Washington University in St. Louis

Washington University Open Scholarship

January 2010

FCS Analysis of Pore Formation by the Human Protein Bax in Lipid Membranes

Olena Ivashyna
Washington University in St. Louis

Follow this and additional works at: https://openscholarship.wustl.edu/etd

WASHINGTON UNIVERSITY

Division of Biology and Biomedical Sciences

Program of Molecular Biophysics

Dissertation Examination Committee:
Paul H. Schlesinger, Chair
Elliot E. Elson
Carl Frieden
Eric A. Galburt
Kathleen B. Hall
Garland R. Marshall

FCS ANALYSIS OF PORE FORMATION BY THE HUMAN PROTEIN BAX

IN LIPID MEMBRANES

By

Olena Anatoliyivna Ivashyna

A dissertation presented to the
Graduate School of Arts and Sciences
of Washington University in
partial fulfillments of the degree
of Doctor of Philosophy

August 2010

Saint Louis, Missouri

<u>AKNOWLEDGEMENTS</u>

First, I would like to thank my thesis advisor, Dr. Paul Schlesinger, for the opportunity to work in his lab, for the research freedom and subtle guidance, for multiple conversations about research and life, and for being an understanding boss.

I would also like to acknowledge two other mentors who have helped me substantially with my thesis work: Dr. Petra Schwille and Dr. Ana Garcia-Saez. Dr. Schwille allowed me to conduct experiments for my thesis research in her laboratory at the BIOTEC, Max Plank Institute for Cell Biology, Dresden, Germany. She has not only provided the lab space and access to the instruments, but also provided financial support for one of my visits to her lab. Dr. Ana Gracia-Saez, at the time a postdoc in the laboratory of Dr. Schwille, helped me to learn a number of experimental techniques which I extensively used in my thesis research. She also mentored me on the design of experiments, critical thinking and she was an invaluable guide to the German way of life and culture.

I would also like to thank the many past and present members of the Schlesinger lab who were helpful to me over the years: Dr. Sean Merlin, Francesca Macaranchas, Dr. Mitsu Saito. I want to especially thank Eric Christenson for his friendship and for being a great lab mate. Eric taught me how to purify proteins and proofread a number of my writings. He was very helpful and supportive in times of need. I would also like to acknowledge some members of the Schwille lab who were very helpful to me inside and outside the lab: Dr. Jonas Ries, Dr. Eugene Petrov, Claudia Schwager, and Karin Crell.

An acknowledgement section would not be complete without thanking my parents, Anatolii and Nadezhda Ivashyna, who guided and supported me in many ways on my path towards a PhD. This work would not be possible without them. I also would like to thank my host family – Frances Agrell and Dick Shaw – who provided me with love and support during my last year of undergraduate training at the University of Maine. I feel very lucky for having them in my life.

Finally, I would like to thank my husband, Jonathan Deering. This PhD thesis would not be possible without his tremendous support, love and understanding.

To my husband Jon and
my parents
Anatolii and Nadezhda

TABLE OF CONTENTS

> Apoptosis
> Bcl-2 protein family and apoptosis
> Sub-groups of the Bcl-2 protein family
> Discovery of the Bcl-2 protein family: retrospective history
> Structure and function of Bax protein
> Bax pore formation mechanism
> References

> Introduction
> Detergent micelles
> Large Unilamellar Vesicles
> Giant Unilamellar Vesicles
> Lipid Bilayers
> Other *in vitro* systems
> References

> Single-Molecule Sensitivity Fluorescence Techniques
> > Physical principles of fluorescence
> > Fluorophores
> > FCS and autocorrelation analysis
> > FCCS and cross-correlation analysis
> > Two-focus scanning FCS
> > Two-focus two-color scanning FCCS
> > Fluorescence intensity distribution analysis
> Assay of liposome permeability
> References

LIST OF FIGURES AND TABLES

Chapter 4

Chapter 5

Chapter 6

Chapter 7

Appendix

LIST OF ABBREVIATIONS

AC	Alternating current
AFM	Atomic force microscopy
APD	Avalanche photo diode
Bax	Bcl-2 associated protein x
BaxΔC	BAX with 19 amino acid truncation on the C-terminus
BAXΔC(G40C)	BAXΔC with G40C, C62A, C126A mutations
fluor-BAXΔC	fluorescently labeled BAXΔC(G40C)
Bax-G	full length Bax protein labeled with Alexa 488
Bax-R	full length Bax protein labeled with Atto 655
Bax-RG	complexes containing Bax-R and Bax-G proteins
Bcl-2	B cell leukemia/lymphoma 2
Bcl-x_L	B cell lymphoma extra large protein
Bid	BH3-interacting domain death agonist (BH3-only protein)
Bik	(BH3-only protein)
Bim	BH3-containing protein (BH3-only protein)
BH domain	Bcl-2 homology domain
CL	bovine heart cardiolipin
cBid	cut Bid, Bid cut with caspases 8
CMC	critical micelle concentration
DLS	Dynamic light scattering
DOPC	1,2-dioleoyl-sn-glycero-3-phosphocoline
DOPA	1,2-dioleoyl-sn-glycero-3-phosphate (monosodium salt)
DOPG	1,2-dioleoyl-sn-glycero-3-phosphoglycerol
DOPE	1,2-dioleoyl-sn-glycero-3-phosphoethanolamine
FCS	Fluorescence correlation spectroscopy
FCCS	Fluorescence cross-correlation spectroscopy
FIDA	Fluorescence intensity distribution analysis
FRET	Fluorescence resonance energy transfer
GUV	Giant unilamellar vesicle
GFP	Green fluorescent protein
ITO-coated cover glass	indium-tin-oxide-coated cover glass
LUV	Large unilamellar vesicle
MAC	Mitochondrial Apoptosis-Induced Channel
Mcl-1	Myeloid cell leukemia sequence 1
MOM	mitochondrial outer membrane
pI	Isoelectric point
p53	tumor protein 53
Puma	(BH3-only protein)
POPC	palmitoyp-oleoyl-sn-glycero-3-phosphocoline
SPR	surface plasmon resonance
tBid	truncated Bid

LIST OF SYMBOLS

$\bar{x}$	geometric mean
$\langle \, \rangle$	Arithmetic mean
A_{eff}	effective detection area
$B(\vec{r})$	spatial brightness distribution function
C	Concentration
δ	deviation from mean value: $\delta F(t) = F(t) - \langle F(t) \rangle$
D	diffusion coefficient
d	distance between two foci
F	Fluorescence intensity
φ	quantum yield of a fluorophore
$G(\tau)$	correlation curve
γ	Euler constant (0.5772)
h	thickness of a membrane
h	Plank constant: $E = h\nu$
q	specific brightness of a fluorophore
k_B	Boltzmann constant
k_r	rate of radiative energy transfer
k_{nr}	rate of non-radiative energy transfer
μ_{mem}	membrane viscosity
μ_{sol}	solution viscosity
N	Number of particles in effective detection volume V_{eff}
$P(n)$	distribution of photon counts
R	radius
S	structural parameter: $S = \omega_z / \omega_{xy}$
T	temperature
T	triplet fraction
T_{count}	counting period
t	time
τ_D	diffusion time: $\tau_D = \omega^2 / 4D$
τ_T	triplet time
$\vec{v}$	flow velocity
V_{eff}	effective detection volume
ω_{xy}	waist: $1/e^2$ - radius of a focused Gaussian beam
ω_z	$1/e^2$ - radius along axial dimension of a focused Gaussian beam

ABSTRACT OF THE DISSERTATION

FCS Analysis of Pore Formation by the Human Protein Bax in Lipid Membranes

by

Olena Anatoliyivna Ivashyna

Abstract

Bax is a pro-apoptotic member of the BCL-2 protein family and its paramount function during apoptosis is to form pores in the mitochondrial outer membrane (MOM). In a simplified apoptosis model, upon apoptotic stimulation, Bax is activated via an unresolved mechanism, translocates to the MOM, where it changes conformation, inserts into the membrane as a monomer, and finally undergoes in-membrane oligomerization to form a pore. Once the Bax pore is formed, cytochrome c and other mitochondria-resident proteins escape into the cytoplasm where they activate the cascade of caspases, which dismantle the cell. To date, the structure of the inactive cytoplasmic form of Bax is known; however, the structure of the membrane-integrated, active form of Bax remains unsolved. The absence of membrane structure for Bax leaves the mechanism of Bax pore formation poorly understood. To investigate the mechanism of Bax pore formation, we developed and used approaches to study fluorescently labeled Bax in solution and in lipid membranes using single-molecule sensitivity fluorescence techniques based on fluorescence correlation spectroscopy – FCS. These single-molecule fluorescence techniques provide us with a non-invasive method to study the mechanism of Bax pore formation reconstituted in giant unilamellar vesicles (GUVs). Our results show, that in the environment of a GUV lipid membrane, Bax can form a complex distribution of coexisting pore sizes ranging from 1 nm to 20 μm in diameter. Evidence is provided by

directly examining oligomerization and mobility changes of Bax molecules in GUVs by fluorescence cross-correlation spectroscopy (FCCS) and observing the large complexes by confocal microscopy. We show that in the presence of Bcl-x_L, an inhibitor of Bax pore formation, membrane-bound Bax was primarily monomeric. We also show, that in the large length-scale format of the GUV, Bax forms mega-pores – structures that reveal its affinity for highly curved membranes. Analysis of the line tension in the rim of Bax mega-pores indicates that Bax dramatically reduces line tension while stabilizing these lipidic pores. Furthermore, our results demonstrate that Bax forms pores by increasing membrane surface energy and by changing the curvature of lipid membranes, thus manifesting an ability to sculpt lipid bilayers.

In addition to studying Bax in lipid membranes, we have investigated the *in vitro* mechanism of Bax activation in detergent micelles, where, due to the formation of large hydrodynamic volume protein-detergent micelles, Bax has been proposed to form homo-oligomers upon activation prior to membrane insertion, which is in contrast to the *in vivo* studies which reported that Bax binds MOM as a monomer and then undergoes homo-oligomerization. Our studies using fluorescence intensity distribution analysis (FIDA) have shown that Bax is a monomer before, during and after interaction with detergent micelles; however, it does form large hydrodynamic volume complexes with detergent micelles. The results of our FIDA study establish the connection between the *in vitro* and *in vivo* mechanism of Bax activation, showing that, prior to the formation of an oligomeric pore in a lipid membrane, Bax binds lipid membranes as a monomer.

CHAPTER 1

"Apoptosis, Bcl-2 Protein Family, and Bax"

Apoptosis

In order to maintain homeostasis and survive, multicellular organisms developed a mechanism to sacrifice certain cells for the good of others. For example, cells in the xylem of plants must die to create a conduction pathway for water; so must do the cells in the finger webs of a human embryo as well as the neuron cells which failed to create the proper cellular connection[1, 2]. Therefore, to selectively kill cells, multicellular organisms developed a mechanism – apoptosis – which is a morphologically defined form of a programmed cell death[3-6]. The distinctive morphological features of apoptosis include nuclear fragmentation, membrane blebbing and the formation of apoptotic bodies. All multicellular organisms employ apoptosis; however, the biochemical details of apoptosis vary among species. For example, vertebrates, during the mitochondrial pathway of apoptosis, rely on the release of cytochrome c from mitochondria to ensure the activation of caspases – the family of proteases responsible for cellular demise – while in *C. elegans* only four proteins are involved in apoptosis without the engagement of cytochrome c[7]. Furthermore, some single-celled organism who form surface biofilms, or live in colonies (such as yeast), also have been shown to have a mechanism to eliminate single cells in the colony to ensure the survival of others[8, 9]. Thus the need to eliminate old, virus-infected or otherwise unwanted cells is universal among the various forms of life.

Apoptosis plays an important role in mammalian development, especially in the nervous system where deficiencies in the execution of the apoptotic program lead to severe neurological disorders. Apoptosis also plays an important role in maintaining homeostasis, for example, in the immune system where it eliminates unwanted B and T cells. Disregulation of apoptosis during the maintenance of homeostasis leads to cancer,

as illustrated by B-cell lymphomas. While disregulation or inhibition of apoptosis at different stages in the life of vertebrates is detrimental, activation of apoptosis, for example, in the cells of the central nervous system upon trauma, or in cardiomyocytes deprived of oxygen upon myocardial infarction, also has a deleterious effect onto the life expectancy of an organism[10, 11]. It is estimated that up to 50% of the cells lost in a heart attack or stroke might be saved by pharmacologic inhibition of apoptosis. The latter can be accomplished only when we understand the molecular and biophysical mechanisms of programmed cell death.

Bcl-2 protein family and apoptosis

Apoptosis can occur via two distinct pathways: the extrinsic and intrinsic pathways[7, 12-15] (Fig. 1-1). The extrinsic pathway, also known as the death-receptor pathway, occurs via activation of the death receptors at the cell surface, leading to the activation of effector caspase 8, which in turn activates the executioner caspases that dismantle the cell. The intrinsic pathway of apoptosis, also known as the mitochondrial pathway, occurs when the cell senses internal damage or is deprived of growth factors. The mitochondrial pathway of apoptosis is controlled by the Bcl-2 protein family, where upon activation, proteins Bax or Bak permeabilize the mitochondrial outer membrane (MOM) resulting in the release of cytochrome c and other mitochondria-resident proteins into the cytoplasm. In the cytoplasm cytochrome c activates the formation of an apoptosome, leading to cell death. The two pathways of apoptosis are connected though caspase 8. Caspase 8 can cleave Bid to produce tBid which activates Bax and Bak to permeabilize the MOM and release cytochrome c, thus killing a cell.
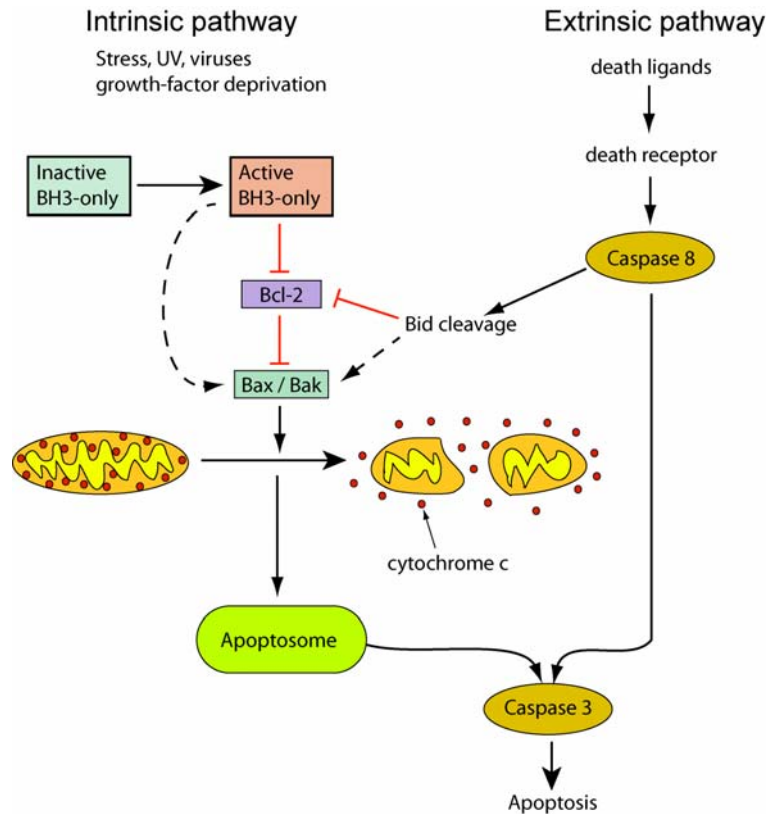
Figure 1-1. The two pathways of apoptosis.

Sub-groups of the Bcl-2 protein family

In humans, twenty-three genes comprise the Bcl-2 protein family and they generate both pro- and anti-apoptotic proteins[13, 16-21]. These two functional protein groups are further divided into three structural groups based on the number of conserved Bcl-2 homology domains (BH1-4) (Fig. 1-2). The first group are the anti-apoptotic multidomain proteins which display sequence conservation through BH1-4 domains, and they include Bcl-2, Bcl-x_L, Mcl1, etc. The other two groups of the Bcl-2 protein family are the pro-apoptotic multidomain proteins (Bax, Bak) and the pro-apoptotic BH3-only proteins (Bid, Bim, Bad, Noxa, Puma, etc.). Interactions between these three groups of the Bcl-2 protein family inform the programmed cell-death decision by altering the
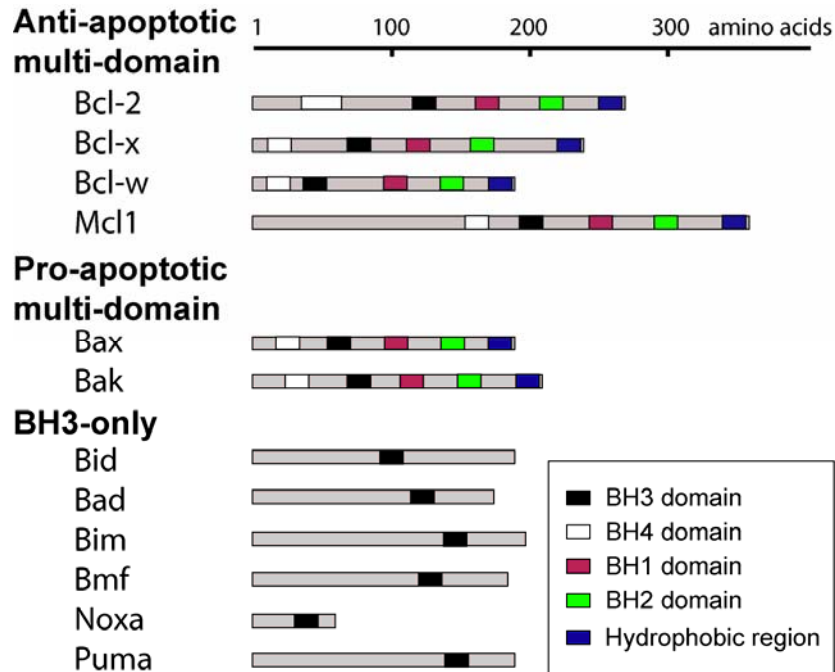
Figure 1-2. The Bcl-2 protein family.

permeability state of the MOM. Alteration of the permeability state of the MOM is done by Bax and Bak, which together[22] or independently[23], can form oligomeric pores in the MOM. The rest of the Bcl-2 family proteins positively and negatively regulate pore formation by Bax and Bak. It has been proposed that the anti-apoptotic proteins such as Bcl-2 and Bcl-x_L inhibit pore formation by Bax and Bak by directly binding these proteins in the MOM. However, it has been shown that Bcl-x_L can prevent Bax pore formation and apoptosis by an independent mechanism where Bcl-x_L does not need to hetero-oligomerize with Bax or Bak[24, 25], though the molecular details of this mechanism have yet to be determined.

The BH3-only proteins, also known as the sentinels of death, transmit the death signal sensed internally inside the cell to Bax and Bak[26]. However, two opposing hypothesis for these proteins function have been proposed. The first hypothesis states that

all BH3-only proteins can bind directly only to the anti-apoptotic proteins which keep Bax and Bak in check. Binding of the BH3-only proteins to the anti-apoptotic proteins releases Bax and Bak to form pores[12-14, 20, 27-29]. The second hypothesis proposes that there are two types of the BH3-only proteins: direct activators and de-repressor/sensitizers[7, 21, 30-34]. The direct activator proteins, which include only Bid, Bim and Puma, activate Bax and Bak by directly binding these proteins, while de-repressor/sensitizer proteins, which include the rest of the BH3-only proteins, initiate apoptosis by binding the anti-apoptotic proteins, preventing them from interacting with the activator BH3-proteins as well as Bax and Bak. However, Puma have been characterized by some groups as a direct activator while by others as a de-repressor/sensitizer[21, 31].

One of the interesting questions about the Bcl-2 protein family in vertebrates is why the family needs to have so many members (over twenty), while in other multicellular organisms, for example, *C. elegans* there are only two homologues of the Bcl-2 protein family (Egl-1 and Ced-9)[35]. A possible answer to this question comes from the tissue-specific expression of the Bcl-2 proteins in vertebrates. For example Bax and Bak are expressed in most tissues while the BH3-only proteins have tissue-specific expression patterns. Additionally, BH3-only proteins receive apoptotic signals from various sources. For example, protein Bim is sequestered to the cytoskeletal structures via association with dynein light chain LC8, and is released form this interaction upon the induction of apoptosis. Free Bim translocates to the mitochondria where it serves as a direct activator of Bax and Bak[36, 37]. Another example is the cytoplasmic protein Bid, which upon cleavage by caspases 8 translocates to the MOM where it serves as a direct

activator of Bax and Bak[38-40]. Puma, another BH3-only protein, is a cytoplasmic protein which is known to interact with p53, a tumor-suppressor protein involved in the regulation of the cell cycle[41]. Upon interaction with p53, Puma influences the activation of Bax and Bak. Therefore, it has been proposed that the reason for the expansion of the number of protein in the Bcl-2 family is the based on three points: (i) a need for redundancy; (ii) a need for functional specialization due to the higher number of tissues in vertebrates compare to invertebrates; (iii) and a need for compensatory regulation[35].

Discovery of the Bcl-2 protein family: retrospective history

The Bcl-2 family of proteins was discovered during a quest to understand the molecular origins of cancer. In the 1940s in the US, an increase in the incidents of cancer was observed and this increase continues. As a result massive research effort has been undertaken to understand the origins of cancer. In 1970s the first viral oncogene, *src*, was discovered[42]. In 1989 Bishop and Varmus were awarded the Nobel Prize in Medicine for the discovery of viral oncogenes, and in particular the *src* oncogene. The discovery of *src* showed that there is a connection between the DNA content of a cell and cancer, and thus opened new avenues of research. As a result it has been shown that a number of non-hereditary cancers are associated with chromosomal translocations[43-45]. For example, it has been shown that translocation from chromosome 14 to chromosome 18, t(14:18), is commonly detected in poorly differentiated lymphocytic lymphomas[44]. However, the state of technology at the time did not allow sequencing of these translocations. In 1980 it became possible to sequence chromosomal DNA at the translocation points and in 1985 three unrelated research groups published independently their results on cloning the gene

located at the t(14:18)[46-49]. This gene was called *bcl-2,* abbreviating the name of cancer cells from which it was cloned – B cell lymphoma. The translocation t(14:18) has coupled the immunoglobulin heavy chain locus from chromosome 14 to the *bcl-2* gene on chromosome 18, thus leading to over-expression of this gene. However, it was unclear how the over-expression of a gene can cause cancer.

In 1988 Vaux *et al* has shown that the over-expression of the Bcl-2 protein results in reduced cell death and the locking of cells in the G_0 state[50]. This observation became the first proof that *bcl-2* was an oncogene which promoted cancer not due to the mutation in the gene, but due to the over-expression of the normal gene. After that point the quest for detailed understanding of the Bcl-2 protein function began. As a result it has been discovered that Bcl-2 is involved in the control of apoptosis. Additionally, it was found that there are a number of proteins which share sequence homology with the Bcl-2 protein, which consequently became the members of the Bcl-2 protein family. These proteins include Bax[51], Bcl-xL[52], Bcl-w[53], Mcl1[54], Bik[55], Bid[40], Bim[56] and others.

In 1993 protein Bax was discovered by coimmunoprecipitation with Bcl-xL[51] and later on it has been shown that to prevent apoptosis, Bcl-2 has to hetero-dimerize with Bax[57, 58]. It has also been shown that during apoptosis the release of cytochrome c is required to initiate the mitochondrial pathway of apoptosis and that Bax and Bak are involved in this process[59].

The biochemical function of the Bcl-2 protein family was revealed after the structure for Bcl-xL was solved[60]. This structure showed a remarkable similarity in fold with the pore-forming subunits of collicin A and diphtheria toxin[61, 62]. Later on the structures of Bid[63], Bax[64] and Bcl-2[65] have been determined and they showed the same

resemblance in protein fold to Bcl-x$_L$ and collicin A. Thus, based on this similarity in protein fold, it has been proposed and later proved that proteins of the Bcl-2 family can form pores in lipid membranes[66-72].

Since the over-expression of the anti-apoptotic proteins has been implicated in causing cancer, an attempt has been made to develop pharmacologic inhibitors of the anti-apototic proteins[73]. As a result, anti-cancer drugs such as ABT-747 and ABT-263 have been developed[74-77]. These drugs have been engineered to bind the hydrophobic pocket on the surface of Bcl-2 and Bcl-x$_L$, where normally the BH3 proteins would bind, thus allowing the BH3 proteins to activate Bax and Bak resulting in the cell death.

Another avenue for the development of anti-cancer drugs would be to develop small molecules able to activate the pro-apoptotic members of the Bcl-2 family, such as Bax and Bak. In addition, development of small molecules which can inhibit the activation of Bax and Bak would be tremendously beneficial in the prevention of apoptosis in the central nervous system after trauma or apoptosis of cardiomyocytes after myocardial infarction. However, all of the above scenarios of activation and inhibition of Bax and Bak are still on hold, since the mechanism of the activation of Bax and Bak is not clear. This demonstrates the need for more basic research to be applied to the problem of understanding the molecular mechanism of action of the proteins of the Bcl-2 family, and in particular of the protein Bax.

Structure and function of protein Bax

Bax is a 21 kDa protein (192 amino acids). According to the solution NMR structure, Bax consists of nine α-helices with 61 % α-helical content[64] (Fig. 1-3). This structure represents the conformation of inactive solution Bax. In contrast to inactive Bax, active Bax is bound to a lipid membrane and has a different protein conformation (Fig. 1-4). It has been shown by cysteine scanning of Bax that in the active membrane bound conformation of Bax has three helices inserted into the lipid membrane[78]. These are helices 5, 6 and 9 (Fig. 1-4, shown in blue and yellow). To achieve such conformation the molecule of Bax needs to be "flexible". The flexibility in changing from one protein conformation to another is possible due to the presence of multiple glycines in the loops connecting the helices of Bax (Fig. 1-5). Glycines constitute 11 % of all amino acids in Bax and 60 % of them are found in the connecting loops.

In order to permeabilize the MOM, Bax needs to translocate from the cytosole to the MOM and undergo a conformational change which is associated with its activation and can be detected by the conformation specific antibodies. In particular, 6A7 antibody against the N-terminus of Bax is used as a "gold standard" for showing the activation of Bax[79, 80]. However, the molecular mechanism of Bax activation is a matter of active debate[21, 28, 81]. In fact, it has been recognized as a "holy grail of apoptosis research"[7].

It has been shown in *in vitro* assays that Bax can be directly activated by a number of BH3 peptides[82], and by the full-length BH3-only proteins[21, 41, 83-86]. In addition, it has been shown that Bax can be directly activated by heat[87], by the direct interaction with p53[88], by elevated pH[89] and by incubation with detergents[79, 80, 90, 91].
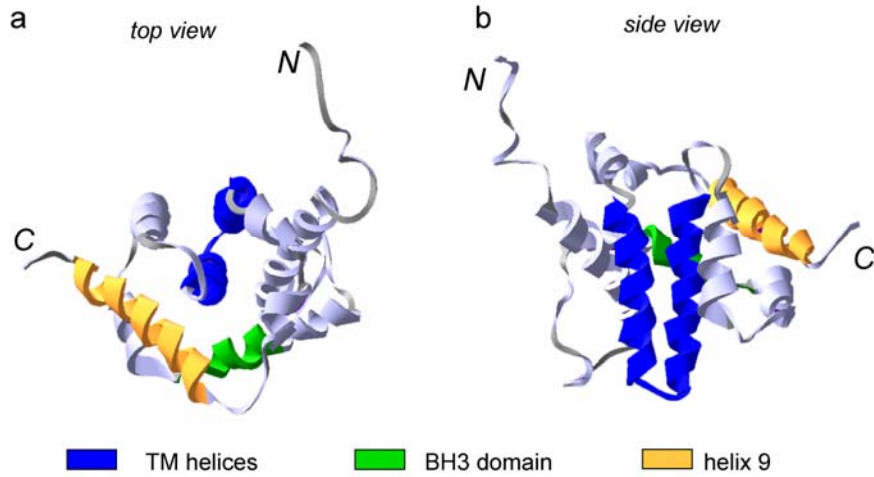
Figure 1-3. Structure of the human Bax protein, alpha isoform[64]. See Appendix I for protein sequence.
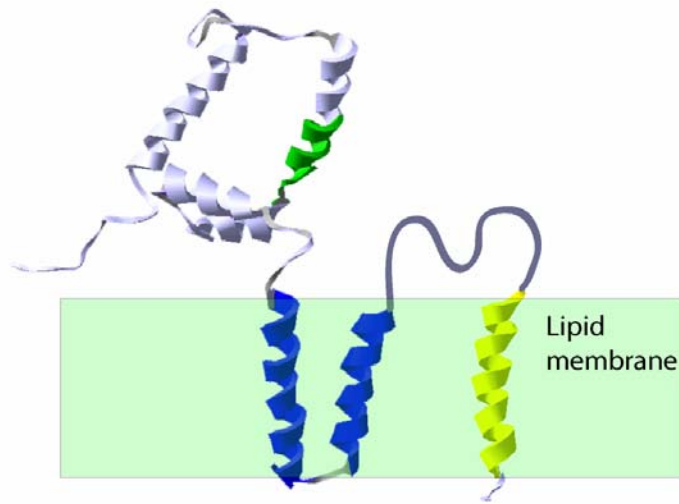
Figure 1-4. Schematic of the protein conformation of Bax in a lipid membrane.
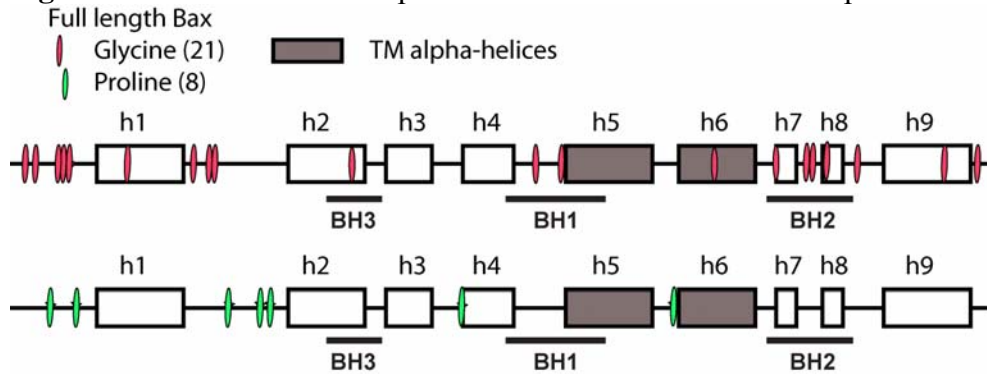
Figure 1-5. Position of glycine and proline amino acids in the Bax protein

Currently, two structural models of Bax activation are being proposed. The first model suggests that the homo- and hetero-oligomerization of Bax with other Bcl-2 family members occurs via a hydrophobic groove on the surface of Bax (formed by domain BH1-3) which in the inactive protein conformation is occupied by the C-terminus of Bax. This model of Bax activation is not supported by the structural studies on Bax, i.e. currently there is no solved structure of Bax where this hydrophobic groove is occluded by the BH3 domain. However, this hypothesis of C-terminus displacement by the BH3 peptides was proposed based on the structural studies with the anti-apoptotic proteins[92] which share a similar fold with Bax. The second model of Bax activation by the BH3 peptides has been proposed by Gavathiotis *et al,* who has shown that the stapled BH3 peptide of Bim binds to Bax at a binding site formed by helices 1 and 6 of Bax[93]. This site is on the opposite side of the Bax protein from the hydrophobic groove occupied by the C-terminus. However, it is possible that *in vivo* both of these binding sites on Bax are used in the homo- and heterotypic interactions.

The importance of various residues and sequences of residues in Bax has been explored in a large number of studies. As a result, it has been shown that the removal of the BH3 domain in Bax renders it inactive *in vivo*[94] and that BH3 domain is important for hetero-and homo-oligomerization among proteins of the Bcl-2 family[95, 96]. It was also shown that the N-terminal end of Bax contains the mitochondrial-targeting sequence[97, 98] and that the C-terminus of Bax, together with helices 5 and 6, is involved in membrane binding[70, 78, 99], while the rest of the helices of Bax play an important role in the activation of Bax by the BH3-only proteins and in the homo-oligomerization of Bax[93, 100, 101]. Therefore, when considering a strategy for the fluorescent labeling of Bax for FCS

studies discussed in Chapter 7, we did not label Bax with GFP (however, it has been done[102]) but instead we labeled Bax with small fluorescent dyes (~0.5 kDa) via genetically engineered cysteine. A similar fluorophore labeling strategy of Bax has been used by Lovell *et al,* where Bax was used in a FRET study[84].

Bax pore formation mechanism

According to a simplified apoptosis model, Bax is found in the cytoplasm of non-dying cells and upon the initiation of the mitochondrial pathway of apoptosis Bax is activated. Then it translocates from the cytoplasm to the mitochondrial outer membrane, where it inserts into the membrane as a monomer and then undergoes self-assembly/oligomerization to form a pore through which cytochrome c and other mitochondria-resident proteins can escape into the cytoplasm[103-105] (Fig. 1-6).
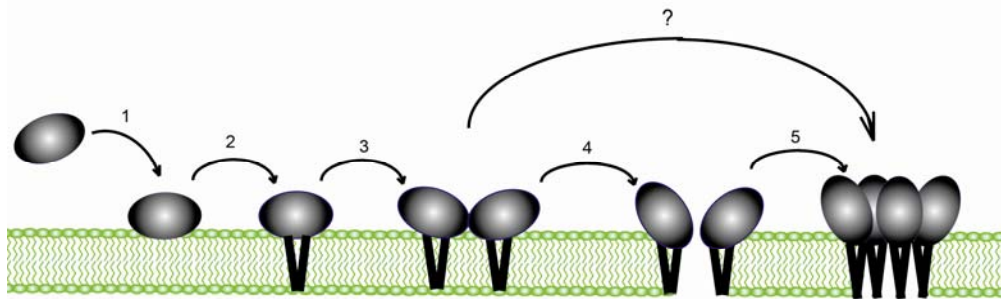
Figure 1-6. Schematic of the mechanism of Bax binding, conformational change, integration, and pore formation in a lipid membrane.

The formation of Bax pores in MOM has not been observed by high resolution electron microscopy. Instead it was shown that Bax was accumulated at the fission site of mitochondria during apoptosis[106]. In addition, it has been shown that disruption of

mitochondrial fission results in the inhibition of apoptosis thus establishing a connection between the function of Bax and that of the proteins involved in mitochondrial fission[107-110]. However, the electrophysiology measurements of membrane conductance in isolated mitochondria from apoptotic cells revealed the existence of a mitochondrial apoptosis-induced channel (MAC). The exact protein composition of a MAC is not clear but it is clear that Bax is its major component[111, 112]. It has been shown that MAC activity is not present in Bax$^{-/-}$, Bak$^{-/-}$ cells, but is present in cells expressing one or both of these proteins[112]. Additionally, it has been shown that the conductivity of a MAC in proteo-liposomes formed from mitochondrial membranes is similar to the conduction properties of the channels formed by the recombinant activated Bax, however, the two do not match exactly. On the other hand, *in vitro* Bax has been shown to form pores in artificial lipid membranes, and its ability to release cytochrome c and other macromolecules from liposomes via the formation of a pore is clearly documented[39, 68, 83, 104, 105, 113]. Therefore, the existence of a MAC in mitochondria during apoptosis and the ability of recombinant Bax to form pores in artificial lipid bilayers indicate that the permeabilization of the OMM during apoptosis must occur via the formation of a Bax-containing pore. Dispite this indication the opponents of this hypothesis do exist.

Studies of the kinetics of liposome poration by Bax revealed that Bax forms pores of various diameters starting with a dimer pore of 1 nm in diameter, continuing to a tetramer pore of 4 nm in diameter[104] (this pore is wide enough for cytochrome c to go though), and continuing to larger pores up to 100 nm in diameter[83, 113, 114]. This heterogeneity in the sizes of pores formed by Bax was assumed to be a controversy,

however, later on it has been shown that the size of a Bax-containing pore in MOM changes with time[111], thus unifying all previous results.

In Chapter 6 of this dissertation we present data showing that Bax is able to form even larger pores with diameter of 5-20 μm. We named these pores as Bax mega-pores and they are wide enough to allow multiple mitochondria to diffuse through them. In all of the observed Bax mega-pores Bax was concentrated at the rim of the pore, however, in GUVs, where the mega-pore was observed to close, no trace of large visible aggregates of Bax was left on the membrane surface of a GUV. This observation indicates that Bax is accumulated at the pore edge, but it does not form tight contacts with neighboring monomers of Bax thus allowing for fast disassembly of the pore. This brings us to the discussion about the type of the pore formed by Bax.

The pore forming proteins and peptides can form two types of pores in lipid membranes – barrel-stave and toroidal pores[115] (Fig. 1-7). The interior of the barrel-stave pore is outlined by protein components, while the interior of the toroidal pore has lipid headgroups outlining the pore interior. Because of its unique structure toroidal pore is occasionally called a lipidic pore since the two leaflets of the lipid bilayer are connected
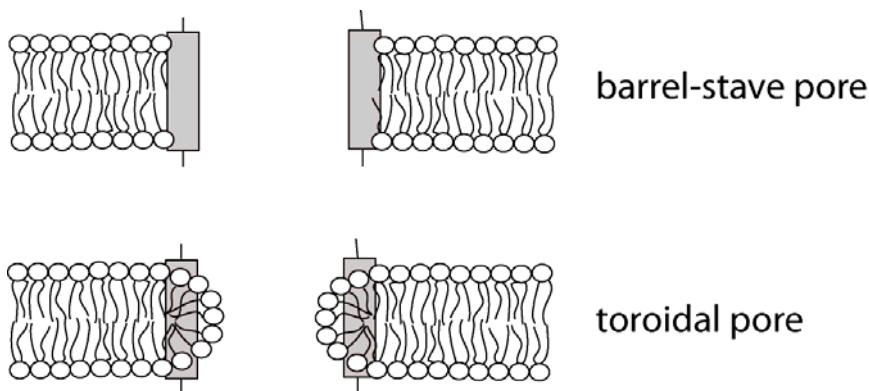
Figure 1-7. Schematic of a cross section for a barrel-stave and for a toroidal pore.

at the pore site. The example of a peptide forming barrel-stave pore is alamethicin[116], while magainin peptide serves as an example of a peptide forming toroidal pores[117].

In case of Bax both models of the pore has been proposed and still are being proposed[118-121]. However, overwhelming number of arguments suggest that Bax forms a toroidal type of pore. The first argument is that Bax accelerates the rate of lipid mixing between the two leaflets of a lipid bilayer[85, 119]. Normally such lipid mixing or transfer has an extremely low rate and can be accelerated only when the two leaflets are connected, for example through a lipidic pore. The second argument comes from the neutron scattering experiments where lipid bilayers treated with pore-forming helix 5 of Bax shows formation of a lipidic pore structure[121]. As a control in these experiments alamethicin was used to show the neutron scattering pattern for a bona fide barrel-stave pore forming peptide. The third argument is based on the experiments where the addition of positive intrinsic curvature promoting lipids (such as lyso-lipids), which energetically favor being in the rim of a lipidic pore, accelerated Bax pore formation, while addition of lipids with negative intrinsic curvature (such as DOPE or cholesterol) inhibited the pore formation by Bax[67, 86]. In addition to this argument, it has been shown that activated Bax can crosslink liposomes to form cuboidal structures – sponge-like structures (unpublished data).

The above-mentioned review of the pore-formation mechanism of Bax together with the enigma of Bax activation, also discussed above, clearly indicates that the mechanism of Bax pore formation is poorly understood and needs to be studied in greater detail. The experiments discussed in this dissertation attempt to answer some of the questions about the mechanism of Bax action.

References

1. Vaux, D. L., Haecker, G. & Strasser, A. An evolutionary perspective on apoptosis. Cell 76, 777-9 (1994).

2. Polard, T. D. & Earnshaw, W. C. Cell Biology (Elsevier Inc., 2004).

3. Meier, P., Finch, A. & Evan, G. Apoptosis in development. Nature 407, 796-801 (2000).

4. Yuan, J. & Yankner, B. A. Apoptosis in the nervous system. Nature 407, 802-9 (2000).

5. Krammer, P. H. CD95's deadly mission in the immune system. Nature 407, 789-95 (2000).

6. Clarke, P. G. & Clarke, S. Nineteenth century research on naturally occurring cell death and related phenomena. Anat Embryol (Berl) 193, 81-99 (1996).

7. Youle, R. J. & Strasser, A. The BCL-2 protein family: opposing activities that mediate cell death. Nat Rev Mol Cell Biol 9, 47-59 (2008).

8. Madeo, F. et al. Apoptosis in yeast. Curr Opin Microbiol 7, 655-60 (2004).

9. Frohlich, K. U. & Madeo, F. Apoptosis in yeast--a monocellular organism exhibits altruistic behaviour. FEBS Lett 473, 6-9 (2000).

10. Abbate, A., Bussani, R., Amin, M. S., Vetrovec, G. W. & Baldi, A. Acute myocardial infarction and heart failure: role of apoptosis. Int J Biochem Cell Biol 38, 1834-40 (2006).

11. Gustafsson, A. B. & Gottlieb, R. A. Bcl-2 family members and apoptosis, taken to heart. Am J Physiol Cell Physiol 292, C45-51 (2007).

12. Adams, J. M. & Cory, S. Bcl-2-regulated apoptosis: mechanism and therapeutic potential. Curr Opin Immunol 19, 488-96 (2007).

13. Adams, J. M. & Cory, S. The Bcl-2 protein family: arbiters of cell survival. Science 281, 1322-6 (1998).

14. Cory, S. & Adams, J. M. The Bcl2 family: regulators of the cellular life-or-death switch. Nat Rev Cancer 2, 647-56 (2002).

15. Danial, N. N. & Korsmeyer, S. J. Cell death: critical control points. Cell 116, 205-19 (2004).

16. Hardwick, J. M. & Youle, R. J. Snapshot: Bcl-2 proteins. Cell 138, 404-5 (2009).

17. Reed, J. C. Proapoptotic multidomain Bcl-2/Bax-family proteins: mechanisms, physiological roles, and therapeutic opportunities. Cell Death Differ 13, 1378-86 (2006).

18. Fesik, S. W. Insights into programmed cell death through structural biology. Cell 103, 273-82 (2000).

19. Kroemer, G. Mitochondrial implication in apoptosis. Towards an endosymbiont hypothesis of apoptosis evolution. Cell Death Differ 4, 443-56 (1997).

20. Adams, J. M. & Cory, S. Life-or-death decisions by the Bcl-2 protein family. Trends Biochem Sci 26, 61-6 (2001).

21. Kim, H. et al. Hierarchical regulation of mitochondrion-dependent apoptosis by BCL-2 subfamilies. Nat Cell Biol 8, 1348-58 (2006).

22. Zhou, L. & Chang, D. C. Dynamics and structure of the Bax-Bak complex responsible for releasing mitochondrial proteins during apoptosis. J Cell Sci 121, 2186-96 (2008).

23. Cheng, E. H. et al. BCL-2, BCL-X(L) sequester BH3 domain-only molecules preventing BAX- and BAK-mediated mitochondrial apoptosis. Mol Cell 8, 705-11 (2001).

24. Billen, L. P., Kokoski, C. L., Lovell, J. F., Leber, B. & Andrews, D. W. Bcl-XL inhibits membrane permeabilization by competing with Bax. PLoS Biol 6, e147 (2008).

25. Cheng, E. H., Levine, B., Boise, L. H., Thompson, C. B. & Hardwick, J. M. Bax-independent inhibition of apoptosis by Bcl-XL. Nature 379, 554-6 (1996).

26. Leber, B., Lin, J. & Andrews, D. W. Embedded together: the life and death consequences of interaction of the Bcl-2 family with membranes. Apoptosis 12, 897-911 (2007).

27. Adams, J. M. & Cory, S. The Bcl-2 apoptotic switch in cancer development and therapy. Oncogene 26, 1324-37 (2007).

28. Willis, S. N. et al. Apoptosis initiated when BH3 ligands engage multiple Bcl-2 homologs, not Bax or Bak. Science 315, 856-9 (2007).

29. Uren, R. T. et al. Mitochondrial permeabilization relies on BH3 ligands engaging multiple prosurvival Bcl-2 relatives, not Bak. J Cell Biol 177, 277-87 (2007).

30. Chipuk, J. E., Moldoveanu, T., Llambi, F., Parsons, M. J. & Green, D. R. The BCL-2 Family Reunion. Mol Cell 37, 299-310 (2008).

31. Chipuk, J. E. & Green, D. R. PUMA cooperates with direct activator proteins to promote mitochondrial outer membrane permeabilization and apoptosis. Cell Cycle 8, 2692-2696 (2009).

32. Chipuk, J. E. et al. Mechanism of apoptosis induction by inhibition of the anti-apoptotic BCL-2 proteins. Proc Natl Acad Sci U S A 105, 20327-32 (2008).

33. Chipuk, J. E. & Green, D. R. How do BCL-2 proteins induce mitochondrial outer membrane permeabilization? Trends Cell Biol 18, 157-64 (2008).

34. Chipuk, J. E., Bouchier-Hayes, L. & Green, D. R. Mitochondrial outer membrane permeabilization during apoptosis: the innocent bystander scenario. Cell Death Differ 13, 1396-402 (2006).

35. Degterev, A., Yuan J. Expansion and evolution of cell death programmes. Nat Rev Mol Cell Biol, 378-390 (2008).

36. Puthalakath, H., Huang, D. C., O'Reilly, L. A., King, S. M. & Strasser, A. The proapoptotic activity of the Bcl-2 family member Bim is regulated by interaction with the dynein motor complex. Mol Cell 3, 287-96 (1999).

37. Bouillet, P. et al. The role of the pro-apoptotic Bcl-2 family member bim in physiological cell death. Ann N Y Acad Sci 926, 83-9 (2000).

38. Billen, L. P., Shamas-Din, A. & Andrews, D. W. Bid: a Bax-like BH3 protein. Oncogene 27 Suppl 1, S93-104 (2008).

39. Korsmeyer, S. J. et al. Pro-apoptotic cascade activates BID, which oligomerizes BAK or BAX into pores that result in the release of cytochrome c. Cell Death Differ 7, 1166-73 (2000).

40.   Wang, K., Yin, X. M., Chao, D. T., Milliman, C. L. & Korsmeyer, S. J. BID: a novel BH3 domain-only death agonist. Genes Dev 10, 2859-69 (1996).

41.   Chipuk, J. E., Bouchier-Hayes, L., Kuwana, T., Newmeyer, D. D. & Green, D. R. PUMA couples the nuclear and cytoplasmic proapoptotic function of p53. Science 309, 1732-5 (2005).

42.   Bishop, J. M. Viral oncogenes. Cell 42, 23-38 (1985).

43.   Klein, G. The role of gene dosage and genetic transposition in carcinogenesis. Nature 294 (1981).

44.   Rowley, J. D. Identification of the chromosome region involved in human hematologic malignancies. Science 216 (1982).

45.   Yunis, J. J. The chromosomal basis of human neoplasia. Science 221, 227-36 (1983).

46.   Bakhshi, A. et al. Cloning the chromosomal breakpoint of t(14;18) human lymphomas: clustering around JH on chromosome 14 and near a transcriptional unit on 18. Cell 41, 899-906 (1985).

47.   Bakhshi, A. et al. Mechanism of the t(14;18) chromosomal translocation: structural analysis of both derivative 14 and 18 reciprocal partners. Proc Natl Acad Sci U S A 84, 2396-400 (1987).

48.   Cleary, M. L. & Sklar, J. Nucleotide sequence of a t(14;18) chromosomal breakpoint in follicular lymphoma and demonstration of a breakpoint-cluster region near a transcriptionally active locus on chromosome 18. Proc Natl Acad Sci U S A 82, 7439-43 (1985).

49.   Tsujimoto, Y., Gorham, J., Cossman, J., Jaffe, E. & Croce, C. M. The t(14;18) chromosome translocations involved in B-cell neoplasms result from mistakes in VDJ joining. Science 229, 1390-3 (1985).

50.   Vaux, D. L., Cory, S. & Adams, J. M. Bcl-2 gene promotes haemopoietic cell survival and cooperates with c-myc to immortalize pre-B cells. Nature 335, 440-2 (1988).

51.   Oltvai, Z. N., Milliman, C. L. & Korsmeyer, S. J. Bcl-2 heterodimerizes in vivo with a conserved homolog, Bax, that accelerates programmed cell death. Cell 74, 609-19 (1993).

52.   Boise, L. H. et al. bcl-x, a bcl-2-related gene that functions as a dominant regulator of apoptotic cell death. Cell 74, 597-608 (1993).

53.   Gibson, L. et al. bcl-w, a novel member of the bcl-2 family, promotes cell survival. Oncogene 13, 665-75 (1996).

54.   Kozopas, K. M., Yang, T., Buchan, H. L., Zhou, P. & Craig, R. W. MCL1, a gene expressed in programmed myeloid cell differentiation, has sequence similarity to BCL2. Proc Natl Acad Sci U S A 90, 3516-20 (1993).

55.   Boyd, J. M. et al. Bik, a novel death-inducing protein shares a distinct sequence motif with Bcl-2 family proteins and interacts with viral and cellular survival-promoting proteins. Oncogene 11, 1921-8 (1995).

56.   O'Connor, L. et al. Bim: a novel member of the Bcl-2 family that promotes apoptosis. Embo J 17, 384-95 (1998).

57.   Yin, X. M., Oltvai, Z. N. & Korsmeyer, S. J. BH1 and BH2 domains of Bcl-2 are required for inhibition of apoptosis and heterodimerization with Bax. Nature 369, 321-3 (1994).

58.   Korsmeyer, S. J., Shutter, J. R., Veis, D. J., Merry, D. E. & Oltvai, Z. N. Bcl-2/Bax: a rheostat that regulates an anti-oxidant pathway and cell death. Semin Cancer Biol 4, 327-32 (1993).

59.   Jurgensmeier, J. M. et al. Bax directly induces release of cytochrome c from isolated mitochondria. Proc Natl Acad Sci U S A 95, 4997-5002 (1998).

60.   Muchmore, S. W. et al. X-ray and NMR structure of human Bcl-xL, an inhibitor of programmed cell death. Nature 381, 335-41 (1996).

61.   Parker, M. W., Pattus, F., Tucker, A. D. & Tsernoglou, D. Structure of the membrane-pore-forming fragment of colicin A. Nature 337, 93-6 (1989).

62.   Bennett, M. J., Choe, S. & Eisenberg, D. Refined structure of dimeric diphtheria toxin at 2.0 A resolution. Protein Sci 3, 1444-63 (1994).

63.   Chou, J. J., Li, H., Salvesen, G. S., Yuan, J. & Wagner, G. Solution structure of BID, an intracellular amplifier of apoptotic signaling. Cell 96, 615-24 (1999).

64.   Suzuki, M., Youle, R. J. & Tjandra, N. Structure of Bax: coregulation of dimer formation and intracellular localization. Cell 103, 645-54 (2000).

65.   Petros, A. M. et al. Solution structure of the antiapoptotic protein bcl-2. Proc Natl Acad Sci U S A 98, 3012-7 (2001).

66.   Basanez, G. et al. Bax, but not Bcl-xL, decreases the lifetime of planar phospholipid bilayer membranes at subnanomolar concentrations. Proc Natl Acad Sci U S A 96, 5492-7 (1999).

67.   Basanez, G. et al. Bax-type apoptotic proteins porate pure lipid bilayers through a mechanism sensitive to intrinsic monolayer curvature. J Biol Chem 277, 49360-5 (2002).

68.   Schlesinger, P. H. et al. Comparison of the ion channel characteristics of proapoptotic BAX and antiapoptotic BCL-2. Proc Natl Acad Sci U S A 94, 11357-62 (1997).

69.   Garcia-Saez, A. J. et al. Peptides derived from apoptotic Bax and Bid reproduce the poration activity of the parent full-length proteins. Biophys J 88, 3976-90 (2005).

70.   Garcia-Saez, A. J. et al. Peptides corresponding to helices 5 and 6 of Bax can independently form large lipid pores. Febs J 273, 971-81 (2006).

71.   Garcia-Saez, A. J., Mingarro, I., Perez-Paya, E. & Salgado, J. Membrane-insertion fragments of Bcl-xL, Bax, and Bid. Biochemistry 43, 10930-43 (2004).

72.   Garcia-Saez, A. J., Ries, J., Orzaez, M., Perez-Paya, E. & Schwille, P. Membrane promotes tBID interaction with BCL(XL). Nat Struct Mol Biol 16, 1178-85 (2009).

73.   Muilenburg, D. J., Coates, J. M., Virudachalam, S. & Bold, R. J. Targeting Bcl-2-Mediated Cell Death as a Novel Therapy in Pancreatic Cancer. J Surg Res (2010).

74.   Ackler, S. et al. ABT-263 and rapamycin act cooperatively to kill lymphoma cells in vitro and in vivo. Mol Cancer Ther 7, 3265-74 (2008).

75.   Ackler, S. et al. The Bcl-2 inhibitor ABT-263 enhances the response of multiple chemotherapeutic regimens in hematologic tumors in vivo. Cancer Chemother Pharmacol.

76.   Park, C. M. et al. Discovery of an orally bioavailable small molecule inhibitor of prosurvival B-cell lymphoma 2 proteins. J Med Chem 51, 6902-15 (2008).

77.   Bruncko, M. et al. Studies leading to potent, dual inhibitors of Bcl-2 and Bcl-xL. J Med Chem 50, 641-62 (2007).

78.   Annis, M. G. et al. Bax forms multispanning monomers that oligomerize to permeabilize membranes during apoptosis. EMBO J 24, 2096-103 (2005).

79.   Hsu, Y. T. & Youle, R. J. Nonionic detergents induce dimerization among members of the Bcl-2 family. J Biol Chem 272, 13829-34 (1997).

80.   Hsu, Y. T. & Youle, R. J. Bax in murine thymus is a soluble monomeric protein that displays differential detergent-induced conformations. J Biol Chem 273, 10777-83 (1998).

81.   Certo, M. et al. Mitochondria primed by death signals determine cellular addiction to antiapoptotic BCL-2 family members. Cancer Cell 9, 351-65 (2006).

82.   Letai, A. et al. Distinct BH3 domains either sensitize or activate mitochondrial apoptosis, serving as prototype cancer therapeutics. Cancer Cell 2, 183-92 (2002).

83.   Kuwana, T. et al. Bid, Bax, and lipids cooperate to form supramolecular openings in the outer mitochondrial membrane. Cell 111, 331-42 (2002).

84.   Lovell, J. F. et al. Membrane binding by tBid initiates an ordered series of events culminating in membrane permeabilization by Bax. Cell 135, 1074-84 (2008).

85.   Terrones, O. et al. Lipidic pore formation by the concerted action of proapoptotic BAX and tBID. J Biol Chem 279, 30081-91 (2004).

86.   Terrones, O. et al. BIM and tBID are not mechanistically equivalent when assisting BAX to permeabilize bilayer membranes. J Biol Chem 283, 7790-803 (2008).

87.   Pagliari, L. J. et al. The multidomain proapoptotic molecules Bax and Bak are directly activated by heat. Proc Natl Acad Sci U S A 102, 17975-80 (2005).

88.   Chipuk, J. E. et al. Direct activation of Bax by p53 mediates mitochondrial membrane permeabilization and apoptosis. Science 303, 1010-4 (2004).

89.   Cartron, P. F., Oliver, L., Mayat, E., Meflah, K. & Vallette, F. M. Impact of pH on Bax alpha conformation, oligomerisation and mitochondrial integration. FEBS Lett 578, 41-6 (2004).

90.   Ivashyna, O. et al. Detergent activated BAX protein is a monomer. J Biol Chem 284, 23935-46 (2009).

91.   Antonsson, B., Montessuit, S., Lauper, S., Eskes, R. & Martinou, J. C. Bax oligomerization is required for channel-forming activity in liposomes and to trigger cytochrome c release from mitochondria. Biochem J 345 Pt 2, 271-8 (2000).

92.   Sattler, M. et al. Structure of Bcl-xL-Bak peptide complex: recognition between regulators of apoptosis. Science 275, 983-6 (1997).

93.   Gavathiotis, E. et al. BAX activation is initiated at a novel interaction site. Nature 455, 1076-81 (2008).

94.   Wang, K., Gross, A., Waksman, G. & Korsmeyer, S. J. Mutagenesis of the BH3 domain of BAX identifies residues critical for dimerization and killing. Mol Cell Biol 18, 6083-9 (1998).

95.   Zha, H., Aime-Sempe, C., Sato, T. & Reed, J. C. Proapoptotic protein Bax heterodimerizes with Bcl-2 and homodimerizes with Bax via a novel domain (BH3) distinct from BH1 and BH2. J Biol Chem 271, 7440-4 (1996).

96.   Sedlak, T. W. et al. Multiple Bcl-2 family members demonstrate selective dimerizations with Bax. Proc Natl Acad Sci U S A 92, 7834-8 (1995).

97.   Cartron, P. F. et al. The N-terminal end of Bax contains a mitochondrial-targeting signal. J Biol Chem 278, 11633-41 (2003).

98.   Cartron, P. F. et al. Involvement of the N-terminus of Bax in its intracellular localization and function. FEBS Lett 512, 95-100 (2002).

99.   Tremblais, K. et al. The C-terminus of bax is not a membrane addressing/anchoring signal. Biochem Biophys Res Commun 260, 582-91 (1999).

100.   Cartron, P. F. et al. The first alpha helix of Bax plays a necessary role in its ligand-induced activation by the BH3-only proteins Bid and PUMA. Mol Cell 16, 807-18 (2004).

101.   Bleicken, S. et al. Molecular details of Bax activation, oligomerization and membrane insertion. J Biol Chem (2009).

102.   Hou, Q. & Hsu, Y. T. Bax translocates from cytosol to mitochondria in cardiac cells during apoptosis: development of a GFP-Bax-stable H9c2 cell line for apoptosis analysis. Am J Physiol Heart Circ Physiol 289, H477-87 (2005).

103.   Antonsson, B., Montessuit, S., Sanchez, B. & Martinou, J. C. Bax is present as a high molecular weight oligomer/complex in the mitochondrial membrane of apoptotic cells. J Biol Chem 276, 11615-23 (2001).

104.   Saito, M., Korsmeyer, S. J. & Schlesinger, P. H. BAX-dependent transport of cytochrome c reconstituted in pure liposomes. Nat Cell Biol 2, 553-5 (2000).

105.   Schlesinger, P. H. & Saito, M. The Bax pore in liposomes, Biophysics. Cell Death Differ 13, 1403-8 (2006).

106.   Karbowski, M. et al. Spatial and temporal association of Bax with mitochondrial fission sites, Drp1, and Mfn2 during apoptosis. J Cell Biol 159, 931-8 (2002).

107.   Karbowski, M., Norris, K. L., Cleland, M. M., Jeong, S. Y. & Youle, R. J. Role of Bax and Bak in mitochondrial morphogenesis. Nature 443, 658-62 (2006).

108.   Youle, R. J. & Karbowski, M. Mitochondrial fission in apoptosis. Nat Rev Mol Cell Biol 6, 657-63 (2005).

109.   Lee, Y. J., Jeong, S. Y., Karbowski, M., Smith, C. L. & Youle, R. J. Roles of the mammalian mitochondrial fission and fusion mediators Fis1, Drp1, and Opa1 in apoptosis. Mol Biol Cell 15, 5001-11 (2004).

110.   Jensen, R. E. Control of mitochondrial shape. Curr Opin Cell Biol 17, 384-8 (2005).

111.   Martinez-Caballero, S. et al. Assembly of the mitochondrial apoptosis-induced channel, MAC. J Biol Chem 284, 12235-45 (2009).

112.   Dejean, L. M., Martinez-Caballero, S., Manon, S. & Kinnally, K. W. Regulation of the mitochondrial apoptosis-induced channel, MAC, by BCL-2 family proteins. Biochim Biophys Acta 1762, 191-201 (2006).

113.   Schafer, B. et al. Mitochondrial outer membrane proteins assist Bid in Bax-mediated lipidic pore formation. Mol Biol Cell 20, 2276-85 (2009).

114.   Epand, R. F., Martinou, J. C., Montessuit, S., Epand, R. M. & Yip, C. M. Direct evidence for membrane pore formation by the apoptotic protein Bax. Biochem Biophys Res Commun 298, 744-9 (2002).

115. Yang, L., Harroun, T. A., Weiss, T. M., Ding, L. & Huang, H. W. Barrel-stave model or torroidal model? A case study on melittin pores. Biophys J 81, 1475-85 (2003).

116. He, K., Ludtke, S. J., Heller, W. T. & Huang, H. W. Mechanism of alamethicin insertion into lipid bilayers. Biophys J 71, 2669-79 (1996).

117. Ludtke, S. J. et al. Membrane pores induced by magainin. Biochemistry 35, 13723-8 (1996).

118. Dewson, G. & Kluck, R. M. Mechanisms by which Bak and Bax permeabilise mitochondria during apoptosis. J Cell Sci 122, 2801-8 (2009).

119. Epand, R. F., Martinou, J. C., Montessuit, S. & Epand, R. M. Transbilayer lipid diffusion promoted by Bax: implications for apoptosis. Biochemistry 42, 14576-82 (2003).

120. Epand, R. F., Martinou, J. C., Montessuit, S. & Epand, R. M. Membrane perturbations induced by the apoptotic Bax protein. Biochem J 367, 849-55 (2002).

121. Qian, S., Wang, W., Yang, L. & Huang, H. W. Structure of transmembrane pore induced by Bax-derived peptide: evidence for lipidic pores. PNAS 105, 17379-83 (2008).

CHAPTER 2

"*In vitro* Systems to Study Protein Bax"

Introduction

Due to the complexity of cellular systems and due to the size limitations of mitochondria, which represent the "battle ground" for the proteins of the Bcl-2 family, it has been recognized that model *in vitro* systems which mimic mitochondria can provide crucial information about the function of Bax and the other Bcl-2 family proteins. In this chapter four model *in vitro* systems used to study Bax are discussed (Fig. 2-1). These *in vitro* systems are introduced in the order of simplicity of preparation, starting with detergent micelles, continuing to large unilamellar vesicles (100-200 nm in diameter), and giant unilamellar vesicles (5-100 μm in diameter), and finishing with supported lipid bilayers. In addition, previous use of these *in vitro* systems and the utility of these systems to the study of the mechanism of Bax pore formation in lipid membranes are discussed.
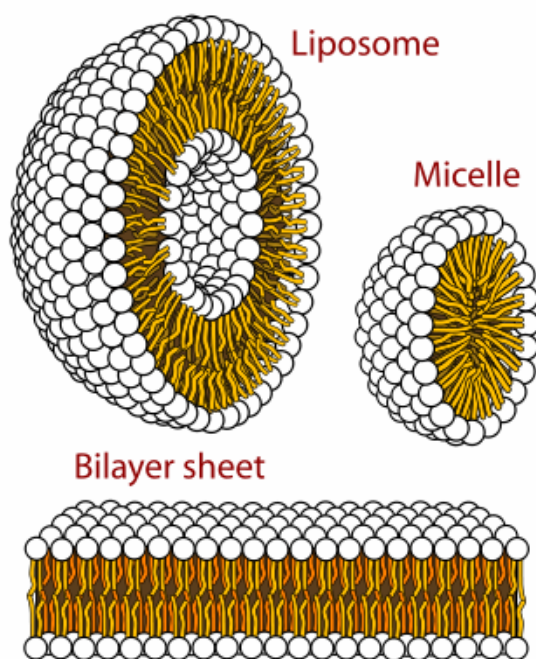
Figure 2-1. *In vitro* systems used to study Bax pore formation. Adopted with permission from Mariana Ruiz Villarreal.

Detergent micelles

After the discovery of the various members of the Bcl-2 family, a number of studies have been done to determine the cellular localization of these proteins prior to and during apoptosis. These studies have shown that, for example, the Bcl-2 protein is found primarily in the membrane compartment of cells[1-3], while Bax and Bcl-x_L changed localization from cytosolic to membrane during the induction of apoptosis[4]. In these studies, detergents were used to extract Bax and other Bcl-2 family proteins from the membrane compartment, and it has been discovered that certain detergents can promote homo- and hetero-dimerization of the Bcl-2 family proteins[4, 5]. In particular, it has been found that certain detergents can lead to the conformational change in Bax which is associated with its activation[5]. As a result, Antonsson *et al.* tested a number of detergents for their ability to activate Bax, allowing it to form pores in liposomes[6]. The results of this study have shown that Bax can be activated by incubation with detergents such as n-octylglucoside, dodecylmaltoside, Nonidet P-40 and Triton X-100 but not with CHAPS. This discovery has led to a number of studies where Bax was activated by incubation with detergents, primarily n-octylglucoside[7-13]. However, before we discuss the important results of the studies of Bax in detergent micelles, it is important to discuss the basic properties of detergent micelles and detergent molecules comprising these micelles.

Detergents are amphipathic molecules which self-assemble into micelles in aqueous solution (Fig. 2-2)[14, 15]. The critical concentration at which detergent molecules start to self-assemble into micelles is known as critical micelles concentration (CMC). The size and shape of detergent micelles together with the CMC depend on the chemical structure of detergent molecules (Table 2-1). In addition, based on their chemical
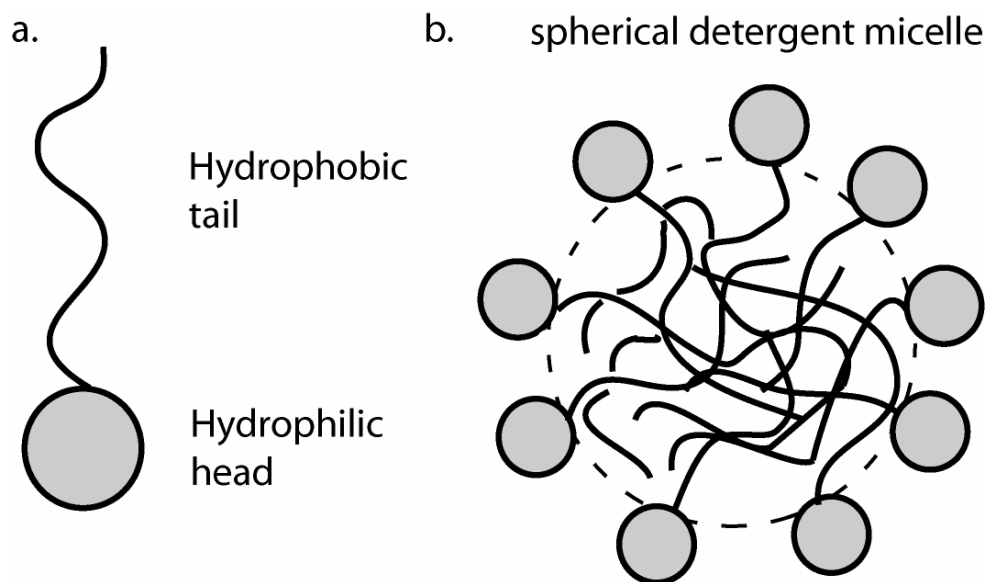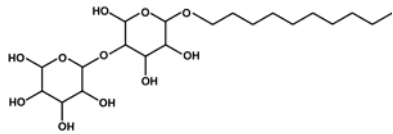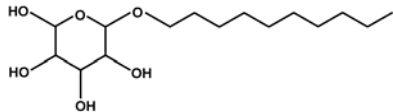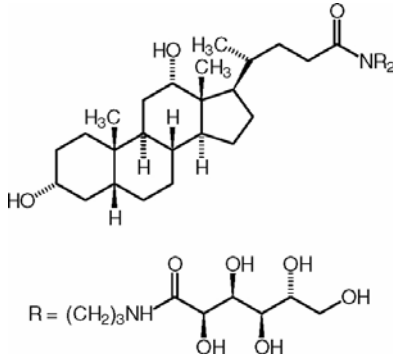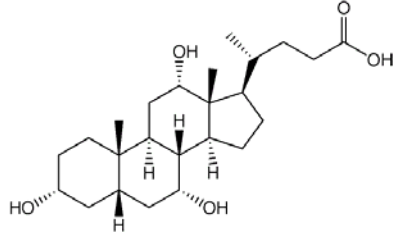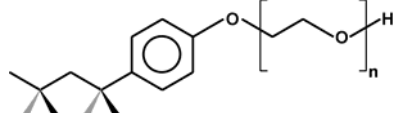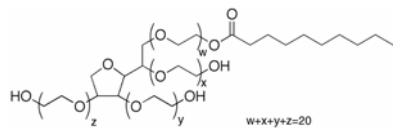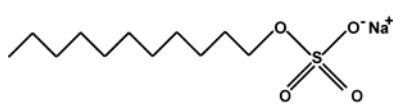
Figure 2-2. a. Schematic of a detergent molecule consisting of a hydrophobic tail and a hydrophilic headgroup. **b.** Schematic cross-section of a spherical detergent micelle[16].

structure detergents are subdivided into two major groups: non-ionic and ionic detergents (Table 2-1). In addition to showing that a range of detergents can activate Bax to form pores in lipid membranes, Antonsson *et al.* has also shown using analytical gel filtration that Bax, when incubated with these activating detergent micelles, eluted together with a high molecular weight marker with the molecular weight larger than the combined weight of one Bax monomer and one detergent micelle[6]. Based on this observation together with the knowledge that Bax oligomerizes in the MOM during apoptosis[17], it was proposed that detergents promote homo-oligomerization of Bax and these homo-oligomers represent active Bax. As a result Bax activated by incubation with detergent micelles was named oligomeric Bax, OG-Bax[13, 18]. In addition to these biochemical studies, Suzuki *et al.* while determining the solution structure of inactive Bax, attempted to determine the structure of Bax in an n-octylglucoside micelle[19], showing that Bax does form large

Table 2-1. Characteristics of various detergents.

Name	MW	CMC, M at 25 °C	Aggregation number	Structure
Non-ionic detergents				
Dodecylmaltoside	510	0.15 mM	98	
n-octylglucoside	292	20-25 mM	84	
CHAPS	615	6 mM	10	
cholic acid	430	14 mM	10	
Triton X-100	625	0.2-0.9 mM	100-155	
Tween 20	1228	0.06 mM		
Ionic detergents				
Sodium lauryl sulfate, SDS	288	7-10 mM	62	

molecular weight complexes in the presence of n-octylglucoside micelles. These n-octylglucoside/Bax complexes had very large hydrodynamic volume, preventing the NMR based determination of the structure of active Bax.

In Chapter 4 of this dissertation, similar studies were undertaken with the fluorescently labeled truncated form of Bax, BaxΔC, with the purpose of determining the number of Bax monomers in the OG-Bax complex[11]. These studies show that indeed BaxΔC, incubated with detergent micelles, forms large macromolecular complexes, but with only one BaxΔC monomer present per complex. This result shows that Bax is able to change the structure of detergent micelles and indicates that the molecular mechanism of Bax activation by detergents is not well understood.

Cholic acid is a naturally occurring bile salt able to activate Bax[5, 11] but without the occurrence of large molecular weight Bax complexes. The latter fact makes cholic acid an interesting candidate for the study of Bax activation.

Detergent micelles were recognized initially as *in vitro* platforms providing a hydrophobic environment for the study of Bax activation. However, it turned out that when present in detergent micelles, Bax has a transformative effect on the detergent micelle structure. For this reason the activation effect of detergents on Bax have been employed widely. However, it is conceivable that in the future, detergents such as cholic acid can be used to determine the protein conformation of active Bax.

Large unilamellar vesicles

Large unilamellar vesicles (LUVs) are widely used as a well characterized, easily manipulated *in vitro* system to study the mechanism of Bax pore formation (Fig. 2-3). LUVs have been used in a wide variety of *in vitro* Bax-related studies: (i) the stoichiometry of Bax pore formation[20]; (ii) the kinetics of Bax pore formation in various conditions such as presence of activating detergents, or activating proteins (such as cBid and Bim), or low pH [6, 7, 9, 13, 20-22]; (iii) the kinetics of Bax binding to lipid membranes[10, 23]; (iv) the morphological changes of lipid membranes upon Bax binding [24]; (v) the effect of curvature-producing and charged lipids on Bax pore formation[7], (vi) the interaction of Bax with other Bcl-2 family proteins [7, 22, 23, 25]; (vii) the ability of Bax to promote mixing of lipids between the internal and external LUV leaflets[26]; (viii) the conformational changes in Bax structure upon membrane binding[27] etc.

The LUVs used in the majority of the aforementioned studies are 200 nm in diameter (similar to the smallest cross-section diameter of mitochondria[28]) and are most commonly composed of a lipid mixture containing combinations of either of following lipids: DOPC, POPC, DOPE, DOPA, DOPG or cardiolipin – lipids which are commonly found in the contact sites of mitochondria[29]. The contact sites in mitochondria are the sites where the outer and inner mitochondrial membranes are in contact. The two most common methods of LUV preparation are the freeze-thaw method[30] and the reverse-phase method[10, 11, 31-33] (See Appendix II for a detailed protocol).

The utility of LUVs to study the mechanism of Bax pore formation is clear, however this *in vitro* system has a number of important limitations: (i) lipid composition of LUVs cannot be 100% identical to the lipid composition of the MOM; (ii) LUVs lack

other mitochondrial proteins present in the MOM during Bax insertion and pore formation which may affect the ability of Bax to form pores; (iii) due to their size, LUVs cannot be used to study the in-membrane diffusion of Bax monomers and the oligomeric Bax pores (GUVs can be used for this purpose).
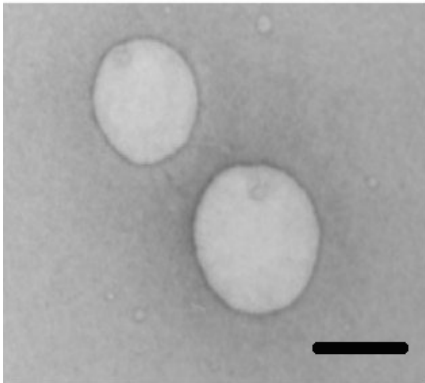
Figure 2-3. Transmission electron microscopy micrograph of LUVs. Scale bar is 200 nm. Adopted from Soman *et al.*[34]

Giant unilamellar vesicles

Giant unilamellar vesicles (GUVs) are another example of a model *in vitro* system used to study the mechanism of Bax pore formation (Fig. 2-4). GUVs have been used successfully to study Bax pore using a patch clamp technique[18], or to study the dye release from a GUV though a single Bax pore using fluorescence microscopy[9]. Due to their size, 5-100 μm in diameter, GUVs can be observed by light microscopy, unlike LUVs, and they can be used to study protein diffusion and oligomerization in a lipid membrane using FCS[35-39] as well as to study the morphological changes in GUVs upon protein binding[40-42]. The use of GUVs to study the diffusion and homo-oligomerization of Bax in lipid membranes using FCS is discussed in Chapter 5.
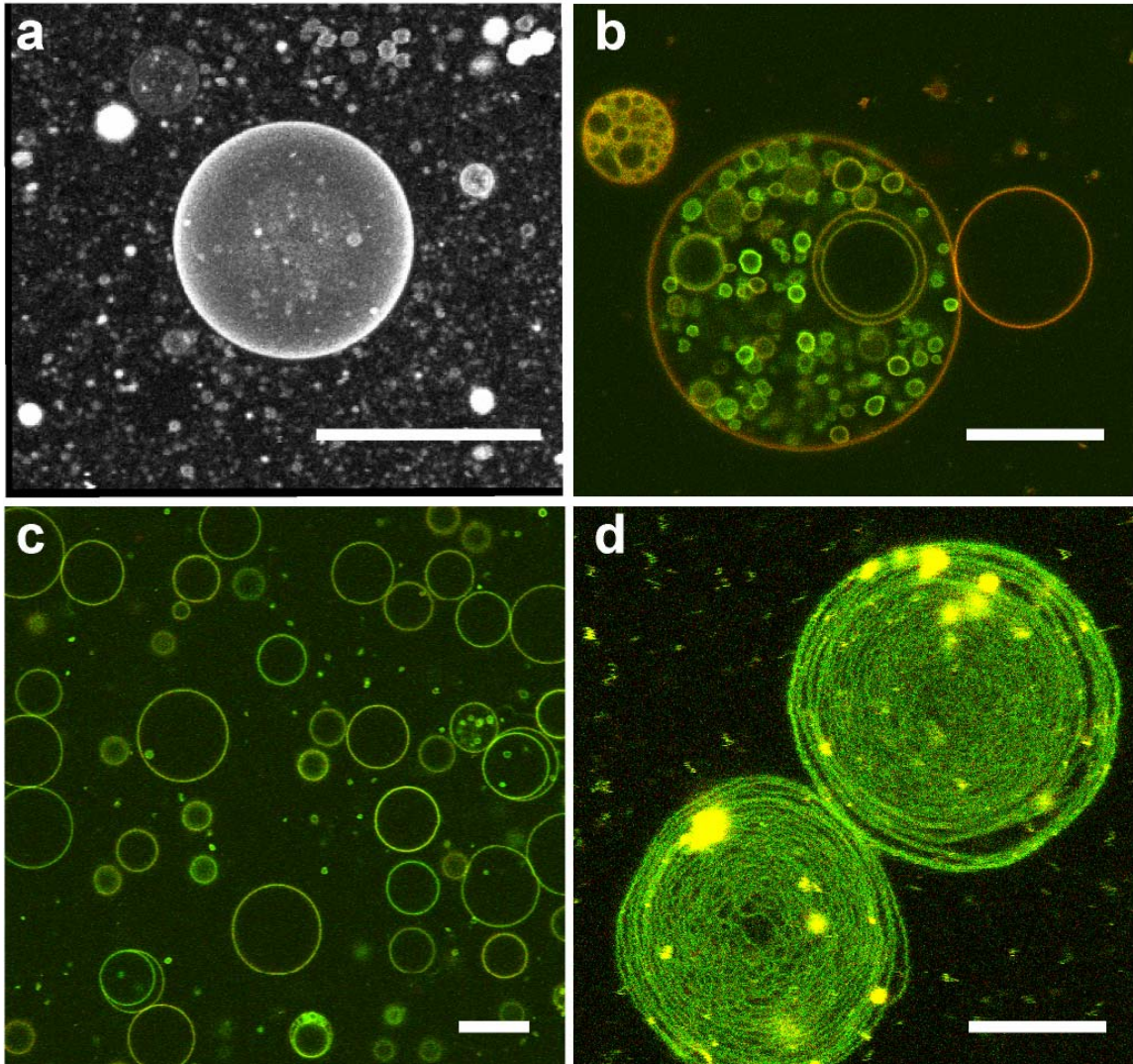
Figure 2-4. Giant unilamellar vesicles: confocal microscopy images.
a. Confocal 3D reconstruction of a field of GUVs (view from the top). One large GUV dominates the field. **b.** Multilamellar giant vesicle. **c.** Cross-section image of a field of GUVs. **d.** Multilamellar GUVs prepared from a lipid mixture of DOPC and cardiolipin (80:20 mol %). Scale bar in each image is 20 μm. All GUVs were prepared by the electroformation method[43].

GUVs can be prepared by three methods: "gentle hydration" method[44, 45], reverse-phase method[46], and by the electroformation method[43, 47-50]. In the "gentle hydration" method, as the name implies, GUVs are formed by the hydration of dried lipid film

deposited on a glass or Teflon surface. In this method, GUVs are formed by the swelling of the lipid film into lipid vesicles. It generally takes up to12 hours to produce GUVs by this method while the electroformation and the reverse-phase methods take up to 2 hours (depending on the lipid composition). In the reverse-phase method, GUVs are made by mixing lipids dissolved in a mixture of diethyl ether and chloroform with aqueous buffer solution forming an emulsion of water in ether/chloroform which is transformed into GUVs after the slow evaporation of ether and chloroform. In the electroformation method, lipids are dried on the surface of two parallel platinum wires[43] or on the surface of two parallel ITO-coated cover glass plates[48], which are then transferred into an aqueous solution (usually 300 mM sucrose) and connected to an AC generator (See Appendix III for detailed protocol). The AC generator generates an alternating electric field between the two electrodes (in this case platinum wires or ITO-coated glass plates) resulting in the swelling of lipid bilayers from the substrate in the form of GUVs.

The electroformation method of GUV preparation is used most commonly due to the relative simplicity of the preparation protocol[51], and it was used to prepare the GUVs described in Chapters 5 though 7. However, this method has a number of drawbacks, such as the difficulty of forming GUVs in solutions containing physiologic salt concentrations[51], the inability to prepare GUVs with heterogeneous lipid distribution between the two lipid leaflets (which would be desirable, since most cellular membranes have asymmetric lipid distribution among the two leaflets), and the artifacts associated with the heterogeneous lipid distribution among the GUVs in the same preparation (Fig. 2-5). In GUVs prepared from a mixture of more than three lipids, it is common to see heterogeneous lipid distribute among the GUVs as shown by arrow and asterisk on
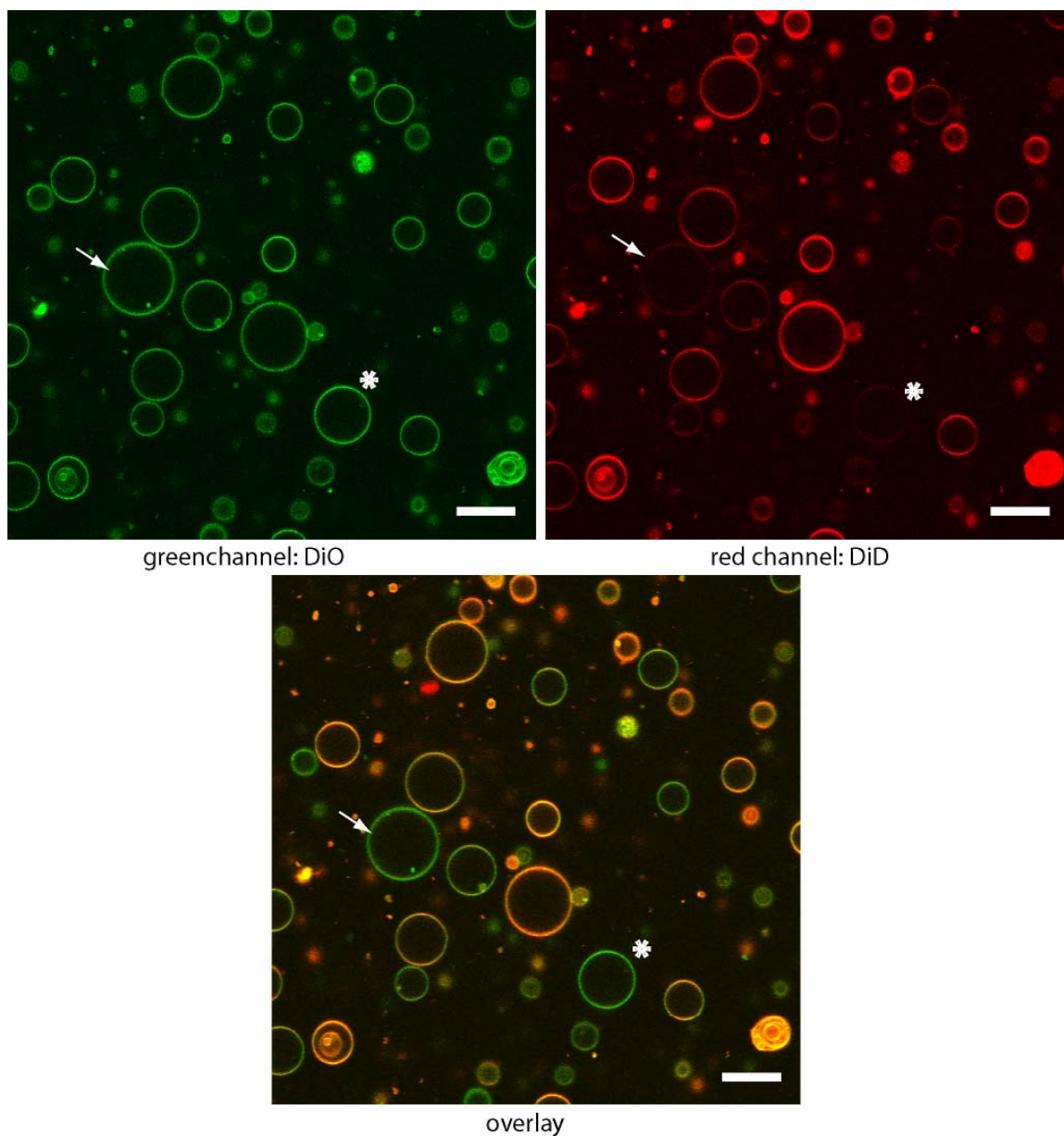
Figure 2-5. Heterogeneity of lipid distribution among the GUV prepared by the electroformation method. GUVs with prominent heterogeneity of lipid distribution are indicated with an arrow and an asterisk. Scale Bar 20 μm.

Figure 2-5, where lipidic dyes DiO and DiD are unevenly redistribute among the GUVs. Another example of heterogeneous lipid distribution is illustrated by the simultaneous formation of unilamellar and multilamellar giant vesicles, electroformed from a lipid

mixture of DOPC:cardiolipin (80:20 mol %) (Fig. 2-4d). This effect will be discussed in greater detail in Chapter 5 of this dissertation.

Lipid bilayers

Lipid bilayers are another example of an *in vitro* system which can be used to study the mechanism of Bax pore formation. Based on the preparation method, lipid bilayers can be divided into supported lipid bilayers (SLBs), which are prepared on a mica surface, and free-standing lipid bilayers which are mostly used in electrophysiology. SLBs can be further subdivided into dry and hydrated lipid bilayers. All three types of lipid bilayers have been used to study the mechanism of Bax pore formation. For example, hydrated SLBs have been used to study by AFM the effect of full length Bax protein and the pore-forming helices of Bax (helices 5 and 6) on hydrated SLB[52, 53] while dry SLBs were used in neutron-scattering experiments to determine whether the pore-forming helix of Bax (helix 5) forms toroidal or barrel-staved type pores[54]. The result of the latter study showed that helix 5 of Bax forms toroidal pores in lipid membranes. Use of free-standing lipid bilayers in the electrophysiology experiments allowed conductance measurements to be performed on Bax pores. It was shown that Bax pores are non selective and can have a variety of diameters[18, 21, 55, 56]. In addition, using free standing lipid bilayers, Basanez *et al.* have shown that upon insertion into the lipid bilayer, Bax reduces the line tension in the bilayer[55], which was further confirmed by Garcia-Saez *et al*. in a study using AFM on a hydrated SLB exposed to the pore forming helix 5 of Bax[57]. These line tension studies together with the measurements presented in Chapter 6 of this dissertation suggest the ability of Bax to stabilize a lipid edge, and provide further

support for the hypothesis that Bax forms lipid stabilized toroidal pores in lipid membranes.

We have also attempted to use hydrated SLBs to study the diffusion and oligomerization of Bax in lipid membranes using FCS (Fig. 2-6). However, because of the hindrance of lipid diffusion in SLBs due to mica-lipid bilayer interaction we reasoned that free-standing bilayers where lipid diffusion in not hindered by the interaction with mica would provide a better model system for studies of the in-membrane diffusion of Bax. Therefore, we have used GUVs as a source of free-standing lipid bilayers in the FCS studies on Bax (Chapter 5).

| BaxΔC | lipidic dye DiD | overlay |
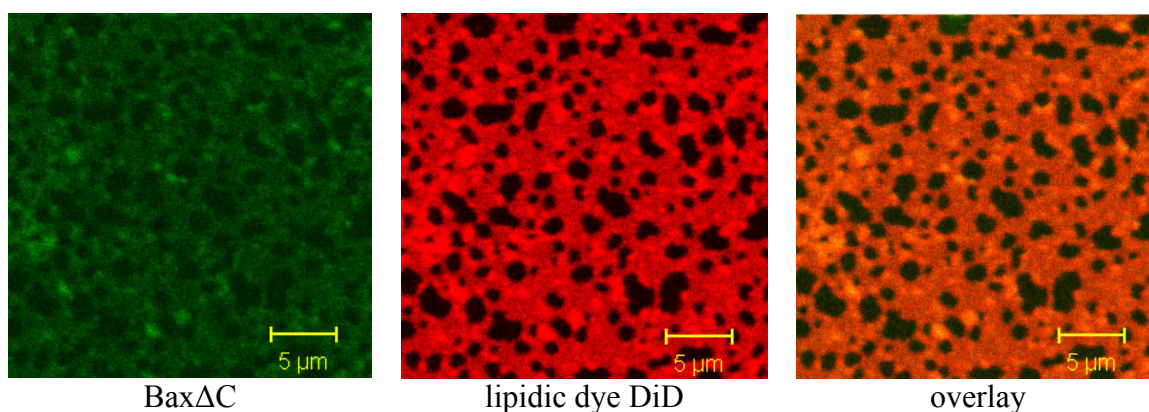
Figure 2-6. Bax binding to a supported lipid bilayer. Lipid bilayer was prepared from a lipid mixture of DOPC:Sphingomeyelin:Cholesterol = 2:2:1 mol%. BaxΔC labeled with Bodipy FL was used in these experiments. Scale bar is 5µm.

Previous studies of Bax in lipid bilayers have shown that this model *in vitro* system is instrumental in the study of the mechanism of Bax pore formation. However, the limited number of studies utilizing this system to study Bax shows that this model system is under-exploited. One of the potential uses of this model system can be combining it with the use of total internal reflection (TIRF) microscopy. Use of hydrated

SLBs in combination with single-molecule TIRF microscopy can be employed to study the sequence of interactions among the Bax and other Bcl-2 family proteins leading to or preventing pore formation by Bax.

Other *in vitro* systems

A description of model *in vitro* systems used to study Bax would not be complete without mentioning a less commonly used model such as lipid monolayers and lipid bicelles. Lipid monolayers have been used to study binding and incorporation of Bax and tBid[58] (Fig. 2-7 a) where it has been shown that upon binding tBid increases pressure in lipid monolayers 12 times higher than the pressure produced by Bax, indicating that tBid has higher binding affinity to lipid membranes than Bax. The results of this study have been recently corroborated by the kinetic measurements of the fluorescent Bax and tBid insertion into lipid membranes[23].

Lipid bicelles present another possible model *in vitro* system for studying the structure of active Bax. Lipid bicelles are discoidal lipid aggregates formed from long-chain phospholipids and either detergents or short-chain phospholipids(Fig. 2-7 b). Bicelles are
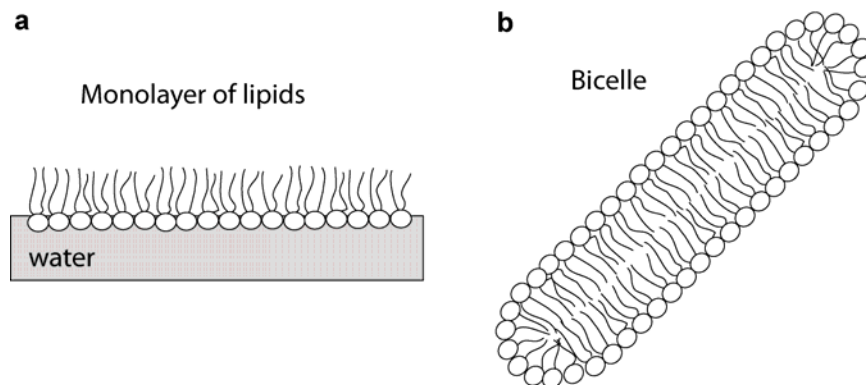
Figure 2-7. Schematic representation of a lipid monolayer and a bicelle.

most commonly used in NMR to study the structure-function relationship of membrane associated and membrane-integrated proteins[59, 60]. Therefore, they can be used to determine the structure of Bax in lipid membranes.

References

1. Hockenbery, D., Nunez, G., Milliman, C., Schreiber, R. D. & Korsmeyer, S. J. Bcl-2 is an inner mitochondrial membrane protein that blocks programmed cell death. Nature 348, 334-6 (1990).

2. Akao, Y., Otsuki, Y., Kataoka, S., Ito, Y. & Tsujimoto, Y. Multiple subcellular localization of bcl-2: detection in nuclear outer membrane, endoplasmic reticulum membrane, and mitochondrial membranes. Cancer Res 54, 2468-71 (1994).

3. Krajewski, S. et al. Investigation of the subcellular distribution of the bcl-2 oncoprotein: residence in the nuclear envelope, endoplasmic reticulum, and outer mitochondrial membranes. Cancer Res 53, 4701-14 (1993).

4. Hsu, Y. T. & Youle, R. J. Nonionic detergents induce dimerization among members of the Bcl-2 family. J Biol Chem 272, 13829-34 (1997).

5. Hsu, Y. T. & Youle, R. J. Bax in murine thymus is a soluble monomeric protein that displays differential detergent-induced conformations. J Biol Chem 273, 10777-83 (1998).

6. Antonsson, B., Montessuit, S., Lauper, S., Eskes, R. & Martinou, J. C. Bax oligomerization is required for channel-forming activity in liposomes and to trigger cytochrome c release from mitochondria. Biochem J 345 Pt 2, 271-8 (2000).

7. Terrones, O. et al. Lipidic pore formation by the concerted action of proapoptotic BAX and tBID. J Biol Chem 279, 30081-91 (2004).

8. Basanez, G. et al. Bax-type apoptotic proteins porate pure lipid bilayers through a mechanism sensitive to intrinsic monolayer curvature. J Biol Chem 277, 49360-5 (2002).

9. Schlesinger, P. H. & Saito, M. The Bax pore in liposomes, Biophysics. Cell Death Differ 13, 1403-8 (2006).

10. Christenson, E., Merlin, S., Saito, M. & Schlesinger, P. Cholesterol effects on BAX pore activation. J Mol Biol 381, 1168-83 (2008).

11. Ivashyna, O. et al. Detergent activated BAX protein is a monomer. J Biol Chem 284, 23935-46 (2009).

12. Ganesan, V. et al. Ceramide and activated Bax act synergistically to permeabilize the mitochondrial outer membrane. Apoptosis 15, 553-62.

13. Kuwana, T. et al. Bid, Bax, and lipids cooperate to form supramolecular openings in the outer mitochondrial membrane. Cell 111, 331-42 (2002).

14. le Maire, M., Champeil, P. & Moller, J. V. Interaction of membrane proteins and lipids with solubilizing detergents. Biochim Biophys Acta 1508, 86-111 (2000).

15. Linke, D. Detergents: an overview. Methods Enzymol 463, 603-17 (2009).

16. Soft Matter Physics (ed. Daoud, M., Williams, C.E.) (Springer, Berlin, 1999).

17. Antonsson, B., Montessuit, S., Sanchez, B. & Martinou, J. C. Bax is present as a high molecular weight oligomer/complex in the mitochondrial membrane of apoptotic cells. J Biol Chem 276, 11615-23 (2001).

18. Dejean, L. M., Martinez-Caballero, S., Manon, S. & Kinnally, K. W. Regulation of the mitochondrial apoptosis-induced channel, MAC, by BCL-2 family proteins. Biochim Biophys Acta 1762, 191-201 (2006).

19. Suzuki, M., Youle, R. J. & Tjandra, N. Structure of Bax: coregulation of dimer formation and intracellular localization. Cell 103, 645-54 (2000).

20. Saito, M., Korsmeyer, S. J. & Schlesinger, P. H. BAX-dependent transport of cytochrome c reconstituted in pure liposomes. Nat Cell Biol 2, 553-5 (2000).

21. Schlesinger, P. H. et al. Comparison of the ion channel characteristics of proapoptotic BAX and antiapoptotic BCL-2. Proc Natl Acad Sci U S A 94, 11357-62 (1997).

22. Terrones, O. et al. BIM and tBID are not mechanistically equivalent when assisting BAX to permeabilize bilayer membranes. J Biol Chem 283, 7790-803 (2008).

23. Lovell, J. F. et al. Membrane binding by tBid initiates an ordered series of events culminating in membrane permeabilization by Bax. Cell 135, 1074-84 (2008).

24. Schafer, B. et al. Mitochondrial outer membrane proteins assist Bid in Bax-mediated lipidic pore formation. Mol Biol Cell 20, 2276-85 (2009).

25. Billen, L. P., Kokoski, C. L., Lovell, J. F., Leber, B. & Andrews, D. W. Bcl-XL inhibits membrane permeabilization by competing with Bax. PLoS Biol 6, e147 (2008).

26. Epand, R. F., Martinou, J. C., Montessuit, S. & Epand, R. M. Transbilayer lipid diffusion promoted by Bax: implications for apoptosis. Biochemistry 42, 14576-82 (2003).

27.   Yethon, J. A., Epand, R. F., Leber, B., Epand, R. M. & Andrews, D. W. Interaction with a membrane surface triggers a reversible conformational change in Bax normally associated with induction of apoptosis. J Biol Chem 278, 48935-41 (2003).

28.   Collins, T. J., Berridge, M. J., Lipp, P. & Bootman, M. D. Mitochondria are morphologically and functionally heterogeneous within cells. Embo J 21, 1616-27 (2002).

29.   Ardail, D. et al. Mitochondrial contact sites. Lipid composition and dynamics. J Biol Chem 265, 18797-802 (1990).

30.   Smirnov, A. A. Liposome preparation by a reverse-phase evaporation method and freezing-thawing. Biull Eksp Biol Med 98, 249-52 (1984).

31.   Skoza, F. & Papahadjopoulos, D. Procedure for preparation of liposomes with large internal aqueous spacce and high capture by reverse-phase evaporation. PNAS 75, 4194-4198 (1978).

32.   Betageri, G. V., Jenkins, S. A., and Parsons, D. J.,. Liposome drug delivery systems. Basel: Technomic Publishing Co. Inc. (1993).

33.   Vemuri, S. & Rhodes, C. T. Preparation and characterization of liposomes as therapeutic delivery systems: a review. Pharm Acta Helv 70, 95-111 (1995).

34.   Soman, N. R. et al. Molecularly targeted nanocarriers deliver the cytolytic peptide melittin specifically to tumor cells in mice, reducing tumor growth. J Clin Invest 119, 2830-42 (2009).

35.   Garcia-Saez, A. J., Ries, J., Orzaez, M., Perez-Paya, E. & Schwille, P. Membrane promotes tBID interaction with BCL(XL). Nat Struct Mol Biol 16, 1178-85 (2009).

36.   Garcia-Saez, A. J. & Schwille, P. Single molecule techniques for the study of membrane proteins. Appl Microbiol Biotechnol 76, 257-66 (2007).

37.   Garcia-Saez, A. J. & Schwille, P. Fluorescence correlation spectroscopy for the study of membrane dynamics and protein/lipid interactions. Methods 46, 116-22 (2008).

38.   Ries, J. & Schwille, P. Studying slow membrane dynamics with continuous wave scanning fluorescence correlation spectroscopy. Biophys J 91, 1915-24 (2006).

39.   Kahya, N., Brown, D. A. & Schwille, P. Raft partitioning and dynamic behavior of human placental alkaline phosphatase in giant unilamellar vesicles. Biochemistry 44, 7479-89 (2005).

40. Schon, P. et al. Equinatoxin II permeabilizing activity depends on the presence of sphingomyelin and lipid phase coexistence. Biophys J 95, 691-8 (2008).

41. Osawa, M., Anderson, D. E. & Erickson, H. P. Reconstitution of contractile FtsZ rings in liposomes. Science 320, 792-4 (2008).

42. Osawa, M., Anderson, D. E. & Erickson, H. P. Curved FtsZ protofilaments generate bending forces on liposome membranes. Embo J 28, 3476-84 (2009).

43. Angelova, M. I. & Dimitrov, S. D. Liposome electroformation. Faraday Discuss. Chem. Soc. 81, 303-311 (1986).

44. Reeves, J. P. & Dowben, R. M. Formation and properties of thin-walled phospholipid vesicles. J Cell Physiol 73, 49-60 (1969).

45. Akashi, K., Miyata, H., Itoh, H. & Kinosita, K., Jr. Preparation of giant liposomes in physiological conditions and their characterization under an optical microscope. Biophys J 71, 3242-50 (1996).

46. Kim, S., Martin, G.M. Preparation of cell-size unilamellar liposomes with high captured volume and defined size distribution. BBA, 1-9 (1981).

47. Girard, P. et al. A new method for the reconstitution of membrane proteins into giant unilamellar vesicles. Biophys J 87, 419-29 (2004).

48. Mathivet, L., Cribier, S. & Devaux, P. F. Shape change and physical properties of giant phospholipid vesicles prepared in the presence of an AC electric field. Biophys J 70, 1112-21 (1996).

49. Pott, T., Bouvrais, H. & Meleard, P. Giant unilamellar vesicle formation under physiologically relevant conditions. Chem Phys Lipids 154, 115-9 (2008).

50. Montes, L. R., Alonso, A., Goni, F. M. & Bagatolli, L. A. Giant unilamellar vesicles electroformed from native membranes and organic lipid mixtures under physiological conditions. Biophys J 93, 3548-54 (2007).

51. Morales-Penningston, N. F. et al. GUV preparation and imaging: Minimizing artifacts. Biochim Biophys Acta.

52. Epand, R. F., Martinou, J. C., Montessuit, S., Epand, R. M. & Yip, C. M. Direct evidence for membrane pore formation by the apoptotic protein Bax. Biochem Biophys Res Commun 298, 744-9 (2002).

53.   Garcia-Saez, A. J., Chiantia, S., Salgado, J. & Schwille, P. Pore formation by a Bax-derived peptide: effect on the line tension of the membrane probed by AFM. Biophys J 93, 103-12 (2007).

54.   Qian, S., Wang, W., Yang, L. & Huang, H. W. Structure of transmembrane pore induced by Bax-derived peptide: evidence for lipidic pores. PNAS 105, 17379-83 (2008).

55.   Basanez, G. et al. Bax, but not Bcl-xL, decreases the lifetime of planar phospholipid bilayer membranes at subnanomolar concentrations. Proc Natl Acad Sci U S A 96, 5492-7 (1999).

56.   Martinez-Caballero, S. et al. Assembly of the mitochondrial apoptosis-induced channel, MAC. J Biol Chem 284, 12235-45 (2009).

57.   Garcia-Saez, A. J., Chiantia, S. & Schwille, P. Effect of line tension on the lateral organization of lipid membranes. J Biol Chem 282, 33537-44 (2007).

58.   Van Mau, N., Kajava, A. V., Bonfils, C., Martinou, J. C. & Harricane, M. C. Interactions of Bax and tBid with lipid monolayers. J Membr Biol 207, 1-9 (2005).

59.   Whiles, J. A., Deems, R., Vold, R. R. & Dennis, E. A. Bicelles in structure-function studies of membrane-associated proteins. Bioorg Chem. 30, 431 42 (2002).

60.   Diller, A. et al. Bicelles: A natural 'molecular goniometer' for structural, dynamical and. Biochimie. 91, 744-46 (2009).

CHAPTER 3

"Techniques to Study Pore Formation in Lipid Membranes

by Protein Bax"

This Chapter provides an overview of single-molecule sensitivity fluorescence techniques and the description of liposome permeability assay, which was used to asses the functionality of all proteins used in the experiments described in this dissertation.

Single-Molecule Sensitivity Fluorescence Techniques

Single-molecule sensitivity fluorescence techniques provide a powerful non-invasive tool to study biological processes *in vivo* and *in vitro* and have been used extensively in a number of experiments described in this dissertation. The following section provides a background on the physical basis of fluorescence and the background of the three single-molecule sensitivity fluorescence techniques: fluorescence correlation spectroscopy (FCS)[1], fluorescence cross-correlation spectroscopy (FCCS)[2], and fluorescence intensity distribution analysis (FIDA)[3].

Physical principles of fluorescence

Luminescence is a physical process of the emission of a photon by a molecule during the transition between the electronic energy states[4, 5]. Depending on the nature of the excited electronic energy states between which the transition occurs, luminescence is divided into two categories – fluorescence and phosphorescence. Fluorescence occurs during the transition from a singlet energy states to the ground state (for example, $S_1 \rightarrow S_0$), while phosphorescence occurs during the transition from a triplet state to the ground state (for example, $T_1 \rightarrow S_0$). The electron in a triplet state has the same spin orientation as the electron in the ground state, and therefore, according to the principles of quantum mechanics transitions between these energy states are forbidden; however, they do occur but with lower probability. Based on the low probability of the $T_1 \rightarrow S_0$

transition, the lifetime of an electron in the triplet state, T_1, is longer than its life time in the excited singlet state, S_1, and therefore, the lifetime of a fluorescence process is generally on the order of 10^{-9} seconds, while the lifetime of a phosphorescence is on the order of 10^{-6} seconds.

The electronic energy states and the transitions among them can be summarized by the Jablonski diagram (Fig. 3-1). On this diagram the excited electronic energy states and the ground state are shown with thick horizontal lines, while the vibrational energy states of each energy state are shown with thinner horizontal lines. According to this diagram, in the absence of excitation the molecule is in the ground electronic energy state, S_0. Upon absorption of a photon with the energy of $h\nu_A$, the molecule is excited into the higher electronic energy state S_1 or S_2. Transition between the energy states is shown by vertical lines. Once in the S_2 state, the molecule rapidly relaxes to the lowest vibrational level of S_1 via internal conversion mechanism. Next, molecule transitions to the ground energy state by emitting a photon with the energy of $h\nu_F$ or by transfering energy via a non-radiative pathway (for example, collision with other molecules). Alternatively, molecules in the S_1 energy state can undergo an intersystem crossing to the triplet state T_1. Such transitions are forbidden by the principles of quantum mechanics but do occur with a low probability. Once in the T_1 state, a molecule undergoes $T_1 \rightarrow S_0$ transition by emitting a photon with energy $h\nu_P$ or by the mechanism of non-radiative energy transfer.

Excitation into higher vibrational energy states followed by the decay into various vibrational ground states results in the lower energy of emitted fluorescence photons than the energy of the adsorbed photon. The difference in the energy of adsorbed and emitted
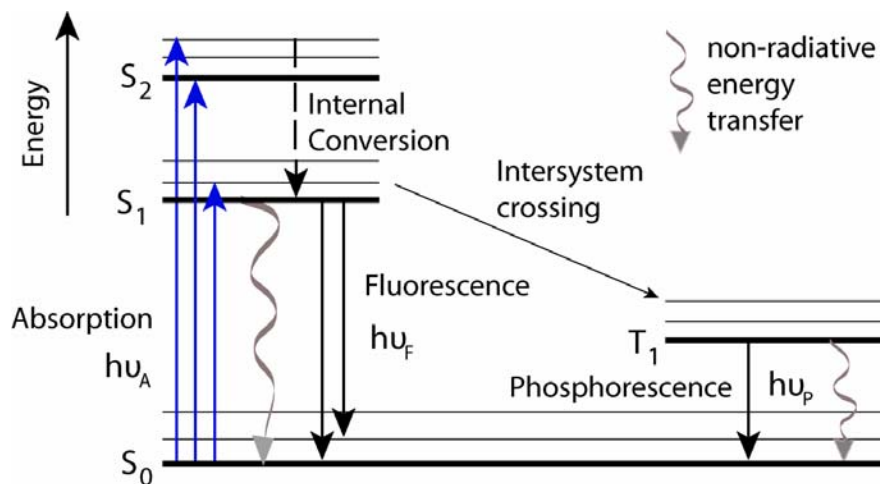
Figure 3-1. Jablonski diagram of the electronic energy states of a molecule.
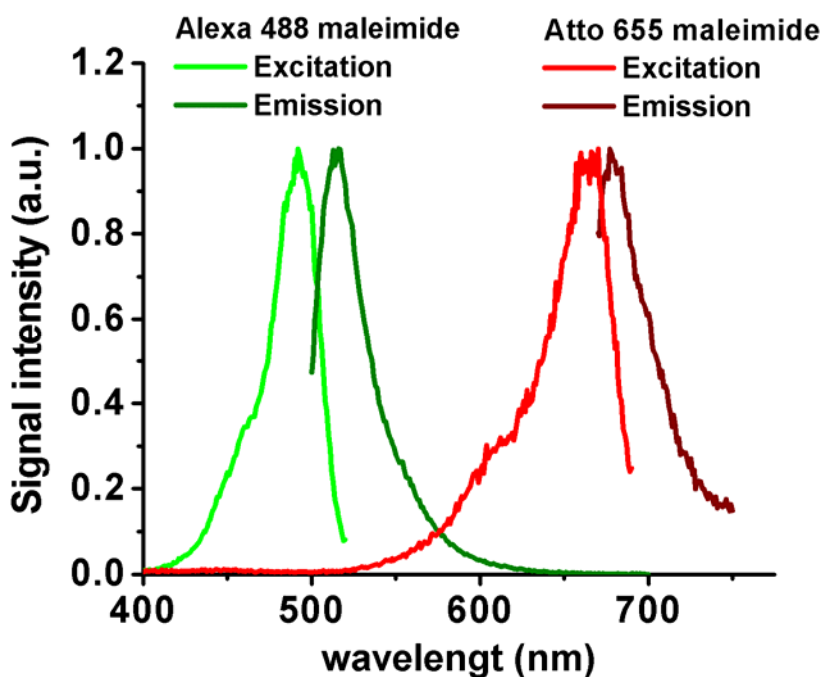
Figure 3-2. Excitation and emission spectra for two fluorophores: Alexa Fluor 488 maleimide and Atto 655 maleimide. These excitation and emission spectra illustrate the phenomenon of a Stokes' shift.

photons is translated into respectively shorter and longer wavelength of the adsorbed and emitted photons which is also known as a Stokes' shift, and is used to separate the excitation photons from the emission photons in the FCS experiments with the use of dichroic mirrors and filters (Fig. 3-2).

Fluorophores

Fluorophores, or fluorescent dyes, are molecules which can emit fluorescent light when excited[4-6]. The major characteristics of fluorophores include excitation and emission spectra, extinction coefficient, quantum yield, singlet-to-triplet quantum yield and photobleaching. Excitation and emission spectra of a fluorophore define the excitation wavelength of a laser and the combination of a dichroic mirror and filters in the FCS experiment (Fig. 3-2). Extinction coefficient defines the efficiency of the fluorophore molecules to absorb excitation light, while the quantum yield of a fluorophore is defined as a ratio of the number of emitted photons per unit of time to the number of absorbed photons. Alternatively, the quantum yield of a fluorophore is defined as

$$\varphi = \frac{k_r}{k_r + k_{nr}}$$
(Eqn. 1)

where, k_r is the rate of radiative energy transfer defined as the transition rate of singlet to the ground state, and k_{nr} is the rate of all non-radiative de-excitation processes.

Photobleaching of a fluorophore is a process of irreversible destruction of a fluorophore. For each fluorophore type there is a characteristic number of photons emitted before the dye undergoes photobleaching. For example, Alexa Fluor 488 is more

photostable than carboxyfluorescein, while both of these fluorophores have identical excitation and emission spectra. Photobleaching in the FCS experiment can be controlled by the illumination levels[7, 8].

For use in FCS experiments fluorophores should have high extinction coefficient, high fluorescence quantum yield, low singlet-to-triplet quantum yield and low photobleaching[7, 8]. However, the majority of biological molecules do not posses such fluorescence properties (GFP would be an exception from this statement). Therefore, in order to study the biological molecules, a number of synthetic fluorophores were developed. These fluorophores are bright and photostable and have engineered reactive groups which allow for their attachment to the biological molecules of interest. In case of Bax we used maleimide reactive group which forms a covalent bond with an engineered cysteine. Examples of chemical structure for some synthetic FCS-compatible fluorophores used in the experiments presented in this dissertation are shown in Figure 3-3. Depending on the chemical structure fluorophores can be used in a variety of applications. For example, small dyes like Alexa Fluor 488, Atto 655 and Bodipy FL can be used to label proteins and nucleic acids, while lipophilic dyes like DiO and DiD are used to visualize lipid membranes.

Alexa Fluor 488 c$_5$ maleimide

Atto 655

BODIPY® FL *N*-(2-aminoethyl)maleimide

DiO

DiD
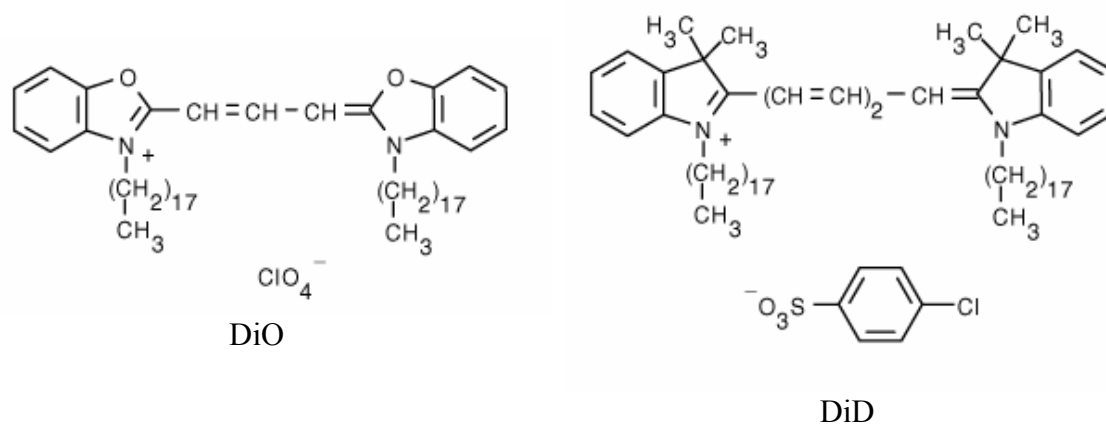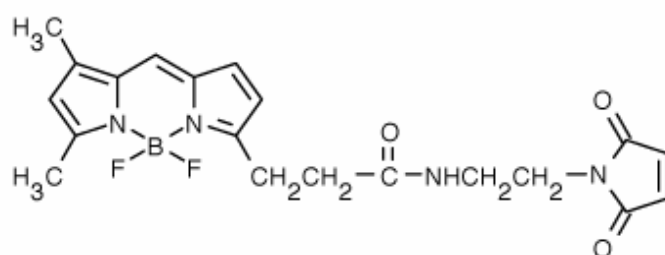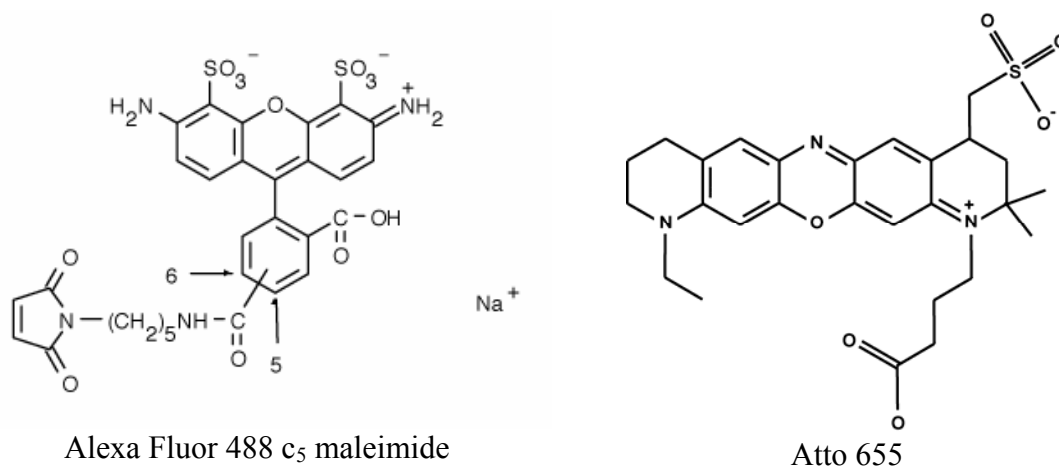
Figure 3-3. Chemical structures for selected FCS-compatible fluorophores. All of these fluorophores were used in the experiments described in Chapters 7 through 7.

FCS and autocorrelation analysis

Fluorescence correlation spectroscopy (FCS)[1] is a single-molecule sensitivity technique uniquely suited for study of biological processes in the 3D space of solution[1, 7, 9-14], in the 2D space of a lipid membrane[15-22], or in 1D space, in the case of the directed flow of fluorophores[8]. It is based on detecting fluorescence intensity fluctuations within a small observation volume (<1 fl) which is achieved by the use of a confocal microscope (Fig. 3-4). Temporal analysis of these fluorescence intensity fluctuations allows determination of the concentration and diffusion coefficients of the fluorophores passing through the observation volume.

Development of FCS: historic prospective

The theoretical basis of FCS has been developed by Madge D., Elson E. and Webb W.W. in 1972[23]. However, due to technical limitations, it did not gain wide use until two decades later; when in 1993, Rigler *et al* implemented FCS in the scheme of a confocal microscope and showed a number of implementation of the technique in biochemistry and biology[9, 24-28]. Since then, FCS has seen a renaissance in its development based on the number of its various implementations such as fluorescence cross-correlation spectroscopy[2, 12, 29], photon-counting histogram (PCH) also known as fluorescence intensity distribution analysis (FIDA)[3, 30-32], high-order correlation FCS (HO-FCS)[33-36], image-correlation spectroscopy[37-40], total internal reflection FCS (TIR-FCS)[41], stimulated emission depletion FCS (STED-FCS)[42-44], FCS with UV fluorophores (UV-FCS)[26, 45], implementation of the FCS *in vivo*[12, 14, 17, 18, 46-49], two-photon FCS[50, 51],

supercritical angle FCS[52], multiple variation of scanning FCS[17, 53-58], FCS in lipid membranes[19-21, 32, 55, 56, 59-62] etc.

The auto-correlation function

In a generic FCS experiment, excitation light from a laser is focused into a small volume (also known as observation volume) in a solution sample with the use of a dichroic mirror and a high numerical aperture objective (Fig. 3-4 a). Here, for the sake of simple explanation, we assume that the sample consists of a dilute solution of freely diffusing non-interacting fluorophores (Fig. 3-4 b). Each time a fluorophore passes through the observation volume, it is excited and emits fluorescence, a portion of which is collected by the objective and directed through the dichroic mirror and a filter to a pinhole positioned in front of the avalanche photo diode (APD) used as a highly sensitive detector in the FCS setup. Pinhole does not allow photons generated outside the observation volume to reach the APD, thus only the photons generated by the fluorophores present in the observation volume are registered and give rise to the fluorescence intensity fluctuations trace $F(t)$ (Fig. 3-4 c). From this intensity trace, the autocorrelation function can be calculated as[1, 8]

$$G(\tau) = \frac{\langle F(t) \cdot F(t+\tau) \rangle}{\langle F(t) \rangle^2} = 1 + \frac{\langle \delta F(t) \cdot \delta F(t+\tau) \rangle}{\langle F(t) \rangle^2} \qquad \text{(Eqn. 2)}$$

where G is the autocorrelation function, F is the fluorescence intensity as a function of time, τ is the correlation time (also known as the "lag time") and the angular brackets refer to time averaging, while $\delta F(t) = F(t) - \langle F(t) \rangle$ and $\langle F(t) \rangle = \frac{1}{T}\int_0^T F(t)dt$.
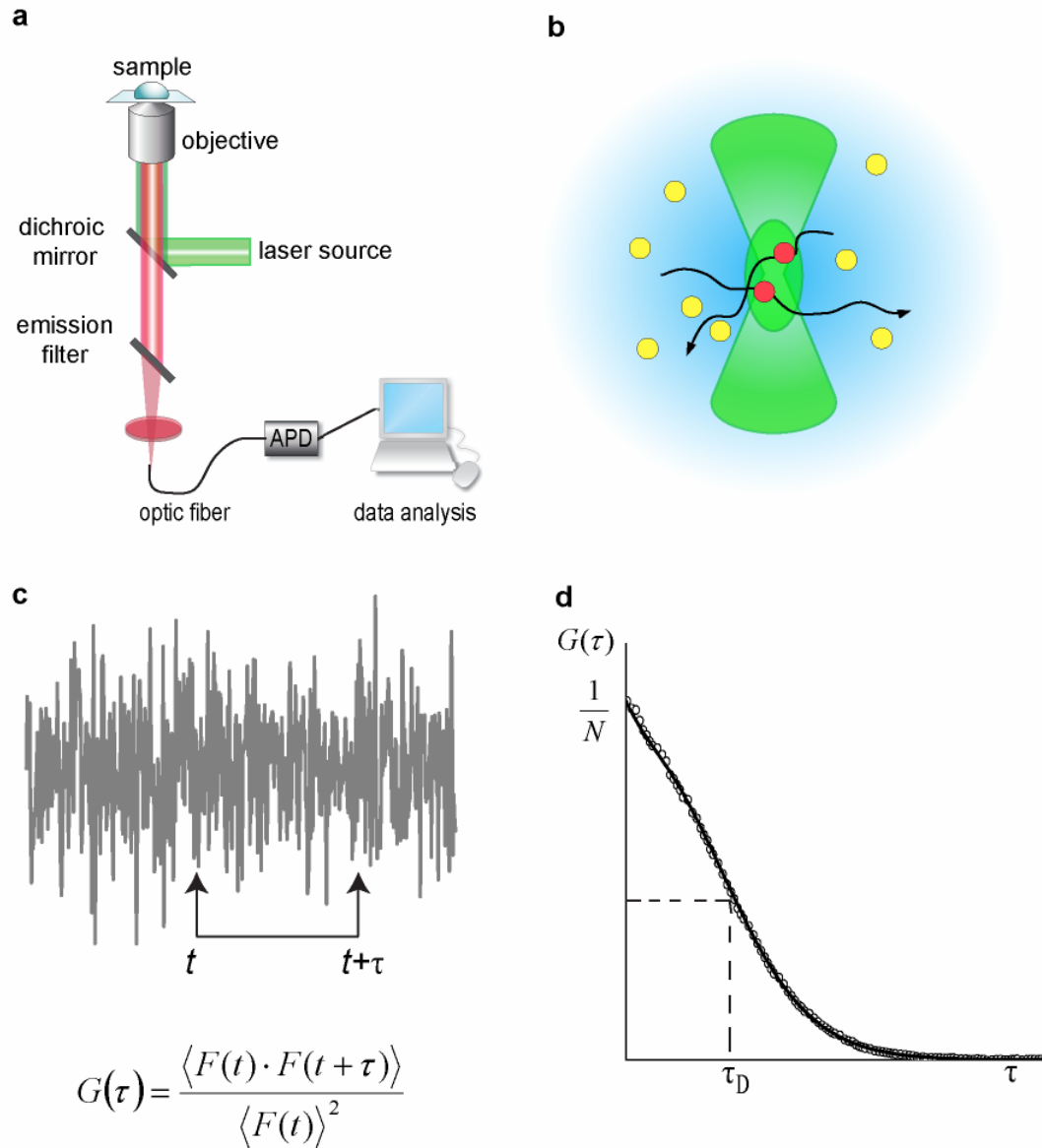
Figure 3-4. Principles of FCS. a. Schematic of the FCS setup. **b.** schematic representation of the FCS observation volume. **c.** Time trace of the fluorescence intensity fluctuations is used to calculate the auto-correlation curve, which measures the self-similarity of the signal. **d.** Fitting of the experimental auto-correlation curve allows determination of the parameters of interest such as diffusion coefficient and the number of fluorescent particles in the observation volume. See next section for the description of selected the fitting correlation functions.

The auto-correlation function measures the self similarity of the fluorescence signal with time by comparing the signal at time t with the signal at time $t + \tau$ (the product carries out this comparison) and averaging over all times (Fig. 3-4 c). During the short lag times τ the fluorophore has not moved out from the observation volume and signal intensity would not change much, thus resulting in high value of the auto-correlation function. For the longer lag times τ the fluorophore would move out from the observation volume resulting in a significance change in the signal intensity and low values for autocorrelation function which decay to zero at long lag times.

The auto-correlation function is characterized by the two major parameters: the diffusion time τ_D and the height of the curve, $G(0)$ (Fig. 3-4 d). The diffusion time τ_D represents the average time the fluorophore spends in the observation volume and is connected to the diffusion coefficient, D, of the fluorophore

$$\tau_D = \omega_{xy}^{\;2} / 4D \qquad \text{(Eqn. 3)}$$

where ω_{xy} is the waist of the observation volume. The heights of the auto-correlation curve, $G(0)$, is proportional to the average number of particles in the observation volume. If we set $\tau = 0$ in the equation 2 and assume the fluorescence intensity to be proportional to the number of particles N in the observation volume, then we find

$$G(0) = \frac{\left\langle \delta F^2 \right\rangle}{\left\langle F \right\rangle^2} = \frac{\left\langle \delta N^2 \right\rangle}{\left\langle N \right\rangle^2} = \frac{1}{N} \qquad \text{(Eqn. 4)}$$

because the number of particles in the observation volume follows a Poisson distribution.

The fluctuations of the fluorescence intensity in the observation volume arise not only due to the Brownian diffusion of fluorophores through the volume, but also due to photophysical fluctuations, internal dynamics, rotation of fluorophores and

photobleaching which lead to the variation in excitation probabilities. Additionally, fluctuations in the excitation power or detection geometry can result in an unwanted change of the fluorescence intensity and thus lead to the distortion of the auto-correlation curve. Therefore, additional controls should be used to account for these possible sources of fluorescence fluctuations.

Once the correlation curve is obtained, it is fitted with a mathematical function which models the fluorescence intensity fluctuations in the observation volume according to the characteristics of the system under study (for example, 3D versus 2D diffusion). IN the fitting function some of the fitting parameters are the concentration of particles and their diffusion coefficient.

Fitting correlation functions

In order to extract meaningful information about the system under study the experimental auto-correlation function needs to be fitted to the fitting correlation function which is derived from the fundamental physical principles. In the case of the Brownian diffusion of a fluorophore in a 3D space the fitting correlation function is defines as

$$G_{3D}(\tau) = \frac{1}{N}\left(1 + \frac{\tau}{\tau_D}\right)^{-1}\left(1 + \frac{\tau}{\tau_D \cdot S^2}\right)^{-1/2}$$

(Eqn. 5)

where N is the average number of fluorescent particles in the observation volume, $N = C\pi^{3/2}\omega_0 S$, C is the concentration of fluorophores and ω_{xy} is the waist radius of the laser focus. The structural parameter $S = \omega_z / \omega_{xy}$ measures the aspect ratio of observation volume which is assumed to have Gaussian shape. Detailed derivation of the Equation 5

can be found in references 1 and 3. However, it is important to point out that this equation was derived using the diffusion equation describing free Brownian diffusion:

$$\frac{\partial C(\vec{r},t)}{\partial t} = D\nabla^2 C(\vec{r},t) \qquad \text{(Eqn. 6)}$$

where $C(\vec{r},t)$ is the concentration of the fluorophores at various positions $\vec{r}$ inside the observation volume at a time point t.

Additionally, equation 5 should take into account the photodynamic state of a fluorophore while it is present in the observation volume, since the timescale of these photodynamic changes is comparable to the diffusion time of a fluorophore. For example, the diffusion time τ_D of the Alexa Fluor 488 is aqueous solution is 30±5 μsec, while the triplet time is 4.7±1.9 μsec (mean±s.d., n=3, measured with the Confocor 2 instrument). Therefore, accounting for the triplet-state population (T) of the fluorophore is done by an additional factor:

$$G_{3D+T} = \left[1 + T(1-T)^{-1} \exp\left(\tau \Big/ \tau_T \right) \right] \cdot G_{3D}(\tau) \qquad \text{(Eqn. 7)}$$

where τ_T is the lifetime of the triplet state of the fluorophore and T is the fraction of fluorophores in the triplet state.

In case of FCS measurement in a lipid membrane, a fitting correlation function that models the 2D motion of fluorescently labeled particles in the plane perpendicular to the laser beam path is:

$$G_{2D}(\tau) = \frac{1}{N}\left(1 + \frac{\tau}{\tau_D} \right)^{-1}$$

$$\text{or} \quad G_{2D} = \frac{1}{A_{eff} \cdot C} \left(1 + \frac{\tau}{\tau_D} \right)^{-1} \qquad \text{(Eqn. 8)}$$

where A_{eff} is the lipid membrane area found in the observation volume, C is the concentration of the fluorophores (in molecules per unit area), and τ_D is calculated using equation 3. In many examples of the FCS measurements of lipid and protein diffusion in lipid membranes, the diffusion time τ_D is on the order of milliseconds and is at least two orders of magnitude longer that the triplet time of the fluorophore. Therefore, those cases the contribution of the triplet state of the fluorophore is not considered.

In case of the active transport of molecules though the observation volume with velocity $\vec{v}$ the fitting auto-correlation function is defined as[8, 63]:

$$G_{1D}(\tau) = \frac{1}{N} \cdot \left(1 + \frac{\tau}{\tau_D} \right)^{-1} \cdot \left(1 + \frac{\tau}{S^2 \tau_D} \right)^{-1/2} \cdot$$

$$\exp\left(-\left(\frac{\left(v_x^2 + v_y^2 \right) \cdot \tau^2}{\omega_{xy}^2} \right) \cdot \left(\frac{1}{1 + \frac{\tau}{\tau_D}} \right) - \left(\frac{v_z^2 \cdot \tau^2}{\omega_z^2} \right) \cdot \left(\frac{1}{1 + \frac{\tau}{S^2 \tau_D}} \right) \right) \qquad \text{(Eqn. 9)}$$

FCCS and cross-correlation analysis

FCS is a powerful technique which allows determination of the diffusion coefficients and concentrations of fluorophores. However, in many biochemical and biological processes this information is insufficient, since the fluorescently labeled molecules of interest undergo chemical reactions such as association (or binding). If the two molecules of interest associate and have similar diffusion coefficient (i.e. similar

molecular weight), then FCS would not be able to differentiate between the hetero-dimer and the individual monomer molecules. To solve this problem FCCS was developed[2].

In FCCS experiments the two molecules of interest are labeled with spectrally different fluorophores and excited with overlapping laser beams (Fig.3-5). Example of the FCCS-compatible pair of fluorophores, Alexa Fluor 488 and Atto 655, is shown in Figure 3-2 and 3-3.

In the FCCS experiment the fluorescence fluctuations are detected in two channels with signals $F_g(t)$ and $F_r(t)$ (Fig. 3-5b). If the labeled species interact, they will diffuse as one particle through the observation volume, resulting in simultaneous fluorescence signal in both channels and positive cross-correlation (Fig. 3-5c). The spectral cross-correlation curve is obtained from the cross-correlation analysis of the fluorescence fluctuations in the two channels:

$$G_{rg}(\tau) = \frac{\left\langle \delta F_r(t) \cdot \delta F_g(t+\tau) \right\rangle}{\left\langle F_g(t) \right\rangle \left\langle F_r(t) \right\rangle}$$

(Eqn. 7)

The degree of binding or percentage of cross-correlation ($\%CC$) can be calculated by comparing the amplitude $G(0)$ from the auto- and cross-correlation curves:

$$\%CC = \frac{C_{rg}}{C_{rg} + C_g} = \frac{G_{rg}(0)}{G_r(0)} \qquad \%CC = \frac{C_{rg}}{C_{rg} + C_r} = \frac{G_{rg}(0)}{G_g(0)}$$

and

(Eqn. 8)

Here C_{rg}, C_r and C_g correspond to the concentrations of bound species rg, and the unbound form r and g respectively.
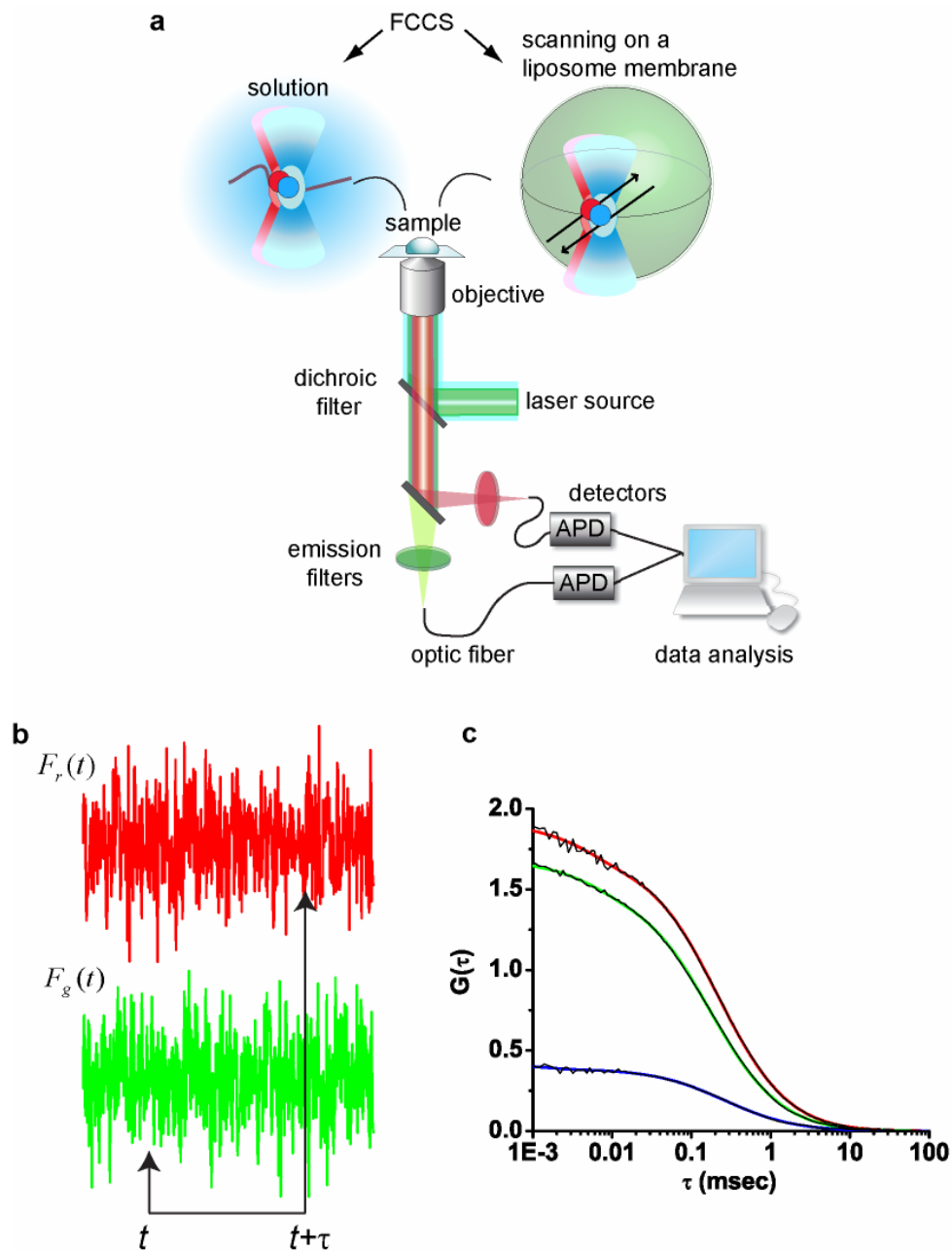
Figure 3-5. Principles of FCCS. a. FCCS setup for measurement in solution and in a lipid membrane of a GUV. **b.** Fluorescence intensity traces for the red and green channels. **c.** Examples for the auto-correlation curves for the red and green channels and the cross-correlation between the two channels (blue line).

FCCS is prone to artifacts and care must be taken to avoid them. The two main artifacts in FCCS measurements are spectral cross-talk, which leads to false-positive cross-correlation, and imperfect overlap between the detection volumes, which leads to decreased cross-correlation[11, 12, 29]. Spectral cross-talk can be corrected by using alternative excitation or alternative pair of fluorophores, while the imperfect overlap between the detection volumes is more difficult to correct. One of the approaches used to account for imperfect overlap between the detection volumes uses measurement of the maximum possible cross-correlation for the instrument (for examples, by using double-labeled DNA) and then correcting all consecutive measurements for the value of this maximum signal.

Two-focus scanning FCCS

Two-focus scanning FCS was developed specifically for the FCS measurement in the lipid membranes of GUVs which tend to undergo multiple undulations (spatial fluctuations) during the time of the measurement (Fig. 3-6). Presence of membrane undulations introduces additional fluctuations in the fluorescence intensity signal which can be incorrectly interpreted as the presence of slowly diffusing molecules[64]. In addition to the possible contribution of membrane undulations to the auto-correlation curve, photobleaching is another problem encountered in FCS in lipid membranes. In a lipid membrane molecules diffuse slower than in solution and thus require longer FCS measurement time which increases the probability of photobleaching. Use of scanning FCS reduces photobleaching during the measurement without shortening the measurement time.
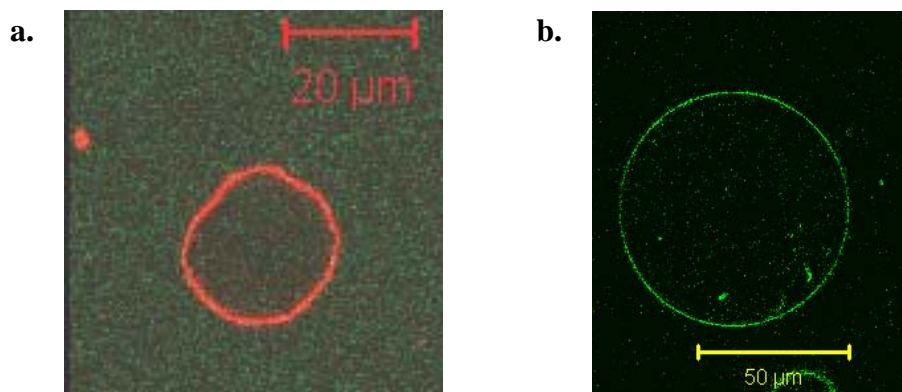
Figure 3-6. Confocal microscopy image of the cross-section of a GUV which **a.** undergoes large membrane undulations due to loss of tension which occurred due to the permeabilization of the GUV by Bax; **b.** tensed GUV which does not have significant membrane undulations.

Before continuing the description of the formalism of the two-focus scanning FCS, it is important to mention the two approaches of performing FCS experiments in GUVs. FCS in GUVs can be done in two spatial positions: at the top or bottom of GUV[20, 47, 61], or in the membrane segment in the equatorial section of a GUV[16, 18, 19, 55] which is used in the two-focus scanning FCS (Fig. 3-7a). In two-focus scanning FCS, the observation volume is scanned perpendicularly through the equatorial section of a GUV along two lines separated by distance d in alternating fashion. Intersection of each scanning line with the GUV membrane creates a detection area on the GUV surface. Scanning of the observation volume is up to 1000 times faster than the diffusion time of a protein or lipid molecule in the lipid membrane, thus allowing sampling of the fluorescent protein or lipid many time before it leaves the observation volume. In addition, scanning of the observation volume through the GUV membrane reduces the photobleaching in the detection each membrane detection area by reducing the residency time of the laser beam
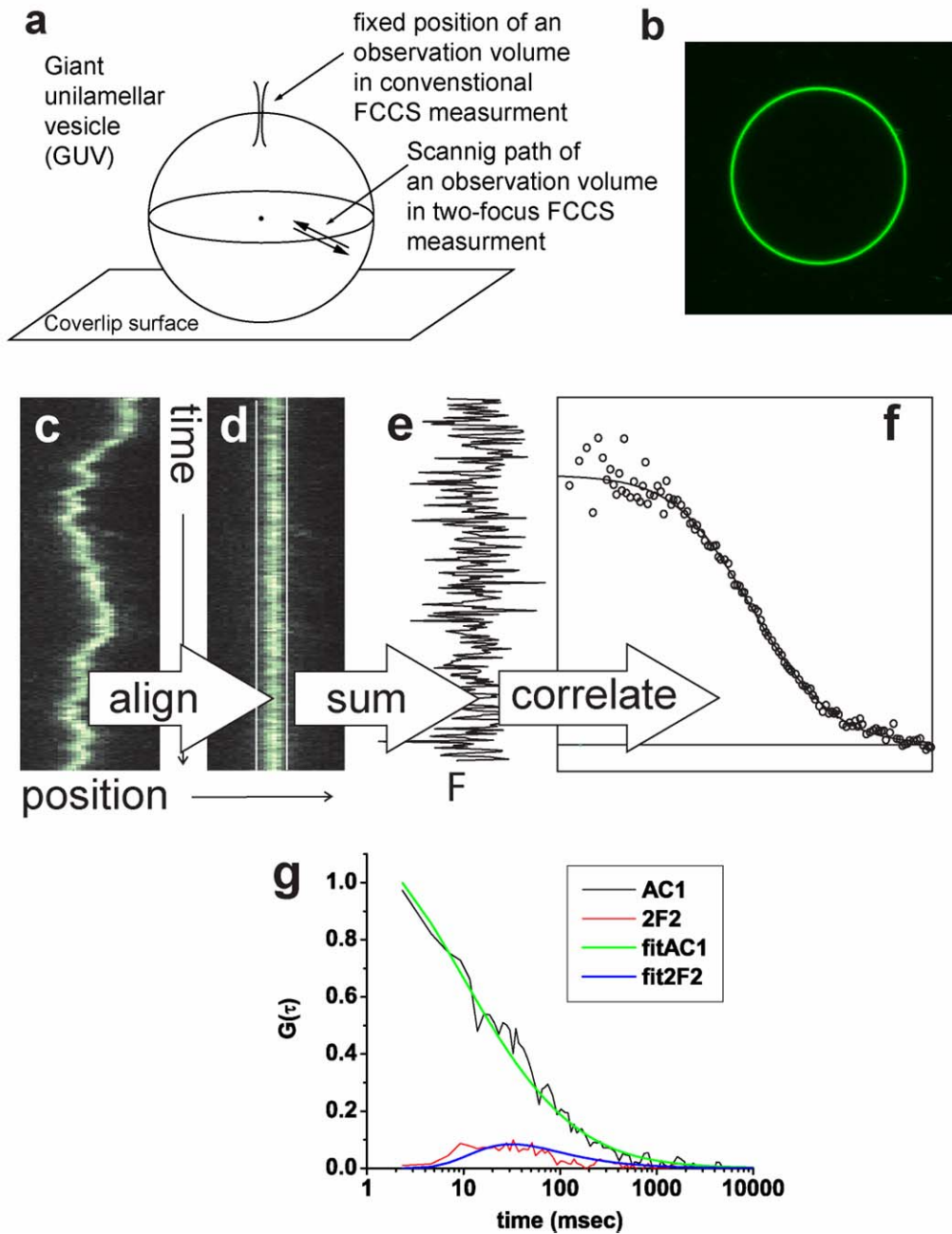
Figure. 3-7. Principles of two-focus scanning FCS. **a.** Schematic of the position of a laser beam with respect to GUV in two types of FCS measurements. **b.** Confocal image of an equatorial cross section of a GUV. **c-f.** Schematic of data analysis in two-focus scanning FCS. **g.** Normalized auto- and cross correlation curve for Bax-G in a lipid membrane measured by two-focus scanning FCS.

65

in the detection areas. Once the scanning is done, a map of change in the fluorescence intensity with time for each of the two detection areas is constructed (Fig. 3-7c) and further processed by software to eliminate the contribution of membrane undulations to the fluorescence intensity trace (Fig. 3-7d). Next, the fluorescence intensity trace for each detection area is auto-correlated and fitted to

$$G(\tau) = \frac{1}{N}\left(1+\frac{\tau}{\tau_D}\right)^{-1/2}\left(1+\frac{\tau}{S^2\tau_D}\right)^{-1/2} \qquad \text{(Eqn. 9)}$$

while the cross-correlation of the fluorescence intensity traces of the detection areas is fitted to

$$G_{cross}(\tau) = \frac{1}{N}\left(1+\frac{\tau}{\tau_D}\right)^{-1/2}\left(1+\frac{\tau}{S^2\tau_D}\right)^{-1/2}\exp\left(-\frac{d^2}{\omega_{xy}^2+4D\tau}\right) \qquad \text{(Eqn. 10)}$$

The cross-correlation curve fitted to this equation shows a maximum at a characteristic lag time, which is the time it takes a fluorophore to move from one detection area to the other. Once the distance between the two detection areas is known, diffusion coefficient D and the structure parameter S can be determined directly by fitting to equation 10. A global fit of the two auto-correlation functions (one for each detection area) and the cross-correlation function improves the accuracy. Example of the auto- and cross-correlation curves obtained by the two-focus scanning FCS is shown in Figure 3-7g.

Due to the alternating data collection between the two foci the resulting cross-correlation curve is shifted by the delay time t_d. If this delay time is comparable to the diffusion time τ_D of the fluorophores, then the shift needs to be taken into account.

66

However, in our two-focus FCS experiments on Bax in GUV membranes the delay time was much smaller than the diffusion time and thus was not taken into account.

Two-color two-focus scanning FCCS

Two-color two-focus scanning FCCS is used to study the formation of in-membrane complexes by molecules labeled with two spectrally different fluorophores (similar to the discussed above FCCS in solution). Data analysis for this technique includes calculation of the auto- and cross-correlation functions for each spectral channel.

In case of perfect overlap between the detection volumes for each spectral channel and negligible cross-talk, the concentrations of the unbound molecules C_r and C_g and of molecules in a complex C_{rg} is calculated from the amplitudes of the correlation functions in following way

$$G_r(0) = \frac{1}{A_{eff}(C_r + C_{rg})}, \qquad G_g(0) = \frac{1}{A_{eff}(C_g + C_{rg})}$$

$$G_{cross}^{rg}(0) = \frac{C_{rg}}{A_{eff}(C_r + C_{rg})(C_g + C_{rg})} \qquad \text{(Eqn. 11)}$$

Fluorescence intensity distribution analysis

Fluorescence intensity distribution analysis (FIDA) is an extension on the FCS technique[3]. While FCS analyzes the temporal characteristics of the fluorescence fluctuations allowing determinations of the concentration and diffusion properties of the fluorophores, FIDA analyzes the instantaneous values of the fluorescence intensity

fluctuations, thus providing information about the distribution of the aggregation states of the fluorophores (Fig. 3-8).

FIDA and FCS share similar experimental setup which is based on confocal microscope (3-4). In this setup fluorophores diffusing thought the observation volume and emit photons, a portion of which is transmitted though the optics of the microscope to the APD. It is estimated that up to 10^5 photons per second can be detected by the APD from a fluorophore passing through the observation volume. The observation volume in FCS is approximated to have Gaussian shape, while in FIDA the shape of the observation volume can not be described by Gaussian and is more complex due to interference caused by diaphragms and aberrations. The observation volume in FIDA is described by the
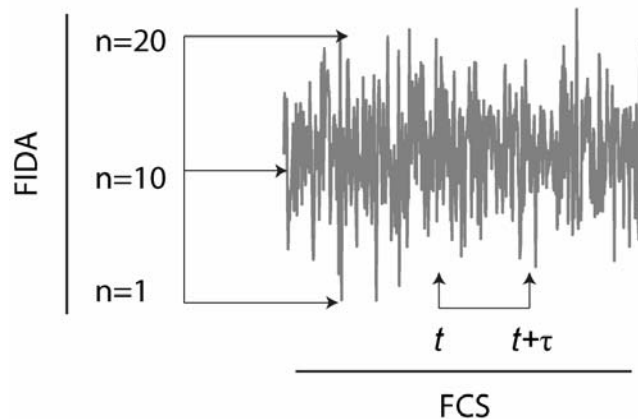
Figure 3-8. FIDA and FCS use the same signal of the fluorescence intensity fluctuations. FIDA utilizes the values for the instantaneous brightness of the fluctuations while FCS utilizes the temporal distribution of the fluorescence fluctuations. On the figure *n* represents the number of photon counts.

three-dimensional spatial brightness function $B(\vec{r})$, which is instrument specific and can be calculated using a calibration measurement with a single dye of known brightness (for example, Alexa Fluor 488 or rhodamine 6G).

Distribution of photon counts, $P(n)$, arising from the observation volume carries information about the specific brightness and concentration of all fluorescent species present in the volume and is calculated according to the Mandel formula[3, 65] which is expressed as

$$P(n) = \int_V \sum_{i=1}^{i=5} \sum_{m=0}^{\infty} \frac{(c_i dV)^m}{m!} \exp(-c_i dV) \cdot \frac{\left(mq_i B(\vec{r})T_{count}\right)^n}{n!} \exp(-mq_i B(\vec{r})T_{count}) \quad \text{(Eqn. 12)}$$

where c_i is the concentration of species with specific brightness of q_i, T_{count} is the length of the counting period, i is the summation index representing the number of fluorescent species, m is summation index representing total number of molecules inside the observation volume, n is summation index representing the number of photon counts. Equation 12 is a double Poissonian first part of which represent the Poisson distribution of the number of molecules within small portion of the observation volume, dV, while the second part of the equation represent the Poisson distribution of the number of photon counts detected from the molecules inside the observation volume. It is stated by Kask *et al* that FIDA can differentiate up to five various fluorescent species in a single experiment.

In FIDA two major assumptions are used: (i) the coordinates of the molecules do not change significantly during the counting period T_{count} which means that the counting period should be shorter than the average time a fluorophore spends inside the observation volume (i.e. $T_{count} < \tau_D$); and (ii) brightness of each molecule can be

expressed as the product of a spatial brightness function $B(\vec{r})$ and specific brightness q, which is characteristic to each fluorescent species. Example of FIDA for monomeric fluorescently labeled BaxΔC and for fluorescently labeled BaxΔC bound to liposomes is shown in Figure 3-9. Furthermore, use of FIDA to determine the oligomeric state of Bax in detergent micelles is discussed in Chapter 4.
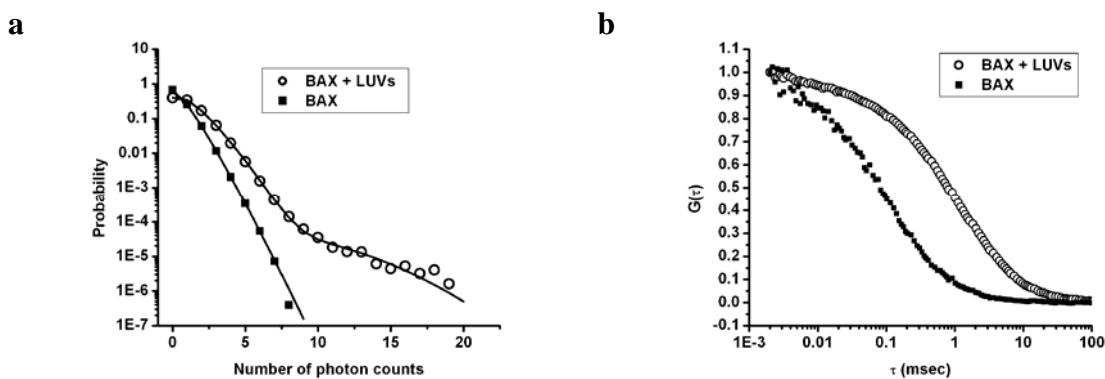
Figure 3-9. Fl-BAXΔC(G40C) bound to liposomes: FCS and FIDA results. **a**. Results of the FIDA fitting for monomeric free fl-BAXΔC(G40C) in solution (squares) and the fl-BAXΔC(G40C)-liposome mixture (circles). According to the single-component FIDA fitting the molecular brightness of free fl-BAXΔC(G40C) monomers in solution was 5.4±0.1 kHz, while two-component FIDA fitting for fl-BAXΔC(G40C)-liposome mixture produced the values for the molecular brightness of 5.4 kHz (fixed component) and 51.7±10.7 kHz which correspond to 9.57±1.99 fl-BAXΔC(G40C) molecules bound per LUV. FIDA analysis was done based on at least six 100 seconds measurements. **b.** Autocorrelation curves (not fitted) for free fl-BAXΔC(G40C) in solution (τ_D=91.3±4.3 μsec) (filled squares) and for fl-BAXΔC(G40C)-LUV mixture (τ_{D1}=91.3 μsec, τ_{D2}=1.12±0.2 msec) (empty circles).

The general idea for analysis of the photon counts have been proposed by Qian and Elson[66, 67] in 1990, while the formalism and experimental implementation of FIDA has been presented by Kask *et al*[3] in 1999. Currently a number of variation of FIDA have

been developed and they include two-dimensional FIDA (2D-FIDA)[68], fluorescence intensity and lifetime analysis (FILDA)[69], fluorescence intensity multiple distributions analysis (FIMDA)[70]. In contrast to FIDA, 2D-FIDA uses two detectors to differentiate between the various dyes, while FILDA and FIMDA perform simultaneous determination of the fluorescence brightness (as done by FIDA) together with fluorescence lifetime or diffusion time respectively.

Assay of liposome permeability

Assay of liposome permeability is used to study the kinetics of the pore formation by Bax and other pore-forming proteins and peptides[71]. For this assay large unilamellar liposomes (100-200 nm in diameter) containing high concentration of a fluorescent dye are prepared (See Appendix II for a detailed protocol). As a fluorescent dyes in this assay carboxyfluorescein or calcein are most commonly used[16, 72]. These dyes are self-quenched and thus do not fluoresce at 20-50 mM concentration and become fluorescent when diluted to µM concentration.

In a generic liposome permeability assay unilamellar liposomes with encapsulated dye have very low background fluorescence signal ($F(0)$) (Fig. 3-10). When the pore forming agent is added (for example, activated Bax), the dye molecules are released from liposomes, becomes diluted and the increase in the fluorescence signal ($F(t)$) is detected. Maximum dye release from liposomes (F_{max}) is achieved by the addition of detergent (for example, 0.1% w/v Triton X-100) which results in the solubilization of all liposomes present in the assay. The curve representing the kinetics of dye release from liposomes is calculated as

$$R(t) = \frac{F(t) - F(0)}{F_{max} - F(0)} \qquad \text{(Eqn. 13)}$$

In many instances the curve of dye release is exponential and can be used to gain quantitative information about the kinetics of the release[73, 74] by fitting to equation

$$R(t) = F(0) + A_1 \times (1 - \exp(-t/\tau_{release})) + m \times t \qquad \text{(Eqn. 14)}$$

where, A_1 is the size of exponential component, $\tau_{release}$ is the time constant of the exponential component, m is the slope of the linear component of the release curve which is occasionally present in release experiments due to the background leakage of dye from liposomes. Saito *et al* used equation 14 to calculate the $\tau_{release}$ values for the various concentrations of activated Bax and then used these values in a Hill plot analysis to determine the stoichiometry of the initial pores formed by Bax[73]. This analysis showed that Bax forms dimer and then tetramer pores. However, due to the small size of the encapsulated dye (0.5 kDa) the formation of higher in stoichiometry Bax pores has not been detected. However, later experiment with liposomes encapsulating larger dye molecules (for example 10 and 70 kDa dextran labeled with carboxyfluorescein) have shown that Bax can form pores large enough to release these dyes[75, 76].

In addition to using self-quenching effect of carboxyfluorescein and calcein in some applications it is advantageous to encapsulate into liposomes dyes together with a quencher. Examples of such quencher-dye pair are Tb/DPA and ANTS/DPX[76-78].
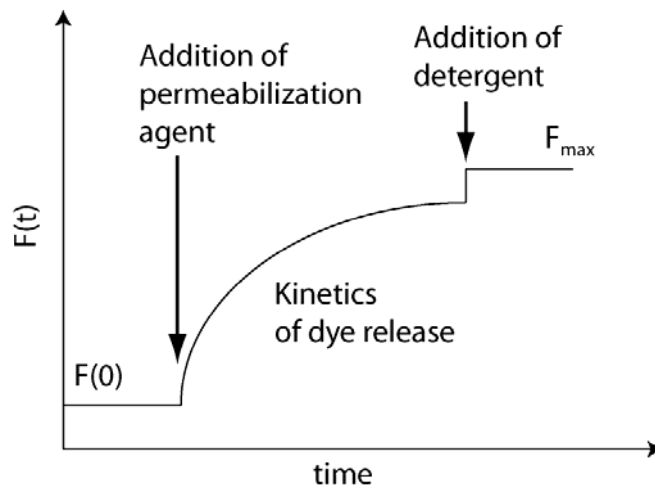
Figure 3-10. Principles of the assay of liposome permeability.

The assay of liposome permeabilization has a number of advantages over other techniques measuring the pore formation in lipid membranes (for example, the electrophysiology methods). These advantages include relative ease of sample preparation (liposomes can be prepared in 30 min and then used within 1 week), fast data acquisition and analysis, and the ability to measure multiple samples at in one experiment by using 96-well format in a fluoremeter. However, the major disadvantage of the technique is that it measures the permeabilization of a population of liposomes and thus doe not allow characterization of individual pores.

References

1.   Fluorescence Correlation Spectrosocpy: Theory and applications (eds. Rigler, R. & Elson, E. L.) (Springer, Berlin, 2001).

2.   Schwille, P., Meyer-Almes, F. J. & Rigler, R. Dual-color fluorescence cross-correlation spectroscopy for multicomponent diffusional analysis in solution. Biophys J 72, 1878-86 (1997).

3.   Kask, P., Palo, K., Ullmann, D. & Gall, K. Fluorescence-intensity distribution analysis and its application in biomolecular detection technology. Proc Natl Acad Sci U S A 96, 13756-61 (1999).

4.   Lakowitcz, J. R. Principles of fluorescence spectroscopy, Second edition (Plenum Publishers, 1999).

5.   Valeur, B. Molecular Fluorescence: Theory and Applications (WILEY-VCH, Germany, 2002).

6.   Haugland, R. P. The Handbook, A Guide to Fluorescent Probes and Labeling Technologies, Tenth Edition (Invitrogen Corp., 2005).

7.   Krichevsky, O. & Bonnet, G. Fluorescence correlation spectrosocopy: the technique and its applications. Rep. Prog. Phys. 65, 251-297 (2002).

8.   Haustein, E. & Schwille, P. Fluorescence correlation spectroscopy: novel variations of an established technique. Annu Rev Biophys Biomol Struct 36, 151-69 (2007).

9.   Rigler, R., Mets, U., Widengren, J. & Kask, P. Fluorescence correlation spectroscopy with high count rate and low background: analysis of translational diffusion. Eur. Biophys. J. 22, 169-175 (1993).

10.   Maiti, S., Haupts, U. & Webb, W. W. Fluorescence correlation spectroscopy: diagnostics for sparse molecules. Proc Natl Acad Sci U S A 94, 11753-7 (1997).

11.   Haustein, E. & Schwille, P. Single-molecule spectroscopic methods. Curr Opin Struct Biol 14, 531-40 (2004).

12.   Bacia, K., Kim, S. A. & Schwille, P. Fluorescence cross-correlation spectroscopy in living cells. Nat Methods 3, 83-9 (2006).

13.   Bacia, K. & Schwille, P. Fluorescence correlation spectroscopy. Methods Mol Biol 398, 73-84 (2007).

14.   Dittrich, P., Malvezzi-Campeggi, F., Jahnz, M. & Schwille, P. Accessing molecular dynamics in cells by fluorescence correlation spectroscopy. Biol Chem 382, 491-4 (2001).

15.   Garcia-Saez, A. J. & Schwille, P. Fluorescence correlation spectroscopy for the study of membrane dynamics and protein/lipid interactions. Methods 46, 116-22 (2008).

16.   Garcia-Saez, A. J., Ries, J., Orzaez, M., Perez-Paya, E. & Schwille, P. Membrane promotes tBID interaction with BCL(XL). Nat Struct Mol Biol 16, 1178-85 (2009).

17.   Ries, J., Yu, S. R., Burkhardt, M., Brand, M. & Schwille, P. Modular scanning FCS quantifies receptor-ligand interactions in living multicellular organisms. Nat Methods 6, 643-5 (2009).

18.   Yu, S. R. et al. Fgf8 morphogen gradient forms by a source-sink mechanism with freely diffusing molecules. Nature 461, 533-6 (2009).

19.   Ries, J. & Schwille, P. New concepts for fluorescence correlation spectroscopy on membranes. Phys Chem Chem Phys 10, 3487-97 (2008).

20.   Kahya, N., Scherfeld, D., Bacia, K. & Schwille, P. Lipid domain formation and dynamics in giant unilamellar vesicles explored by fluorescence correlation spectroscopy. J Struct Biol 147, 77-89 (2004).

21.   Garcia-Saez, A. J., Carrer, D. C. & Schwille, P. Fluorescence correlation spectroscopy for the study of membrane dynamics and organization in giant unilamellar vesicles. Methods Mol Biol 606, 493-508 (2010).

22.   Garcia-Saez, A. J. & Schwille, P. Stability of lipid domains. FEBS Lett 584, 1653-8 (2009).

23.   Magde, D., Elson, E. L., Webb, W. W. Thermodynamic fluctuations in a reacting system: Measurement by fluorescence correlation spectroscopy. Phys Rev Lett 4, 390-401 (1972).

24.   Pramanik, A., Thyberg, P. & Rigler, R. Molecular interactions of peptides with phospholipid vesicle membranes as studied by fluorescence correlation spectroscopy. Chem Phys Lipids 104, 35-47 (2000).

25. Eigen, M. & Rigler, R. Sorting single molecules: application to diagnostics and evolutionary biotechnology. Proc Natl Acad Sci U S A 91, 5740-7 (1994).

26. Wennmalm, S., Blom, H., Wallerman, L. & Rigler, R. UV-Fluorescence correlation spectroscopy of 2-aminopurine. Biol Chem 382, 393-7 (2001).

27. Korn, K., Wennmalm, S., Foerster, H. H., Hahn, U. & Rigler, R. Analysis of the RNase T1 mediated cleavage of an immobilized gapped heteroduplex via fluorescence correlation spectroscopy. Biol Chem 381, 259-63 (2000).

28. Wennmalm, S., Edman, L. & Rigler, R. Conformational fluctuations in single DNA molecules. Proc Natl Acad Sci U S A 94, 10641-6 (1997).

29. Bacia, K. & Schwille, P. Practical guidelines for dual-color fluorescence cross-correlation spectroscopy. Nat Protoc 2, 2842-56 (2007).

30. Chen, Y., Muller, J. D., So, P. T. & Gratton, E. The photon counting histogram in fluorescence fluctuation spectroscopy. Biophys J 77, 553-67 (1999).

31. Malengo, G. et al. Fluorescence correlation spectroscopy and photon counting histogram on membrane proteins: functional dynamics of the glycosylphosphatidylinositol-anchored urokinase plasminogen activator receptor. J Biomed Opt 13, 031215 (2008).

32. Saffarian, S., Li, Y., Elson, E. L. & Pike, L. J. Oligomerization of the EGF receptor investigated by live cell fluorescence intensity distribution analysis. Biophys J 93, 1021-31 (2007).

33. Melnykov, A. V. & Hall, K. B. Revival of high-order fluorescence correlation analysis: generalized theory and biochemical applications. J Phys Chem B 113, 15629-38 (2009).

34. Palmer, A. G., 3rd & Thompson, N. L. High-order fluorescence fluctuation analysis of model protein clusters. Proc Natl Acad Sci U S A 86, 6148-52 (1989).

35. Palmer, A. G., 3rd & Thompson, N. L. Molecular aggregation characterized by high order autocorrelation in fluorescence correlation spectroscopy. Biophys J 52, 257-70 (1987).

36. Palmer, A. G., 3rd & Thompson, N. L. Theory of sample translation in fluorescence correlation spectroscopy. Biophys J 51, 339-43 (1987).

37.   Palmer, A. G., 3rd & Thompson, N. L. Fluorescence correlation spectroscopy for detecting submicroscopic clusters of fluorescent molecules in membranes. Chem Phys Lipids 50, 253-70 (1989).

38.   Gielen, E. et al. Measuring diffusion of lipid-like probes in artificial and natural membranes by raster image correlation spectroscopy (RICS): use of a commercial laser-scanning microscope with analog detection. Langmuir 25, 5209-18 (2009).

39.   Brown, C. M. et al. Raster image correlation spectroscopy (RICS) for measuring fast protein dynamics and concentrations with a commercial laser scanning confocal microscope. J Microsc 229, 78-91 (2008).

40.   Raub, C. B. et al. Image correlation spectroscopy of multiphoton images correlates with collagen mechanical properties. Biophys J 94, 2361-73 (2008).

41.   Ries, J., Petrov, E. P. & Schwille, P. Total internal reflection fluorescence correlation spectroscopy: effects of lateral diffusion and surface-generated fluorescence. Biophys J 95, 390-9 (2008).

42.   Neumann, D., Buckers, J., Kastrup, L., Hell, S. W. & Jakobs, S. Two-color STED microscopy reveals different degrees of colocalization between hexokinase-I and the three human VDAC isoforms. PMC Biophys 3, 4.

43.   Wildanger, D., Medda, R., Kastrup, L. & Hell, S. W. A compact STED microscope providing 3D nanoscale resolution. J Microsc 236, 35-43 (2009).

44.   Kastrup, L., Blom, H., Eggeling, C. & Hell, S. W. Fluorescence fluctuation spectroscopy in subdiffraction focal volumes. Phys Rev Lett 94, 178104 (2005).

45.   Lippitz, M., Erker, W., Decker, H., van Holde, K. E. & Basche, T. Two-photon excitation microscopy of tryptophan-containing proteins. Proc Natl Acad Sci U S A 99, 2772-7 (2002).

46.   Ohrt, T., Merkle, D., Birkenfeld, K., Echeverri, C. J. & Schwille, P. In situ fluorescence analysis demonstrates active siRNA exclusion from the nucleus by Exportin 5. Nucleic Acids Res 34, 1369-80 (2006).

47.   Bacia, K., Scherfeld, D., Kahya, N. & Schwille, P. Fluorescence correlation spectroscopy relates rafts in model and native membranes. Biophys J 87, 1034-43 (2004).

48.   Bacia, K. & Schwille, P. A dynamic view of cellular processes by in vivo fluorescence auto- and cross-correlation spectroscopy. Methods 29, 74-85 (2003).

49. Schwille, P. Fluorescence correlation spectroscopy and its potential for intracellular applications. Cell Biochem Biophys 34, 383-408 (2001).

50. Berland, K. M., So, P. T. & Gratton, E. Two-photon fluorescence correlation spectroscopy: method and application to the intracellular environment. Biophys J 68, 694-701 (1995).

51. Sanchez, S. A. & Gratton, E. Lipid--protein interactions revealed by two-photon microscopy and fluorescence correlation spectroscopy. Acc Chem Res 38, 469-77 (2005).

52. Ries, J., Ruckstuhl, T., Verdes, D. & Schwille, P. Supercritical angle fluorescence correlation spectroscopy. Biophys J 94, 221-9 (2008).

53. Petersen, N. O. Scanning fluorescence correlation spectroscopy. I. Theory and simulation of aggregation measurements. Biophysical Journal 49, 809-815 (1986).

54. Petersen, N. O., Johnson, D. C. & Schlesinger, M. J. Scanning fluorescence correlation spectroscopy. II. Application to virus glycoprotein aggregation. Biophysical Journal 49, 817-820 (1986).

55. Ries, J. & Schwille, P. Studying slow membrane dynamics with continuous wave scanning fluorescence correlation spectroscopy. Biophys J 91, 1915-24 (2006).

56. Ries, J., Chiantia, S. & Schwille, P. Accurate determination of membrane dynamics with line-scan FCS. Biophys J 96, 1999-2008 (2009).

57. Kis-Petikova, K. & Gratton, E. Distance measurement by circular scanning of the excitation beam in the two-photon microscope. Microsc Res Tech 63, 34-49 (2004).

58. Levi, V., Ruan, Q., Kis-Petikova, K. & Gratton, E. Scanning FCS, a novel method for three-dimensional particle tracking. Biochem Soc Trans 31, 997-1000 (2003).

59. Korlach, J., Schwille, P., Webb, W. W. & Feigenson, G. W. Characterization of lipid bilayer phases by confocal microscopy and fluorescence correlation spectroscopy. Proc Natl Acad Sci U S A 96, 8461-6 (1999).

60. Schwille, P., Korlach, J. & Webb, W. W. Fluorescence correlation spectroscopy with single-molecule sensitivity on cell and model membranes. Cytometry 36, 176-82 (1999).

61. Kahya, N., Brown, D. A. & Schwille, P. Raft partitioning and dynamic behavior of human placental alkaline phosphatase in giant unilamellar vesicles. Biochemistry 44, 7479-89 (2005).

62. Kahya, N., Scherfeld, D., Bacia, K., Poolman, B. & Schwille, P. Probing lipid mobility of raft-exhibiting model membranes by fluorescence correlation spectroscopy. J Biol Chem 278, 28109-15 (2003).

63. Magde, D., Webb, W. W. & Elson, E. L. Fluorescence correlation spectroscopy. III. Uniform translation and lamellar flow. Biopolymers 17, 361-376 (1978).

64. Petrov, E. P., Schwille, P. Standartization and quality assurance in fluorescence measurements: state-of-the-art and future challenges (ed. Resch-Genger, U.) (Springer, Berlin, Heidelberg, New York, 2008).

65. Nadarajah, S. Models for Mandel formula. J Math Chem 44, 184-196 (2008).

66. Qian, H. & Elson, E. L. On the analysis of high order moments of fluorescence fluctuations. Biophys J 57, 375-80 (1990).

67. Qian, H. & Elson, E. L. Distribution of molecular aggregation by analysis of fluctuation moments. Proc Natl Acad Sci U S A 87, 5479-83 (1990).

68. Kask, P. et al. Two-dimensional fluorescence intensity distribution analysis: theory and applications. Biophys J 78, 1703-13 (2000).

69. Palo, K. et al. Fluorescence intensity and lifetime distribution analysis: toward higher accuracy in fluorescence fluctuation spectroscopy. Biophys J 83, 605-18 (2002).

70. Palo, K., Mets, U., Jager, S., Kask, P. & Gall, K. Fluorescence intensity multiple distributions analysis: concurrent determination of diffusion times and molecular brightness. Biophys J 79, 2858-66 (2000).

71. Torchilin, V. P., Weissig, V. . Liposomes, Second edition (Oxford University Press, New York, 2003).

72. Ivashyna, O. et al. Detergent activated BAX protein is a monomer. J Biol Chem 284, 23935-46 (2009).

73. Saito, M., Korsmeyer, S. J. & Schlesinger, P. H. BAX-dependent transport of cytochrome c reconstituted in pure liposomes. Nat Cell Biol 2, 553-5 (2000).

74.   Schlesinger, P. H. & Saito, M. The Bax pore in liposomes, Biophysics. Cell Death Differ 13, 1403-8 (2006).

75.   Kuwana, T. et al. Bid, Bax, and lipids cooperate to form supramolecular openings in the outer mitochondrial membrane. Cell 111, 331-42 (2002).

76.   Lovell, J. F. et al. Membrane binding by tBid initiates an ordered series of events culminating in membrane permeabilization by Bax. Cell 135, 1074-84 (2008).

77.   Nir, S., Duzgunes, N. & Bentz, J. Binding of monovalent cations to phosphatidylserine and modulation of Ca2+- and Mg2+-induced vesicle fusion. Biochim Biophys Acta 735, 160-72 (1983).

78.   Billen, L. P., Kokoski, C. L., Lovell, J. F., Leber, B. & Andrews, D. W. Bcl-XL inhibits membrane permeabilization by competing with Bax. PLoS Biol 6, e147 (2008).

79.   Besenicar, M., Macek, P., Lakey, J. H. & Anderluh, G. Surface plasmon resonance in protein-membrane interactions. Chem Phys Lipids 141, 169-78 (2006).

80.   Cooper, M. A. Advances in membrane receptor screening and analysis. J Mol Recognit 17, 286-315 (2004).

81.   Cho, W., Bittova, L. & Stahelin, R. V. Membrane binding assays for peripheral proteins. Anal Biochem 296, 153-61 (2001).

82.   Mozsolits, H. & Aguilar, M. I. Surface plasmon resonance spectroscopy: an emerging tool for the study of peptide-membrane interactions. Biopolymers 66, 3-18 (2002).

CHAPTER 4

"Protein Bax is a Monomer in Detergent Micelles"

Abstract*

BAX is a pro-apoptotic member of the BCL-2 protein family. At the onset of apoptosis, monomeric, cytoplasmic BAX is activated and translocates to the outer mitochondrial membrane, where it forms an oligomeric pore. The chemical mechanism of BAX activation is controversial and several *in vitro* and *in vivo* methods of its activation are known. One of the most commonly used *in vitro* methods is activation with detergents, such as n-octylglucoside. During BAX activation with n-octylglucoside, it has been shown that BAX forms high molecular weight complexes which are larger than combined molecular weight of BAX monomer and one detergent micelle. These large complexes have been ascribed to the oligomerization of BAX prior to its membrane insertion and pore formation. This is in contrast with the *in vivo* studies which suggest that active BAX inserts into the outer mitochondrial membrane as a monomer and then undergoes oligomerization. Here, to simultaneously determine the molecular weight and the number of BAX proteins per BAX-detergent micelle during detergent activation we have used an approach which combines two single-molecule sensitivity techniques – fluorescence correlation spectroscopy (FCS) and fluorescence-intensity distribution analysis (FIDA). We have tested a range of detergents: n-octylglucoside, dodecylmaltoside, Triton X-100, Tween 20, CHAPS and cholic acid. With these detergents we observe that BAX is a monomer before, during and after interaction with micelles. We conclude that detergent activation of BAX is not congruent with oligomerization and that in physiologic buffer conditions BAX can assume two stable monomeric conformations: one inactive and one active.

Introduction

BAX is a pro-apoptotic member of the BCL-2 protein family. In a simplified apoptosis model, monomeric inactive BAX is localized in the cytoplasm of healthy non-dying cells[1]. During apoptosis BAX is activated, and translocates to the OMM[2] where it inserts as a monomer[3], undergoes oligomerization[4] and forms a pore through which cytochrome c and other apoptotic factors are released into the cytoplasm. Once in the cytoplasm, these apoptotic factors induce the activation of the effector caspases which execute the cell death process. This mechanism, which is generally correct, requires that soluble BAX becomes integrated into the mitochondrial membrane where it forms a functional oligomeric pore capable of cytochrome c release. However, the molecular mechanism of BAX activation remains controversial[5, 6].

It has been understood for some time, but frequently ignored, that activity of the BCL-2 family proteins are exhibited in cells when these proteins are associated with the hydrophobic environment of membranes. Therefore, it has always seemed that attention to the effect of hydrophobic environments on the BCL-2 family proteins would be rewarding. It has been shown that BAX can be directly activated by treatment with non-ionic detergents such as n-octylglucoside, dodecylmaltoside, and Triton X-100[1, 7]. During activation by non-ionic detergents, in order to gain the ability to form pores in a bilayer membrane, BAX needs to undergo a major conformational transition from a globular protein with two pore-forming alpha-helices 5 and 6 hidden in the protein core[8] to a conformation in which these two helices are exposed and inserted into a lipid membrane[3, 5, 9]. The nature of this active conformation of BAX is important for the understanding of the death decision in cells. Most proposals suggest that in a cell this activated form of

BAX protein is initiated and maintained by the interactions with other proteins, such as tBID, or by BAX itself as a homo-oligomer[7, 10].

Non-ionic detergents have been commonly used to activate BAX for *in vitro* studies because they are reliably effective and simple to employ. However, little is known about the detailed molecular mechanism of BAX activation by these detergents and its comparability with *in vivo* activation of BAX. What is known is that concentrations of detergent above their critical micelle concentration (CMC) are necessary for BAX activation. This suggests that, in order to be activated, BAX needs to interact with detergent micelles instead of monomeric detergent molecules. For example, in the case of BAX activation by n-octylglucoside, it has been shown that n-octylglucoside concentration should be 1 % (w/v)[7], which is well above the CMC for this detergent (0.6 % w/v)[11]. In addition, it has also been shown that above their individual CMC concentrations most BAX activating detergents produce a change in BAX conformation which can be detected by a conformation-sensitive 6A7 antibody against BAX[1, 12, 13]. In cellular experiments this feature of BAX reactivity to 6A7 antibody is commonly associated with the onset of apoptosis[14, 15]. However, CHAPS does not generate the antibody detected conformational change or the activation of BAX. The small micelle size of this detergent (10 kDa) suggests that perhaps BAX can not adopt an activated state with this detergent. However, cholic acid with even smaller micelle size (4 kDa) can partially activate BAX[1].

Many important detergent properties are associated with micelles. The formation of detergent micelles in solution is concentration dependent beginning at the CMC. The CMC value for a detergent has a practical importance since in most cases only monomers

of detergent can be removed by dialysis, and therefore, it is easier to remove detergent monomers for a detergent with high CMC value than for a detergent with low CMC[11]. For BAX this same consideration applies to its activation with n-octylglucoside (CMC~23 mM) as compared to its activation with Triton X-100 (CMC~0.25 mM). The ease of dialysis is why, in most cases, OG is used to activate BAX *in vitro.*

It has been shown by analytical gel filtration that, when incubated with n-octylglucoside, BAX creates complexes with molecular weight larger than the combined size of a BAX monomer (21 kDa) and an n-octylglucoside micelle (~26 kDa)[7, 11]. It has also been shown that in defined liposomes BAX pore formation requires oligomerization[16]. These data combined with the knowledge that oligomerization is important for the biological function of BAX led to a hypothesis that BAX oligomerizes during its detergent activation prior to membrane insertion[7]. However, it has been shown that *in vivo* activated BAX inserts into the OMM as a monomer[3] and in order to create a pore, BAX undergoes oligomerization in this membrane[4]. This discrepancy between the oligomeric state of active BAX prior to its insertion into a lipid membrane *in vivo* (monomer) and *in vitro* (possibly hexamer or octamer) led us to study the oligomerization state of BAX in detergent micelles. The important issue is whether BAX activation requires protein oligomerization or whether active BAX conformation can be generated from a single protein monomer. To solve this issue we used two single-molecule sensitivity techniques: fluorescence correlation spectroscopy (FCS)[17] and fluorescence-intensity distribution analysis (FIDA)[18]. Combined use of FCS and FIDA allows simultaneous determination of the apparent molecular weight and the number of fluorescently labeled BAX monomers per protein-detergent micelle. Our results are

consistent with previously established results in which BAX forms high molecular weight protein-detergent micelles with n-octylglucoside[4] and show that BAX is present as a monomer in these complexes. In addition, we determined the apparent molecular weight and the number of BAX proteins bound per protein-detergent micelles formed by BAX and micelles of five additional detergents (dodecylmaltoside, Triton X-100, Tween 20, cholic acid and CHAPS). Our data show that BAX is a monomer before, during and after interaction with the micelles of all tested detergents.

Results

Detergent-activated fluorescently labeled BAXΔC can release cytochrome c from isolated mitochondria.

For the FCS and FIDA experiments, we prepared recombinant, fluorescently-labeled, human BAXΔC containing a fluorophore at a single cysteine residue (Fig. 1.A, B). Human BAXΔC contains two indigenous cysteines (C62 and C126) which we considered inappropriate for fluorophore conjugation due to structural and functional reasons[8]. Previously full-length BAX with G40C, C62A and C126A mutations has been reported to be functional *in vivo*[3]. Therefore, we removed cysteines, C62 and C126, by mutation to alanine and added an additional cysteine residue in place of glycine 40 creating BAXΔC(G40C) (Fig. 4-1.A). BAXΔC(G40C) labeled with Bodipy FL maleimide fluorophore became fluor-BAXΔC.

To check the biological activity of the fluor-BAXΔC protein, we studied its ability to release cytochrome c using mitochondria isolated from HeLa cells (Fig. 4-1.C). Our results show that fluor-BAXΔC activated with 2% (w/v) n-octylglucoside releases
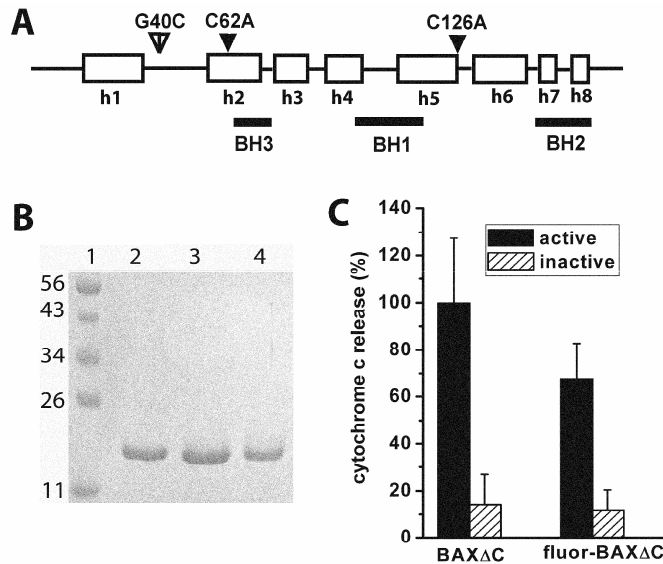
Figure 4-1. **A.** Schematic structure of human BAXΔC(G40C). Introduced mutations and their relative position with respect to the helices and BH domains are indicated with arrows. **B.** SDS-PAGE of purified recombinant proteins: Protein standards with molecular weight indicated (lane 1), human BAXΔC(G40C) (lane 2), human BAXΔC (lane 3), human fluor-BAXΔC (lane 4). **C.** Cytochrome c release from mitochondria isolated from HeLa cells. Mitochondria isolated from HeLa cells were incubated for 20 min at 37 °C with 100 nM of the indicated recombinant protein. Where indicated, protein was activated by incubation with 2% (w/v) n-octylglucoside for 1 hour at 4°C after which protein/detergent mixture was diluted to obtain final detergent concentration of 0.5% (w/v) and the 100 nM protein concentration used in the assays. Cytochrome c content of each fraction was normalized for the basal release of cytochrome c in mitochondria samples with only detergent added and in mitochondria samples without detergent or protein added. Error-bars were calculated based on three independent experiments.

cytochrome c from isolated mitochondria similar to BAXΔC but with slightly lower efficiency. For both proteins significant cytochrome c release required detergent activation, suggesting that the detergent activation of fluor-BAXΔC was comparable to the detergent activation of the BAXΔC[7, 12, 19]. In each cytochrome c release experiment final concentration of n-octylglucoside was 0.005% (w/v) or lower, which is well below the CMC for this detergent (0.6% w/v)[11], so that detergent micelles played no role in the release of cytochrome c or the maintenance of the active BAXΔC conformation during the assay.

Surface plasmon resonance studies of membrane binding and integration by BAXΔC and fluor-BAXΔC.

Direct analysis of the membrane binding and integration by detergent activated fluor-BAXΔC was compared to that of BAXΔC using surface plasmon resonance (SPR) as previously described[20] (Fig. 4-2). SPR has been applied to the study of membrane binding and integration of a number of pore forming proteins and peptides[21, 22] including BAX[20]. Using this technique it is not necessary to label or chemically modify the protein under study. Therefore, we could use this method to determine the effect of the mutations and the added fluorophore on fluor-BAXΔC membrane binding and integration by comparison with the same properties of BAXΔC.

These SPR experiments were done using cardiolipin-containing liposomes (DOPC:DOPA:cardiolipin 70:20:10 mol%) immobilized on the SPR-chip surface and the protein of interest were injected over this surface. Both BAXΔC and fluor-BAXΔC

required n-octylglucoside activation to generate significant interaction with liposomes membrane (Fig. 4-2.A, B).

To determine the concentration-dependence of BAX integration into the liposome membranes, we sequentially injected increasing concentrations of BAX over the same liposome-covered surface and determined the amount of BAX integrated into the lipid membrane based on sensorgram response after 300 seconds of washing. Our results show that, when activated with n-octylglucoside, fluor-BAXΔC and BAXΔC have comparable integration into the liposome membrane (Fig. 4-2.C). This similarity in membrane integration suggests that the slight decrease in cytochrome c release by fluor-BAXΔC (Fig. 4-1.C) is not the result of reduced membrane retention of the labeled protein, but possibly a result of reduced stability of the in-membrane open pore conformation. However, despite a possible reduction in the stability of fluor-BAXΔC pores, the cytochrome c release experiments (Fig 4-1.C) together with the SPR binding data (Fig. 4-2) suggest that both BAXΔC and fluor-BAXΔC, when activated with n-octylglucoside, follow a similar mechanism of membrane interaction and pore formation.

Analytical gel filtration of BAXΔC(G40C) with n-octylglucoside or CHAPS present.
To show that fluor-BAXΔC interacts with detergent micelles of n-octylglucoside and CHAPS comparably to BAXΔC, we performed analytical gel filtration following a procedure of Antonsson *et al.*[7] We carried out our analytical gel filtration studies using BAXΔC(G40C) incubated with either 2% (w/v) of n-octylglucoside or CHAPS (Fig. 4-3). The obtained results show that in the absence of detergents BAXΔC(G40C) eluted as a monomer with molecular weight of slightly less than 25 kDa (Fig. 4-3.A), while in the

presence of 2% (w/v) n-octylglucoside, protein eluted at a molecular weight slightly below 440 kDa (Fig. 4-3.C). In contrast, when BAXΔC(G40C) was incubated with and eluted in the presence of 2% (w/v) CHAPS in the column, protein eluted mostly (73%) as a monomer in a broad peak (Fig. 4-3.B). These results are consistent with previously reported analytical gel filtration of BAXΔC (7) and show that mutant BAXΔC(G40C) interacts with micelles of n-octylglucoside and CHAPS similarly as BAXΔC.
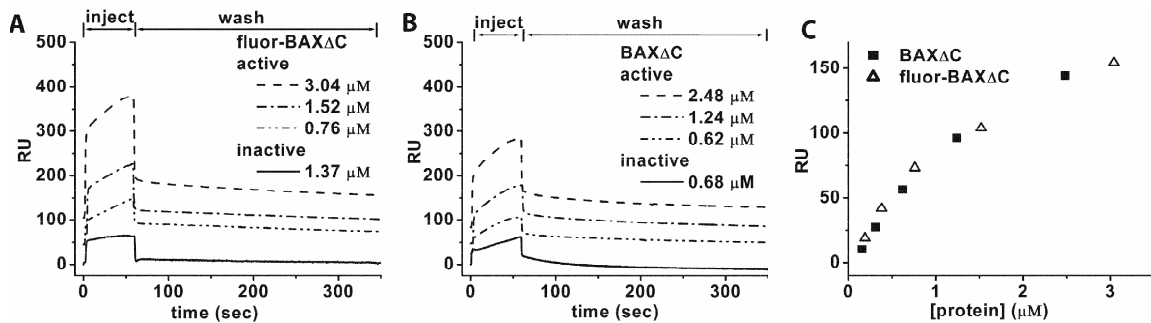
Figure 4-2. Surface plasmon resonance data of fluor-BAXΔC and BAXΔC binding to cardiolipin-containing liposomes (200 nm in diameter; DOPC:DOPA:CL 70:20:10 mol%). Increasing concentrations of protein activated with 2% (w/v) n-octylglucoside was flowed over immobilized on surface liposomes A. Data for fluor-BAXΔC binding. B. Data for BAXΔC binding. C. Results of concentration-dependence analysis of protein integration into liposomes for BAXΔC (squares) and fluor-BAXΔC (triangles).
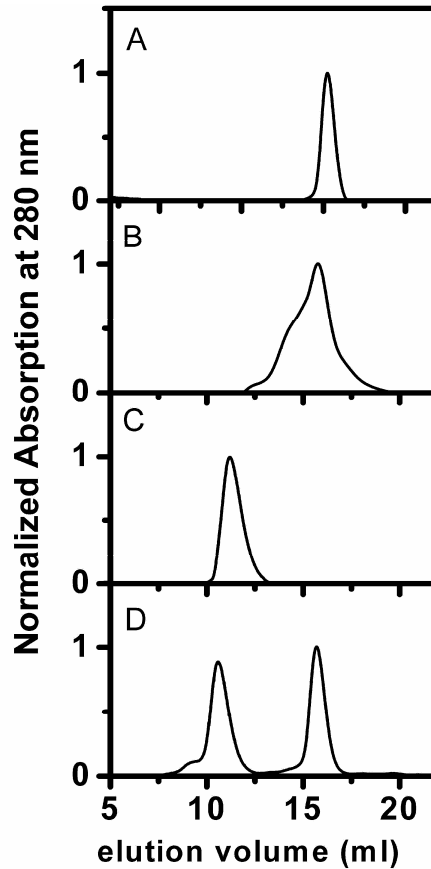
Figure 4-3. Analytical gel filtration of BAXΔC(G40C) incubated with indicated detergents. BAXΔC(G40C) was incubated with 2% (w/v) of indicated detergent for 1 hour at 4 °C. BAXΔC(G40C) incubated with detergent was passed through a Superdex-200 column equilibrated with 10 mM HEPES/KOH, pH 7.0, 300 mM KCl buffer containing 2% (w/v) of the same detergent in which BAX was incubated. The Superdex-200 column was calibrated with two protein standards. A. BAXΔC(G40C) without detergents. B. BAXΔC(G40C) + 2% (w/v) CHAPS. C. BAXΔC(G40C) + 2% (w/v) n-octylglucoside. D. Standards (chymotrypsinogen, 25 kDa, and ferritin, 438.7 kDa).

Activation of BAX with non-ionic detergents.

Compared to the amount of protein required for the analytical gel filtration studies, the amount of fluor-BAXΔC required for the FCS and FIDA analyses is at least 100 times lower. Therefore, we decided to extend the range of the detergents used in our study. We chose n-octylglucoside, CHAPS, Triton X-100, dodecylmaltoside and Tween 20 since these detergents have specific and known effects on BAXΔC activity[7, 19]. We also chose cholic acid due to its similarity in structure to CHAPS, because it is a physiologic detergent and because it can activate BAX[1]. In all cases the 2% (w/v) concentration of the detergent was well above the CMC[11].

Before proceeding to the FCS and FIDA studies, we first tested the ability of all chosen detergents to activate BAXΔC using an assay of carboxyfluorescein release from liposomes (Fig. 4.A)[20]. For these experiments we used recombinant human BAXΔC purified from *E. coli* cells without detergent. This BAXΔC protein was monomeric (23 ± 4 kDa as determined by dynamic light scattering) and had very low (<10%) carboxyfluorescein release activity. Upon 1 hour incubation at 4°C with selected non-ioninc detergents (n-octylglucoside, dodecylmaltoside, Triton X-100 and Tween 20) BAXΔC released carboxyfluorescein from liposomes (Fig. 4-4.A), indicating that protein became activated. Incubation with cholic acid, an ionic detergent, also resulted in activation of BAXΔC. However, upon similar 1 hour incubation at 4°C with CHAPS (detergent known for its inability to activate BAX) no significant carboxyfluorescein release was observed. Similar carboxyfluorescein release results were obtained for BAXΔC(G40C) incubated with all six detergents (Fig. 4-4.B). Comparison of the maximum carboxyfluorescein release values for both proteins after 90 min presents two

instructive observations (Fig. 4-4.C). First, upon incubation with all detergents BAXΔC has almost 20% higher carboxyfluorescein releasing activity than its mutant, BAXΔC(G40C). Second, for both proteins incubation with Triton X-100 resulted in the most activated form of BAX followed by n-octylglucoside, dodecylmaltoside, cholic acid and Tween 20, while CHAPS failed to activated either of the two proteins.

CD spectroscopy on BAXΔC in detergent micelles.

Circular dichroism measurements were performed to determine whether any significant secondary structure changes occur in BAXΔC during interaction with detergent micelles. BAXΔC without detergent produced CD spectra with strong α-helical pattern (Fig. 4-5). In the presence of micelles of Triton X-100, Tween 20 or cholic acid no significant changes in the BAXΔC spectra were observed. However, in the presence of micelles of n-octylglucoside or dodecylmaltoside slight increase in the alpha-helical content of BAXΔC CD spectra was observed. The CD spectra of BAXΔC in the presence of CHAPS were not collected because of high CD signal from CHAPS (due to presence of amide bond in CHAPS structure).
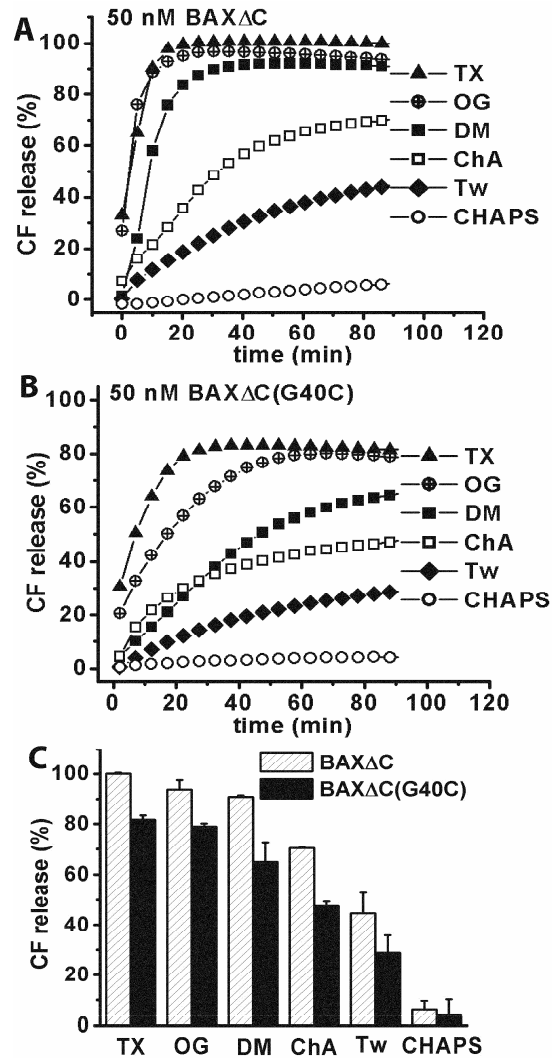
Figure 4-4. Release of carboxyfluorescein (CF) from liposomes by the detergent activated BAXΔC and BAXΔC(G40C). **A.** Monomeric inactive BAXΔC was incubated for 1 hour at 4°C with 2% (w/v) n-octylglucoside (OG), 0.6% (w/v) dodecylmaltoside (DM), 0.076% (w/v) Triton X-100 (TX), 0.038% (w/v) Tween 20 (Tw), 2% (w/v) CHAPS, or 2% (w/v) cholic acid (ChA). During this incubation the concentration of each detergent was above the CMC while protein concentration was 70 μM. Before addition to liposomes protein was diluted to 50 nM. Total lipid mass in each assay was 175 μg. Liposomes composition was DOPC:DOPA 70:30 mol%. Final detergent concentration in the release assays was below the CMC for each detergent. Releases were normalized to carboxyfluorescein release by 20% Triton X-100 and corrected for basal carboxyfluorescein release by each detergent. Each release curve represents an average of at least three independent experiments. **B.** Release of carboxyfluorescein from liposomes by detergent activated BAXΔC(G40C). Protein was treated the same way as BAXΔC in panel A. **C.** Single point comparison of the carboxyfluorescein release values at 90 minutes for BAXΔC and BAXΔC(G40C) activated with indicated detergents. Representative error bars are shown for each release curve.
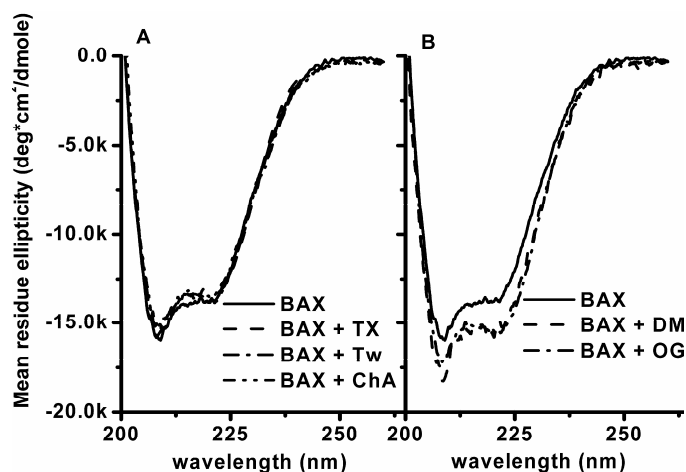
Figure 4-5. CD spectroscopy of BAXΔC in the presence of detergent micelles in 10 mM HEPES, pH 7.0, 100 mM KCl. A. Comparison of the CD spectra for BAXΔC alone and in the presence of either 0.08% Triton X-100 (TX), or 0.04% Tween 20 (Tw), or 2% cholic acid (ChA). B. Comparison of the CD spectra for BAXΔC alone and in the presence of either 2% n-octylglucoside (OG), or 0.6% dodecylmaltoside (DM).

FCS detection volume is not affected by the presence of detergents.

The maintenance of consistent detection volume is critical for accurate comparison of FCS characteristics of different particles. Size and shape of the FCS detection volume depend on a number of parameters, one of which is the refractive index of solution[23, 24]. The latter can be affected by the presence of detergents leading to the distortion of the FCS detection volume.

Commonly AlexaFluor 488 dye is used for calibration of the FCS detection volume[24, 25]. During this calibration procedure the diffusion time (τ_D) of the dye molecules and the structure parameter of the FCS detection volume (ω) are obtained by

fitting the measured autocorrelation curve using Equation 1. Using such analysis for AlexaFluor 488 diffusing freely in solution in the absence of detergent we get following values: τ_D=22.7±0.9 µsec, ω=5.5±0.8. To determine whether presence of detergent has an effect on our FCS measurements we determined τ_D and ω values for AlexaFluor 488 in solution containing increasing concentrations of n-octylglucoside detergent (Fig. 4-6). The results of these experiments show that over the range of 0% to 5% (w/v) of n-octylglucoside the diffusion time of the dye and the structure parameter of the detection volume do not change indicating that the FCS detection volume is not affected by the detergent presence. Similar experiments were done with the rest of the detergents and they yielded analogous results (data not shown).
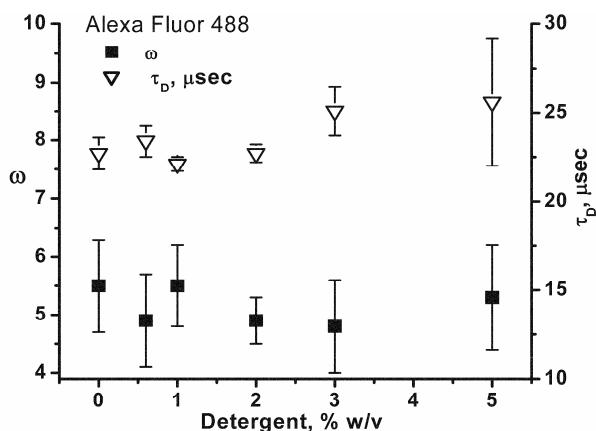
Figure 4-6. Effect of detergent on the shape and size of the FCS detection volume. Measurement of the diffusion time (τ_D) of Alexa Fluor 488 and the structure parameter of the detection volume (ω) at various detergent concentrations. N-octylglucoside was used as a detergent of choice, while buffer composition was 10 mM HEPES, pH 7.2, 100 mM KCl. Error bars were calculated based on nine 10 sec measurements. For some data points error bars are smaller than the symbol.

FCS characterization of fluor-BAXΔC in detergent micelles.

We used fluorescence correlation spectroscopy to confirm the detergent dependent change in the apparent molecular weight of BAXΔC protein as seen by analytical gel filtration. The diffusion characteristics of fluor-BAXΔC were studied in the absence and in the presence of 2% (w/v) of selected detergents (Fig. 4-7, Table 4-1). The FCS diffusion times were obtained by fitting the autocorrelation curves (Fig. 4-7) and are shown in Table 1. Fluor-BAXΔC incubated with 2% (w/v) of either n-octylglucoside, dodecylmaltoside, Triton X-100 or Tween 20 had a significant increase in diffusion time, τ_D, compared with the diffusion time of fluor-BAXΔC monomer in the absence of detergent. In contrast, the diffusion time of fluor-BAXΔC in the presence of 2% (w/v) CHAPS or cholic acid did not increase significantly (Table 4-1).

Using Equation 6 and the diffusion time of the fluorescent particles we calculated the apparent molecular weight (MW) of the BAXΔC-detergent micelle complexes for each detergent (Table 4-1). The apparent MW of fluor-BAXΔC in the presence of n-octylglucoside and CHAPS calculated from the FCS data are the same as the MW obtained by analytical gel filtration of BAX in the presence of these detergents (Fig. 4-3). The large MW complexes of BAX generated in the presence of n-octylglucoside, dodecylmaltoside and Triton X-100 detergents were significantly larger than the sum of BAX and micelle of the respective detergents.
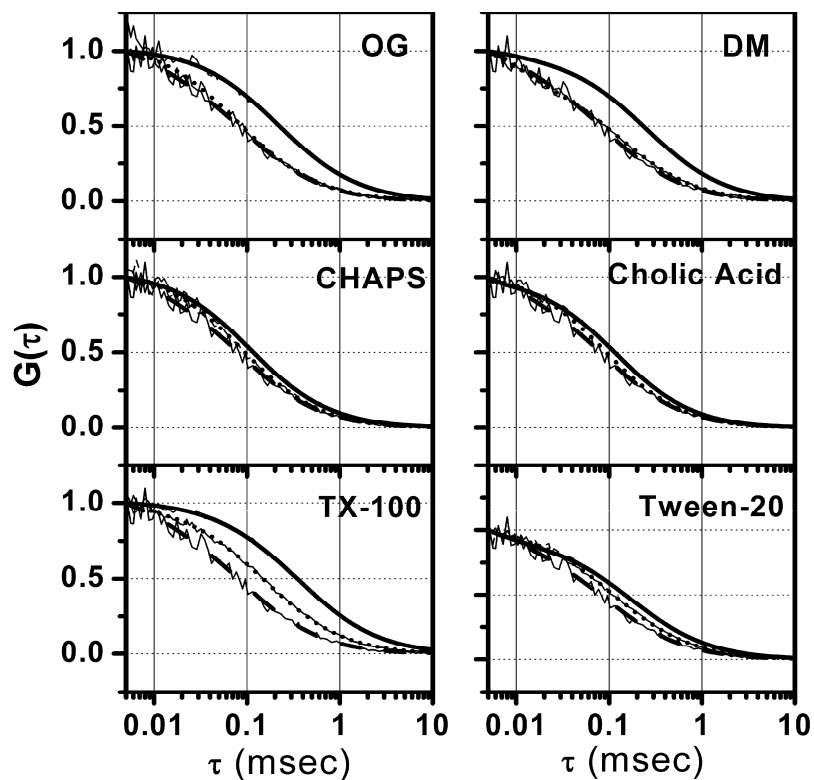
Figure 4-7. Normalized FCS autocorrelation curves of fluor-BAXΔC incubated with various detergents, as indicated (OG - n-octylglucoside, DM − dodecylmaltoside, TX-100 − Triton X-100). For each autocorrelation experiment protein was incubated in 10 mM HEPES/KOH, pH 7.2, 100 mM KCl, with 2% (w/v) of indicated detergent at 4 °C for 1 hour. In each graph: normalized autocorrelation curve for fluor-BAXΔC in the absence of detergent (dashed line), normalized autocorrelation curve for fluor-BAXΔC incubated with 2% (w/v) of the indicated detergent (solid line), and normalized autocorrelation curve for fluor-BAXΔC after detergent was diluted to the concentration below its CMC (dotted line). Raw data for each autocorrelation curve are shown with thin jagged line. See Table 1 for the numerical results of the analysis of these autocorrelation curves.

To determine the size of fluor-BAXΔC after interaction with detergent micelles we removed micelles by diluting detergent concentration below CMC. In most cases this resulted in dissociation of the protein-detergent micelles as well as of the detergent micelles in solution. Each measurement of fluor-BAXΔC size after detergent dilution was done at least one hour after dilution to allow dissociation of the detergent micelles bound to the protein. In all cases the diffusion time of fluor-BAXΔC decreased significantly upon detergent dilution (Table 4-1, Fig. 4-7). For all detergents, except Triton X-100, the diffusion time decreased close to that of fluor-BAXΔC monomer. These observations indicate that upon detergent dilution the molecular weight of the protein-detergent micelle complexes is reduced, and for most of the detergents this molecular weight is reduced to that of a fluor-BAXΔC monomer. In addition, it should be mentioned that n-octylglucoside treated fluor-BAXΔC used in the FCS dilution experiments was used with similar dilution as in the cytochrome c release experiments (Fig. 4-1.C).

Table 4-1. Results of the FCS studies with fluor-BAXΔC-detergent micelles.
The molecular weight of the fluor-BAXΔC-detergent micelles was calculated using Equation 6.

Sample: fluor-BAXΔC+	Detergent concentration 2% (w/v)		After detergent dilution		
	τ_D, μsec	Molecular weight, kDa	Detergent concentration, % (w/v)	τ_D, μsec	Molecular weight, kDa
no detergent	91 ± 4		0	91 ± 4	
n-octylglucoside	223 ± 5	280 ± 12	0.003	100 ± 5	25±1
Triton X-100	366 ± 8	1236 ± 223	0.003	158 ± 4	99±2
dodecylmaltoside	262 ± 21	453 ± 31	0.003	90 ± 4	18±1
CHAPS	115 ± 4	38 ± 1	0.004	87 ± 3	17±1
cholic acid	124 ± 5	48 ± 1	0.003	86 ± 2	17±1
Tween 20	161 ± 12	105 ±2	0.003	112 ± 3	35±1

Fluorescence intensity distribution analysis of fluor-BAXΔC in detergent micelles.

Analysis of the distribution of the photon counts in the FCS data sets was used to determine the number of fluor-BAXΔC molecules per protein-detergent micelle formed with micelles of all tested detergents. This analysis used the FIDA algorithm developed by Kask *et al.*[26] Using FIDA we determined fluorescence brightness of BAX molecules before, during and after interaction with detergent micelles. Comparison of these fluorescence brightness values shows that BAX is a monomer in all cases (Table 4-2). However, in case of dodecylmaltoside and Triton X-100 the calculated values of fluorescence brightness per protein-detergent micelle were 90% higher than the fluorescence brightness of the fluor-BAXΔC monomer. It is possible that BAX is dimerized in micelles of these detergents. Interestingly, in the presence of cholic acid or Tween 20 protein fluorescence brightness decreased by 36% and 15% respectively, while in the presence of the rest of the detergents protein fluorescence brightness increased or stayed the same as in the absence of detergents. Therefore, since protein fluorescence brightness was clearly affected by the detergent we studied this effect directly.

For three detergents where micelle size was significantly increased by the addition of BAX (n-octylglucoside, dodecylmaltoside and Triton X-100) we varied the degree of protein to detergent ratio while holding either detergent or protein concentration constant. First, we varied the concentration of the fluor-BAXΔC from 25 µM to 3 µM while keeping detergent concentration constant at 2% (w/v). We reasoned that, if fluor-BAXΔC forms oligomers in micelles, then decrease in protein concentration while keeping detergent concentration constant would lead to a change, e.g. reduction, of the oligomeric state of protein in detergent micelles. Such change in the oligomeric state

of protein with increasing detergent concentration has been previously demonstrated for some transmembrane peptides in detergent micelles[27]. In this case there was no significant change in the fluorescence brightness of the fluor-BAXΔC-detergent micelles (Table 4-2).

Table 4-2. Analysis of the fluorescence-intensity distribution of the fluor-BAXΔC protein detergent-micelle complexes. Protein (at concentration indicated in the table) was preincubated with detergent for 1 hour at 4 °C. Upon incubation with detergent, the protein was diluted below 0.5 µM into a solution containing identical detergent concentration as during activation. The measurements were done immediately upon this dilution. Mean and standard deviations of the brightness values were calculated based on 9 measurements 50 seconds each.

Sample: fluor-BAXΔC+	Detergent concentration 2% (w/v)		After detergent dilution	
	Fluorescence brightness for 25 µM BAX, kHz	Fluorescence brightness for 3 µM BAX, kHz	Detergent concentration, % (w/v)	Fluorescence brightness, kHz
no detergent			0	5.5 ± 0.1
n-octylglucoside	7.4 ±0.2	7.2 ±0.3	0.003	4.7 ± 0.2
Triton X-100	10.5 ± 0.1	10.4 ± 0.1	0.003	7.1 ± 0.1
dodecylmaltoside	8.5 ± 0.1	10 ± 0.1	0.003	5.0 ± 0.1
CHAPS	5.9 ± 0.1	5.8 ± 0.1	0.004	5.6 ± 0.1
cholic acid	3.49 ± 0.06		0.003	4.71 ± 0.09
Tween-20	4.70 ± 0.24		0.003	5.41 ± 0.06

Second, we measured the effect of increasing detergent concentration on the fluorescence brightness of fluor-BAXΔC at constant protein concentration. If protein fluorescence brightness increases due to the presence of detergent, then the total fluorescence intensity of the sample containing constant protein concentration will increase with increasing detergent concentration. As shown in Fig. 4-8.A (empty circles), for constant protein concentration in the presence of increasing n-octylglucoside concentrations total fluorescence intensity increases. Furthermore, fluorescence brightness per particle of protein-detergent micelles determined by single-component fitting of resulting FCS auto-correlation curves also increased (Fig. 4-8.A. filled squares). The ratio of the total fluorescence intensity to the fluorescence brightness per particle (a.k.a. cpp) represents average number of particles in the FCS observation volume. As expected, this number stayed constant for all n-octylglucoside concentrations clearly showing that increase in n-octylglucoside concentration leads to increase in protein fluorescence brightness. For n-octylglucoside the FCS and FIDA yield similar protein fluorescence brightness values (Table 4-2, Fig. 4-8). Such an agreement between FCS and FIDA results further shows that fluor-BAXΔC is present as a monomer in n-octylglucoside micelles.

Analogous detergent titration experiments were performed for the rest of the detergents giving the same result that protein fluorescence brightness of the fluor-BAXΔC is changing with increasing concentration of detergent (Fig 4-8.C). In addition, in the n-octylglucoside titration experiment gradual increase in the protein diffusion time was observed together with increase in protein fluorescence brightness. This observation

suggests that with increasing n-octylglucoside concentration protein-detergent micelles grow in size (Fig 4-8.B).
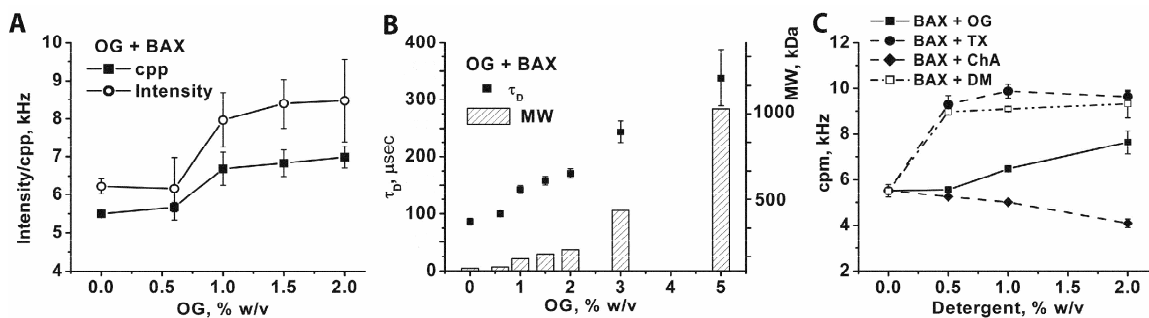
Figure 4-8. Enhancement of the fluor-BAXΔC fluorescence intensity upon interaction with detergents. A. Constant concentration (3 µM) of fluor-BAXΔC was incubated with increasing concentrations of n-octylglucoside for 1 hour at 4 °C. The fluorescence intensity of the protein samples incubated with detergent was measured using ConfoCor 3 (Zeiss, Germany). For each measurement the protein incubated with detergent was diluted to a final concentration of 24 nM in EB buffer containing the same detergent concentration as in the protein sample. All measurements were done at 22 °C. Counts per particle (cpp) values were determined using single-component fit of the FCS autocorrelation curves. B. Increase in the apparent molecular weight of BAXΔC upon interaction with micelles of n-octylglucoside. MW values were calculated using Equation 6. C. Change in the cpp value of fluor-BAXΔC with increasing detergent concentration. Samples were prepared and measurements were done similar to the Fig. 6.A. Detergent abbreviations are similar to Fig. 5.

For all tested detergents after micelle removal by dilution the fluorescence brightness of the fluor-BAXΔC returned to that of a protein monomer. However, upon removal of Triton X-100 protein fluorescence brightness decreased but was still 29% higher than that for the protein monomer in the absence of the detergent. This result suggests incomplete dissociation of the Triton X-100 molecules from BAX and is in accordance with the FCS diffusion time which shows that upon Triton X-100 dilution below CMC, the apparent MW of the fluor-BAXΔC was higher than that of a protein monomer.

FCCS analysis of BAXΔC in detergent micelles.

To show the absence of BAX oligomerization in detergent micelles fluorescence cross-correlation (FCCS) analysis was used. FCCS is a variation of the FCS which allows determination of the degree of interaction between two fluorescent molecules or macromolecular assemblies. In these experiments we used two types of fluorescently labeled BAX: fluor-BAXΔC and Bodipy 630/650 maleimide-BAXΔC. The degree of interaction between these two proteins in detergent micelles is proportional to the cross-correlation value which is determined by FCCS analysis. The results of these FCCS experiments show low cross-correlation values between two fluorescent forms of BAXΔC compared to the theoretically predicted cross-correlation value of BAXΔC dimer. These FCCS results suggest absence of interaction between the two fluorescent variants of BAXΔC in detergent micelles of all tested detergents (Fig. 4-9).
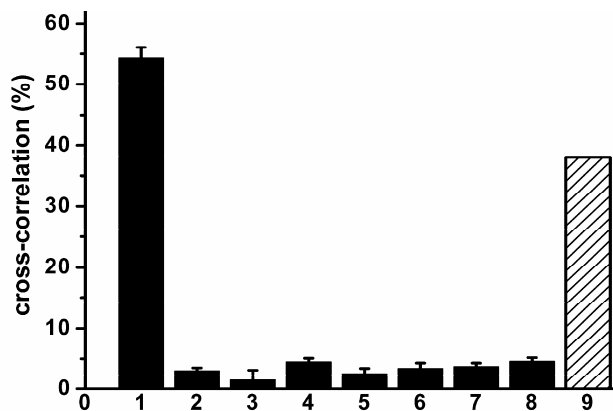
Figure 4-9. Results of the FCCS experiments with fluor-BAXΔC (50% labeled) and Bodipy 630/650 maleimid-BAXΔC (80% labeled) in the presence of indicated detergents: lane 1 - cross correlation standard (double-stranded RNA with Alexa Fluor 488, Cy5 labels); lane 2 - no detergent present; lane 3 - + 2% n-octylglucoside; lane; 4 - + 2% Triton X-100; lane 5 - + 2% CHAPS; lane 6 - + 2% Cholic acid; lane 7- + 2% Tween 20; lane 8 - + 2% dodecylmaltoside; lane 9 – maximum expected cross-correlation value for a formation of protein dimer from a mix of 50 % and 80 % labeled protein. Experiments were done in 10 mM HEPES, pH 7.2, 100 mM KCl buffer at 22 °C. All detergent concentrations are given in % of w/v.

Discussion

Fluorescently labeled BAXΔC is active.

In order to apply FCS to the study of BAX we generated a soluble form of the protein. We employed the BAXΔC in these solution studies of the protein activity and oligomerization because we found that it remained in solution and could be activated by detergent throughout all the manipulations that were used in these studies. In order to label this protein with a fluorophore we substituted endogenous cysteines with alanine (C62A, C126A) and converted glycine 40 in an unstructured region of BAX to a cysteine.

The position of these changes in the BAXΔC protein are shown not to interfere with the function of the full-length BAX *in vivo*[3] and the resulting protein was well expressed by bacteria. The added cysteine was exposed in the engineered protein and formed disulfide cross linked BAXΔC(G40C) dimers at high concentrations (data not shown). After substitution with the fluorescent probe the disulfide formation did not occur. Therefore, further characterization of the activity of the engineered protein was performed on the fluor-BAXΔC.

To assess the functional capability of fluor-BAXΔC we tested its ability to promote cytochrome c release from isolated mitochondria as compared to that of BAXΔC. Since our engineered BAXΔC was based upon the human protein we used mitochondria isolated from HeLa cells to study cytochrome c release[28]. In these experiments we observed that activated with n-octylglucoside fluor-BAXΔC releases 71±15 % of the mitochondrial cytochrome c while BAXΔC releases 100±30 % (Fig. 4-1). Based on this result we conclude that mutation and fluorophore labeling of BAXΔC alter pore forming activity of this protein but only in a minor way. In addition, to these experiments we also studied the ability of various detergents to activate BAXΔC and its mutant in liposomes (Fig. 4-4). Again we saw a reduction in pore activation by the mutant protein. However, it is clear that the reduction is consistent across the range of tested detergents (Fig 4-4.C). Finally, we compared the integration of BAXΔC and its mutant into lipid membranes using SPR. We have recently developed methods to quantitatively study binding and integration of BAX to membranes using SPR[20]. In those studies protein integration into lipid membranes was critical for pore formation and only occurred after protein incubation with n-octylglucoside. In the SPR comparison mutant of

BAXΔC, BAXΔC(G40C), was fully functional and integrated into lipid membranes as well as BAXΔC (Fig. 4-2). Taken together these studies indicate that BAXΔC(G40C) is fully functional but its specific activity for pore formation is slightly lessened by the introduced mutations, possibly due to lower oligomerization rate or changed pore topology.

Fluor-BAXΔC forms high MW protein-detergent micelles with most activating detergents. BAXΔC has been shown to form high molecular weight complexes with n-octylglucoside but not with CHAPS[7]. To show that our mutated BAX, BAXΔC(G40C), can form high molecular weight complexes with n-octylglucoside and not with CHAPS we performed analytical gel filtration studies similar to those in reference 7. The results of these analytical gel filtration experiments show that in the presence of 2% (w/v) of n-octylglucoside BAXΔC(G40C) elutes at molecular weight slightly below 440 kDa , while in the presence of 2% (w/v) CHAPS this protein elutes mostly as a monomer (73%). These results are similar to the previously published results for BAXΔC (7) indicating that mutations introduced into BAXΔC do not interfere with formation of high molecular weight complexes of this protein with n-octylglucoside.

Next we proceeded to measure the molecular weight of fluor-BAXΔC in the presence of n-octylglucoside and CHAPS using FCS. In the FCS experiments we measured the diffusion time, τ_D, of fluor-BAXΔC molecules in the presence of 2% (w/v) of these detergents. Then using Equation 6 we calculated the molecular weight of the fluor-BAXΔC protein-detergent micelle complexes (Table 4-1). The molecular weight of BAXΔC protein-detergent micelle complexes determined by FCS and analytical gel filtration were fairly similar, further demonstrating that mutagenesis and fluorescent

labeling of BAXΔC does not affect the interactions of this protein with n-octylglucoside and CHAPS. This result also shows that FCS can be used to determine apparent molecular weight BAXΔC with other detergents. Therefore, we extended the range of detergents used in our study to dodecylmaltoside, Triton X-10, Tween 20 and cholic acid. As a result of these FCS studies we determined that fluor-BAXΔC forms high molecular weight complexes in the presence of activating non-ionic detergents (n-octylglucoside, dodecylmaltoside, Triton X-100, Tween 20). However, in the presence of cholic acid, activating ionic detergent, fluor-BAXΔC does not form high molecular weight complexes. Fluor-BAXΔC also did not form high molecular weight complexes with CHAPS, a zwitter-ionic detergent known for its inability to activate BAXΔC. In addition, all of the tested activating detergents did not induce significant secondary structure changes in the BAXΔC protein (Fig. 4-5).

For the studies of BAXΔC pore-formation in lipid membranes it is desirable that detergent is removed after BAXΔC activation since detergent at concentrations above the CMC can alter the integrity of lipid membranes. Therefore, it is important to know the molecular weight of BAXΔC after interaction with detergent micelles. To determine the latter, excess detergent was removed from fluor-BAXΔC by dilution below the CMC. After removal of detergent micelles the molecular weight of fluor-BAXΔC decreased to that of the fluor-BAXΔC monomer for the most of the detergents (Table 4-1). The results for fluor-BAXΔC treated with Triton X-100 were an exception. Upon Triton X-100 dilution the molecular weight of fluor-BAXΔC was five times larger than that of fluor-BAXΔC monomer. There are two possible explanations of this result. The first explanation is based on incomplete dissociation of Triton-X-100 molecules bound to

fluor-BAXΔC upon detergent dilution, while the second explanation is possible formation of fluor-BAXΔC homo-oligomers. To differentiate between these two explanations and to determine the stoichiometry of fluor-BAXΔC before, during and after interactions with detergent micelles we performed FIDA.

BAXΔC is present as a monomer in protein-detergent micelles.

To further investigate the stoichiometry of the fluor-BAXΔC-detergent micelles we performed FIDA on the FCS data (Table 4-2). The fluorescence brightness of the individual protein-detergent micelles varied approximately 90% as a function of the detergent used, but all of them contained one BAX protein molecule. The reason for such variation of the fluorescence brightness of the protein monomer in various detergents was due to the enhancement or quenching of the Bodipy FL fluorophore brightness upon transfer into hydrophobic environment of a detergent micelle. Similar effect of the fluorophore brightness enhancement were reported previously for the fluorescently-labeled diphtheria toxin T-domain interacting with detergent micelles[29]. In our case there appears to be an enhancement of the fluorescence brightness of fluor-BAXΔC in the presence of n-octylglucoside, dodecylmaltoside, Triton X-100 detergents and decrease in protein fluorescence brightness in the presence of cholic acid and Tween 20. Studies of detergent titration into constant protein concentration show that this effect is due to the enhancement of the fluorophore brightness and not due to protein oligomerization (Fig. 4-8). In addition, detergent dilution studies show that upon detergent dilution, which leads to the dissolution of the fluor-BAXΔC-detergent micelles, the fluorophore

brightness of the protein returns to that of the protein monomer prior to the interaction with detergent micelles (Table 4-2).

The FIDA results mean clearly that before, during, and after interaction with detergent micelles the fluor-BAXΔC protein is a monomer. This observation suggests that BAXΔC interaction with micelles is fundamentally different from the interaction which it establishes in bilayer membranes. In a bilayer membrane BAXΔC assumes conformation which allows assembly of homo-oligomers resulting in pore formation. In contrast, in a detergent micelle BAXΔC assumes conformation which in case of non-ionic detergents leads to a dramatic enlargement of resulting protein-detergent micelle without necessary protein homo-oligomerization (Table 4-1, Fig. 4-3). Since this increase in size can no longer be attributed to additional BAX molecules per micelle, it must be due to the incorporation of additional detergent.

To study the interaction of the fluor-BAXΔC with detergent micelles we used detergents at 2% (w/v) concentration which is well above the CMC for all tested detergents. If expressed in molar units, this detergent concentration will be on the order of mM for all tested detergents (n-octylglucoside – 68 mM, Triton X-100 – 32 mM, CHAPS – 33 mM; dodecylmaltoside – 40 mM). In contrast, in all of the experiments the concentration of fluor-BAXΔC during incubation with detergent was 20-30 μM. Solution containing 20-30 μM protein and >30 mM detergent has an excess of detergent micelles over the number of protein molecules. Fleming *et al.* have shown that an excess of detergent micelles moves the protein to a more dissociated state[27]. Fleming *et al.* also show that for a glycophorin A transmembrane α-helix, 40% of dimers of this α-helix are detected for a 40 times lower mole ratio of protein to detergent than was used in our

experiments. This demonstrates that if fluor-BAXΔC is forming oligomers in detergent micelles, then we would not have been prevented from detecting them. The above outlined argument together with the FCCS results (Fig. 4-9) lead us to a conclusion that fluor-BAXΔC is present as a monomer in detergent micelles.

The outcome of this conclusion is that during and after detergent activation BAXΔC is a monomer. Therefore this protein has two stable monomeric conformations in physiological buffer conditions: one inactive and one active. Second this implies that the detergent-activated species of BAX is a monomeric protein and the large molecular weight in the presence of the micelles of non-ionic detergents is a result of the detergent component of the complex.

Consequences for the physiological activation of BAX.

These studies suggest that detergent activation of BAX is not merely a mimicry of the physiologic BAX activation. The characteristics of the detergent activation indicate two intriguing characteristics which may concern *in vivo* activation of BAX. First, since BAX remains active after we effectively remove the detergent substrate upon which it has activated, there must be two stable conformations of monomeric solution BAX, one active and the other inactive. Since this activation requires a large template and is distinct from the oligomer-competent conformation which BAX assumes in membranes, we can consider the possibility that BAX is activated as a soluble protein and then integrates into the membrane. Second, the existence of a soluble active form of BAX suggests that this process can be reversed which is a potential therapeutic approach.

Conclusion

In this work we studied in detail the process of BAXΔC activation by non-ioninc detergents. Based on the results of our study we conclude that BAXΔC is a monomer before, during and after interaction with detergent micelles. In this study we used fluorescently labeled analogue of BAXΔC in combination with two single-molecule sensitivity techniques (FCS and FIDA). Since the determination of the oligomeric state of proteins in detergent micelles is important for structural and functional studies of integral membrane proteins[30, 31], we are hopeful that the method presented here can be used for other proteins.

Experimentals

All chemicals used in this paper were from Sigma-Aldrich, St. Louis, USA, unless otherwise stated. All lipids were obtained from Avanti Polar Lipids, USA. Fluorescent dyes for protein labeling were purchased from Molecular Probes, USA.

Protein constructs, protein purification and protein labeling.

The cDNA for human BAX with 19 amino acid truncation on the C-terminus (BAXΔC) was fused to the C-terminal intein/chitin-binding domain of pTYB1 vector (New England BioLabs, USA)[8]. Three mutations (G40C, C62A, C126A) were introduced into each of the DNA plasmids using a QuikChange mutagenesis kit (Stratagene) and presence of mutations was confirmed by sequencing. Resulting construct and purified protein was dubbed as BAXΔC(G40C). All proteins (human BAXΔC and human BAXΔC(G40C)) were purified from BL21(DE3) *E. coli* cells without detergent. Briefly, bacterial cultures were grown at 37 °C in Terrific Broth[32] to an OD_{600} of 1.5-2.0, then the cultures were

induced with 0.1 mM IPTG (RPI, Illinois, USA) and the temperature was dropped to 25 °C. After 12-15 hours, bacteria were collected via centrifugation, the resulting pellet resuspended in lysis buffer (PBS, pH 7.2, 1mM EDTA, 0.25 mM PMSF), and cells broken by four passages through a Microfluidizer (Microfluidics, USA) at 1000 bar. Lysate was clarified by centrifugation and the supernatant containing BAX incubated with chitin affinity resin (New England BioLabs, USA) overnight at 4°C on a rocker. Resin was subjected to a high salt wash then equilibrated in cleavage buffer (10 mM HEPES/NaOH, pH 8.0, 100 mM NaCl, 50 mM DTT) and incubated for 48 hours at 4°C. The purity of the proteins were assessed by SDS-PAGE. BAXΔC(G40C) was labeled with Bodipy FL c_5-maleimide (Molecular Probes, USA) according to the manufacturer's protocol. Labeled protein was separated from the free dye using a Sephadex G-25 column. The degree of protein labeling was determined using a NanoDrop spectrophotometer (Thermo Scientific) by measuring absorbance at 280 nm (for protein concentration) and 504 nm (for Bodipy FL concentration). Resulting protein was ~ 80 % labeled and was stored in EB buffer (10 mM HEPES/KOH, pH 7.2, 100 mM KCl) at 4°C.

Incubation of BAX with detergent micelles.

Prior to FCS studies, cytochrome c and carboxyfluorescein release experiments, fluorescently labeled BAXΔC(G40C) or BAXΔC (20-30 µM) were incubated with 2% (w/v) of indicated detergent in EB buffer for 1 hour at 4 °C. For FCS studies of the fluor-BAXΔC in detergent micelles, after incubation with detergent, protein was diluted to a concentration below 0.5 µM in a solution containing the same detergent concentration as the activated protein. This dilution was done to insure that the fluorescent signal emitted by the protein sample is within the dynamic range of the detector in the ConFocor 3

(Zeiss, Germany). To remove detergent micelles for the cytochrome c release and for the FCS studies of post-micelle-activated fluor-BAXΔC, the BAX-detergent mixture was diluted below the CMC of each particular detergent. The disappearance of micelles occurred at different rates (< 1 minute for OG and longer but <60 minutes for TX-100) but was allowed to finish before further studies on the sample (cytochrome c release or FCS) proceeded.

Cytochrome c release assay.

Mitochondria from HeLa cells were isolated using previously published procedure[33]. Isolated mitochondria were resuspended in 10 mM HEPES/KOH, pH 7.4, 100 mM KCl, 1 mM EGTA, 200 mM sucrose. For the cytochrome c release assay isolated mitochondria were incubated with 100 nM of protein that was detergent activated but micelle diluted as described in the preceding section or inactive protein at 37 °C for 20 min. After the incubation with BAX protein or detergent control solutions, mitochondria were spun down at 10,000 g for 10 min at 4 °C, then pellet and supernatant fractions were collected and stored at -20 °C. For the cytochrome c release assay we used 0.5 μg of mitochondria in 30 μl volume. Protein concentration in the preparation of isolated mitochondria was determined by Bio-Rad Protein Assay (Bio-Rad Laboratories, USA). Cytochrome c content in the pellet and supernatant fractions was determined using TiterZyme EAI human cytochrome c Enzyme Immunimetric Assay Kit (Assay Designs, USA) in combination with Synergy HT plate reader (Bio-Tek Instruments, Inc., USA).

Surface plasmon resonance studies of BAX binding to liposomes.

These studies were done using Biacore X instrument (Biacore Division of GE Healthcare, Sweden) at ambient temperature of 25 °C. Liposome with lipid composition of DOPC:DOPA: bovine heart cardiolipin (70:20:10 mol %) were prepared using the reverse-phase evaporation method[34] following procedure described in detail in[20]. The buffer was EB unless otherwise noted. The rest of the experimental conditions, experimental protocol and data analysis were the same as described in (20).

Analytical gel filtration.

Analytical gel filtration experiments were performed on a Superdex 200 HR 10/30 column (GE Healthcare, UK) equilibrated with 20mM Hepes/KOH pH 7.5, 300mM KCl, 0.2mM dithiothreitol. In the corresponding samples, 2% (w/v) of the indicated detergent was included in the equilibration buffer. Prior to loading the sample on the column 2.5 nmol of BAXΔC(G40C) were incubated in 2% (w/v) of the corresponding detergent for 1h at 4° C. Then, samples were loaded into the column and run at 0.5 ml/min. BAXΔC(G40C) elution was detected by light absorption at 280 nm.

Carboxyfluorescein release assay.

Liposomes containing 50 mM carboxyfluorescein (CF) were prepared following procedure described in (20). Incubation with detergents protein was diluted into wells in a black bottom 96 well-plate (NUNC, Denmark) using EB buffer. Liposomes (200 nm in diameter, DOPC:DOPA 70:30 mol%) were added to the wells last. Immediately upon addition of liposomes measurement of CF fluorescence was done using Synergy HT plate reader (Bio-Tek Instruments, Inc., USA). CF releases for all protein samples containing

detergent were corrected for the baseline CF release in the presence of detergents without protein. Data were analyzed in Origin 6.1 (OriginLab Corp. USA).

Circular dichroism spectroscopy.

Samples for circular dichroism (CD) spectroscopy were prepared at 5 µM protein concentration in 10 mM potassium phosphate buffer, pH 7.0. Detergents (n-octylglucoside (2% w/v), dodecylmaltoside (0.6% w/v), Triton X-100 (0.08%), Tween 20 (0.04% w/v), cholic acid (2% w/v)) were added to protein samples 1 hour prior to measurements and stored at 4 °C. Samples were measured at 20 °C on Jasco J-715 spectrapolarimeter using a 1 mm path-length cell. Data were collected every 0.1 nm at 50 nm/min scan speed from 260 to 200 nm, and results were averaged from five scans. Due to high CD signal from Triton X-100 at 200 nm for samples containing this detergent data were collected from 240 to 205 nm. Spectra for all protein samples containing detergent were corrected for the baseline of detergents in the absence of protein.

FCS, FCCS and FIDA analyses: instrumentation and measurements.

LSM 510 ConfoCor 3 system coupled with Zeiss Axiovert 200M inverted microscope (Zeiss, Germany) was used for FCS and FIDA experiments. A water immersion C-Apochromat 40x objective (Zeiss, Germany) focused the excitation light to a diffraction-limited spot. The pinhole size was set to 70 µm for 488 nm excitation laser light. The excitation light of a 25 mW 488 nm Argon laser was set at 1% of the acusto-optical tunable transmission. Laser power in the sample was 7 µW. In front of the detector LP 530 nm filter was used. For the FCS and FIDA analyses each sample was measured at least nine times for 50 seconds. The detection volume was previously calibrated with free

Bodipy FL maleimide in solution (diffusion time 22.6 ± 0.5 μsec, structure parameter 5.0 ± 0.4).

FCS analysis.

FCS measurements provide three characteristic parameters for interpretation: τ_D - the diffusion time of a fluorescent particle (i.e. the average time a particle spends in the detection volume), N - the number of fluorescent particles in the detection volume, and the counts per particle (cpp) or the average fluorescent intensity per particle. These parameters are extracted by performing a fit of FCS auto-correlation data to one component diffusion model which takes into account photophysical dynamics of fluorophores

$$G(\tau) = \frac{1}{N} \cdot \left(1 + \frac{T \exp(-\tau/\tau_T)}{1-T}\right) \cdot \left(1 + \frac{\tau}{\tau_D}\right)^{-1}$$

$$\cdot \frac{1}{\sqrt{1 + \tau/\omega^2 \tau_D}}$$
  (Eq.1)

In this formula $G(\tau)$ is auto-correlation function, τ is the lag time, T is the fraction of molecules in the triplet state, τ_T triplet decay time, ω is the structure parameter (aspect ratio) of the Gaussian detection volume. Fitting of the FCS auto-correlation curves was done using Equation 1 with software written in MATLAB (Mathworks, NA) using a weighted non-linear least squares fitting algorithm.

Calculation of protein-detergent micelle molecular weight based on FCS diffusion time.

For a particle in solution the diffusion time is inversely proportional to the diffusion coefficient

$$\tau_D = \frac{\omega^2}{4D} \qquad \text{(Eq. 2)}$$

In general protein molecules diffusing in solution are assumed to approximate a spherical shape permitting the Einstein-Stokes relationship to be used in evaluating the diffusion constant

$$D = \frac{k_B T}{6\pi\eta R} \qquad \text{(Eq. 3)}$$

where, k_B is the Boltzmann constant, T is temperature in degrees Kelvin, η is viscosity of solution in which particle is diffusing, and R is the radius of the spherical particle. The radius of diffusing particle depends on the molecular weight of the particle ($R \propto (MW)^{1/3}$). Under these conditions a relationship can be established between the FCS diffusion time of a particle and its molecular weight

$$\tau_D = \frac{\omega^2}{4} \cdot \frac{6\pi\eta}{k_B T} \cdot R \qquad \text{(Eq. 4)}$$

$$\tau_D \propto \frac{\omega^2}{4} \cdot \frac{6\pi\eta}{k_B T} \cdot (MW)^{1/3} \qquad \text{(Eq. 5)}$$

In case of BAXΔC, we know diffusion time of a BAXΔC monomer, $\tau_{D,monomer}$, and its molecular weight, $MW_{monomer} = 19$ kDa. We also know the diffusion time of BAXΔC

118

protein-detergent micelle, $\tau_{D,oligomer}$. Using Equation 5 we can determine the apparent molecular weight of the BAXΔC protein-detergent micelle

$$MW_{oligomer} = MW_{monomer}\left(\frac{\tau_{D,oligomer}}{\tau_{D,monomer}}\right)^3 \quad \text{(Eq. 6)}$$

FCCS analysis. Fluorescence cross-correlation spectroscopy (FCCS) employing BAX labeled with dyes having non-overlaping fluorescence spectra and two channel collection of data, was used to determine the presence or absence of BAX homo-oligomers in detergent micelles (23,24). Using Bodipy FL maleimide-BAXΔC and Bodipy 630/650 maleimid-BAXΔC we studied cross-correlation in micelle associated protein. The cross-correlation value, a ratio of the number of the fluorescent complexes containing both proteins of interest to the number of the fluorescent species of one of the proteins, was used to estimate the micelles with more than one BAX molecule. As a positive control and as a calibration sample the 21 base pair long double-stranded RNA labeled with Alexa Fluor 488 and Cy5 on each 3'-end was used[35].

Fluorescence intensity distribution analysis, FIDA.

Analysis of the fluorescence brightness of a particle can provide an additional measure of the number of fluorescent proteins associated with a detergent micelle. The particle fluorescence brightness determined by FIDA is extracted by fitting the distribution of the number of photon counts and is similar to the cpp value determined by FCS for a monodisperse fluorophore solution. Determination of the particle brightness of the BAX-detergent micelle and comparison with particle brightness of monomeric BAX molecules estimates the number of BAX molecules in detergent micelles. FIDA was performed

according to Kask *et al.*[18]. The raw data of photon arrival times was binned to 20 µs and photon counting histograms were constructed. Parameters describing the detection volume were determined in a solution of fluor-BAXΔC in absence of detergent. As indicated, histograms were fitted to model functions for one or two components, described in Kask *et al.*[18] subtracting a background of 310 Hz for the buffer solution.

References:

1.   Hsu, Y. T. & Youle, R. J. Bax in murine thymus is a soluble monomeric protein that displays differential detergent-induced conformations. J Biol Chem 273, 10777-83 (1998).

2.   Wolter, K. G. et al. Movement of Bax from the cytosol to mitochondria during apoptosis. J Cell Biol 139, 1281-92 (1997).

3.   Annis, M. G. et al. Bax forms multispanning monomers that oligomerize to permeabilize membranes during apoptosis. EMBO J 24, 2096-103 (2005).

4.   Antonsson, B., Montessuit, S., Sanchez, B. & Martinou, J. C. Bax is present as a high molecular weight oligomer/complex in the mitochondrial membrane of apoptotic cells. J Biol Chem 276, 11615-23 (2001).

5.   Lalier, L. et al. Bax activation and mitochondrial insertion during apoptosis. Apoptosis 12, 887-96 (2007).

6.   Youle, R. J. & Strasser, A. The BCL-2 protein family: opposing activities that mediate cell death. Nat Rev Mol Cell Biol 9, 47-59 (2008).

7.   Antonsson, B., Montessuit, S., Lauper, S., Eskes, R. & Martinou, J. C. Bax oligomerization is required for channel-forming activity in liposomes and to trigger cytochrome c release from mitochondria. Biochem J 345 Pt 2, 271-8 (2000).

8.   Suzuki, M., Youle, R. J. & Tjandra, N. Structure of Bax: coregulation of dimer formation and intracellular localization. Cell 103, 645-54 (2000).

9.   Garcia-Saez, A. J., Mingarro, I., Perez-Paya, E. & Salgado, J. Membrane-insertion fragments of Bcl-xL, Bax, and Bid. Biochemistry 43, 10930-43 (2004).

10.   Lovell, J. F. et al. Membrane binding by tBid initiates an ordered series of events culminating in membrane permeabilization by Bax. Cell 135, 1074-84 (2008).

11.   le Maire, M., Champeil, P. & Moller, J. V. Interaction of membrane proteins and lipids with solubilizing detergents. Biochim Biophys Acta 1508, 86-111 (2000).

12.   Yethon, J. A., Epand, R. F., Leber, B., Epand, R. M. & Andrews, D. W. Interaction with a membrane surface triggers a reversible conformational change

in Bax normally associated with induction of apoptosis. J Biol Chem 278, 48935-41 (2003).

13.   Hsu, Y. T. & Youle, R. J. Nonionic detergents induce dimerization among members of the Bcl-2 family. J Biol Chem 272, 13829-34 (1997).

14.   Dewson, G., Snowden, R. T., Almond, J. B., Dyer, M. J. & Cohen, G. M. Conformational change and mitochondrial translocation of Bax accompany proteasome inhibitor-induced apoptosis of chronic lymphocytic leukemic cells. Oncogene 22, 2643-54 (2003).

15.   Hou, Q. & Hsu, Y. T. Bax translocates from cytosol to mitochondria in cardiac cells during apoptosis: development of a GFP-Bax-stable H9c2 cell line for apoptosis analysis. Am J Physiol Heart Circ Physiol 289, H477-87 (2005).

16.   Saito, M., Korsmeyer, S. J. & Schlesinger, P. H. BAX-dependent transport of cytochrome c reconstituted in pure liposomes. Nat Cell Biol 2, 553-5 (2000).

17.   Haustein, E. & Schwille, P. Single-molecule spectroscopic methods. Curr Opin Struct Biol 14, 531-40 (2004).

18.   Kask, P., Palo, K., Ullmann, D. & Gall, K. Fluorescence-intensity distribution analysis and its application in biomolecular detection technology. Proc Natl Acad Sci U S A 96, 13756-61 (1999).

19.   Kuwana, T. et al. Bid, Bax, and lipids cooperate to form supramolecular openings in the outer mitochondrial membrane. Cell 111, 331-42 (2002).

20.   Christenson, E., Merlin, S., Saito, M. & Schlesinger, P. Cholesterol effects on BAX pore activation. J Mol Biol 381, 1168-83 (2008).

21.   Anderluh, G., Macek, P. & Lakey, J. H. Peeking into a secret world of pore-forming toxins: membrane binding processes studied by surface plasmon resonance. Toxicon 42, 225-8 (2003).

22.   Bavdek, A. et al. Sterol and pH interdependence in the binding, oligomerization, and pore formation of Listeriolysin O. Biochemistry 46, 4425-37 (2007).

23.   Enderlein, J., Gregor, I., Patra, D. & Fitter, J. Art and artefacts of fluorescence correlation spectroscopy. Curr Pharm Biotechnol 5, 155-61 (2004).

24.   Meacci, G. et al. Mobility of Min-proteins in Escherichia coli measured by fluorescence correlation spectroscopy. Phys Biol 3, 255-63 (2006).

25. Saffarian, S., Li, Y., Elson, E. L. & Pike, L. J. Oligomerization of the EGF receptor investigated by live cell fluorescence intensity distribution analysis. Biophys J 93, 1021-31 (2007).

26. Kask, P. et al. Two-dimensional fluorescence intensity distribution analysis: theory and applications. Biophys J 78, 1703-13 (2000).

27. Fleming, K. G. Standardizing the free energy change of transmembrane helix-helix interactions. J Mol Biol 323, 563-71 (2002).

28. Jurgensmeier, J. M. et al. Bax directly induces release of cytochrome c from isolated mitochondria. Proc Natl Acad Sci U S A 95, 4997-5002 (1998).

29. Rodnin, M. V. et al. Interactions of fluorinated surfactants with diphtheria toxin T-domain: testing new media for studies of membrane proteins. Biophys J 94, 4348-57 (2008).

30. Bamber, L., Harding, M., Butler, P. J. & Kunji, E. R. Yeast mitochondrial ADP/ATP carriers are monomeric in detergents. Proc Natl Acad Sci U S A 103, 16224-9 (2006).

31. MacKenzie, K. R. & Fleming, K. G. Association energetics of membrane spanning alpha-helices. Curr Opin Struct Biol 18, 412-9 (2008).

32. Tartof & Hobbs. Improved media for growing plasmid and cosmid clones. Focus 9, 12 (1987).

33. Frezza, C., Cipolat, S. & Scorrano, L. Organelle isolation: functional mitochondria from mouse liver, muscle and cultured fibroblasts. Nat Protoc 2, 287-95 (2007).

34. Skoza, F. & Papahadjopoulos, D. Procedure for preparation of liposomes with large internal aqueous spacce and high capture by reverse-phase evaporation. PNAS 75, 4194-4198 (1978).

35. Ohrt, T., Merkle, D., Birkenfeld, K., Echeverri, C. J. & Schwille, P. In situ fluorescence analysis demonstrates active siRNA exclusion from the nucleus by Exportin 5. Nucleic Acids Res 34, 1369-80 (2006).

CHAPTER 5

"Effect of Bax onto the Morphology of GUVs: Imaging Study"

Abstract

This Chapter provides an overview of the various effects of Bax onto GUV morphology, permeabilization and collapse as studied by the confocal microscopy with the use of fluorescently labeled Bax. In addition, to establishing the effects of Bax binding and pore formation in GUVs, the confocal microscopy experiments described in this chapter establish a time frame for the FCCS measurements on Bax presented in Chapter 7. Furthermore, using the confocal microscopy we compare the ability of Bax to transform the morphology of GUVs to the similar ability of detergents, thus establishing that Bax has a detergent-like effect onto the morphology of GUVs. In this chapter, we also show that the fluorescently labeled full-length Bax used in this and the following two chapters is functional.

Introduction

Upon binding and pore formation, Bax changes the physical properties of lipid membranes such as line tension and surface tension[1-3], which in place would lead to changes in the morphology of lipid bilayers. Therefore, before proceeding to the FCCS studies of Bax diffusion and self-assembly in GUV membranes we used confocal microscopy to characterize the morphological changes in GUVs upon, during and after Bax binding and pore formation. These confocal microscopy studies allow us to establish the time frame for the FCCS experiments which is defined by the span of time during which there is sufficient amount of the fluorescently labeled Bax in a GUV membrane and the GUV is not deformed. As a result of these studies, we determined the optimal concentration of Bax for the FCCS experiments and the time frame for the FCCS experiments. We also have found that the ability of Bax to transform the morphology of GUVs is similar to that of detergent n-octylglucoside suggesting that Bax and n-octylglucoside disrupt lipid bilayer coupling in a similar fashion.

Results and Discussion

Fluorescently labelled Bax is active

FCCS is a fluorescence-correlation technique with the sensitivity to detect the co-diffusion of single molecules which need to be labeled with distinct fluorophores[4]. For our FCCS and imaging experiments human full-length Bax with a single cysteine residue engineered at position 4 and the two endogenous cysteines, C62 and C126, mutated to serine and alanine respectively was produced in *E. coli* without use of detergent as described in Appendix V. This protein was labeled with Alexa Fluor 488 dye (Bax-G) or with Atto 655 dye (Bax-R). The activity of both fluorescently labeled proteins was checked using assay of carboxyfluorescein release from liposomes[5, 6] (also described in Chapter 3). In this assay cBid was used to activate the pore formation by Bax. However, without the addition of cBid, Bax produced a slow release of carboxyfluorescein from liposomes (Fig 5-1). Interestingly, addition of Bcl-x_L, an inhibitor of Bax pore formation, inhibited only the cBid activation of Bax but not the auto-activation of Bax[7] (Fig. 5-1b). However, the auto-activation of Bax was inhibited by Bcl-x_L when both proteins were added simultaneously to liposomes.

Another check of the ability of the fluorescently labelled Bax to form pores was done using GUVs (Fig. 5-2). In these experiments Bax-R (25 nM), Bax-G (25 nM), cBid (4 nM) and free dye Alexa 546 (1 µM) were added to the GUVs and the time series of images were taken to follow the GUV permeabilization. As a result Bax bound and permeabilized GUVs (Fig 5-2). Bax binding to the GUVs can be seen from the time-dependent increase in the fluorescence in the GUV membranes while permeabilization of GUVs can be seen from the filling of GUV lumen with free dye and with Bax (Fig. 5-2).
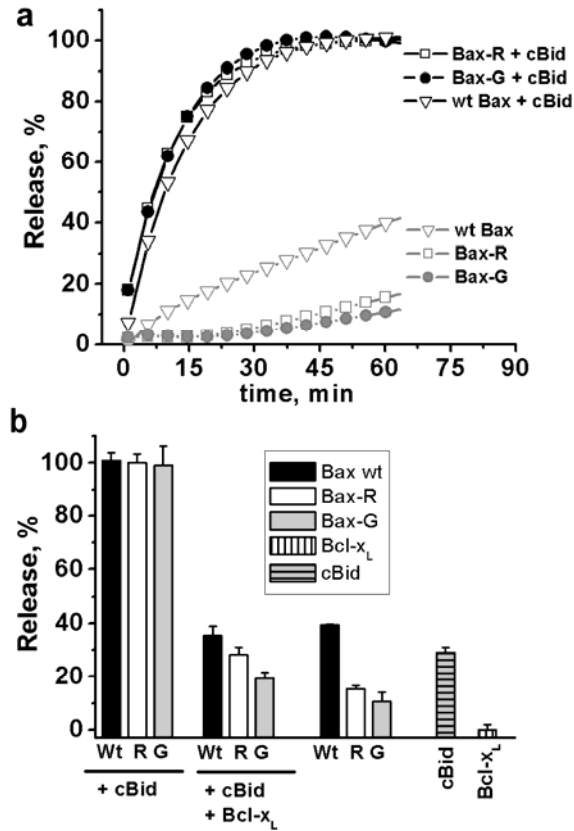
Figure 5-1. Assay of liposomes permeabilization by Bax. a. Kinetics of the carboxyfluorescein release from the liposomes. Each release curve is normalized and represents an average of three independent measurements. **b.** End point measurement of the % release 60 minutes after addition of indicated proteins to liposomes filled with carboxyfluorescein.

However, GUVs presented on Fig. 5-2 were not permeabilized simultaneously reflecting the stochastic nature of the Bax pore formation. Nevertheless, all the GUVs in the well were permeabilized by 45 min after addition of proteins to GUVs. Without activator protein, cBid, fluorescently labeled Bax did bind to GUVs but much weaker than in the presence of cBid (Fig. 5-3h). This result of low Bax-R and Bax-G binding to GUVs is

consistent with an observation of slow release of carboxyfluorescein from liposomes (Fig 5-1) suggesting that the fluorescently labeled Bax has some intrinsic activity[7].

We have also tested the effect of Bcl-x_L on Bax binding and permeabilization of GUVs (Fig. 5-3). In these experiments as expected Bcl-x_L prevented pore formation by Bax without inhibiting the ability of Bax to bind GUV membranes (Fig. 5-3f). However, when liposomes were initially preincubated with Bcl-x_L and cBid for one hour and then Bax was added no Bax binding to GUVs was observed, suggesting that Bcl-x_L when present in a lipid membrane inhibits Bax binding to the membrane[8]. Taken together, these results show that both fluorescently labelled Bax proteins can bind lipid membranes and form pores in liposomes and thus behave similarly to the wild-type full length Bax.
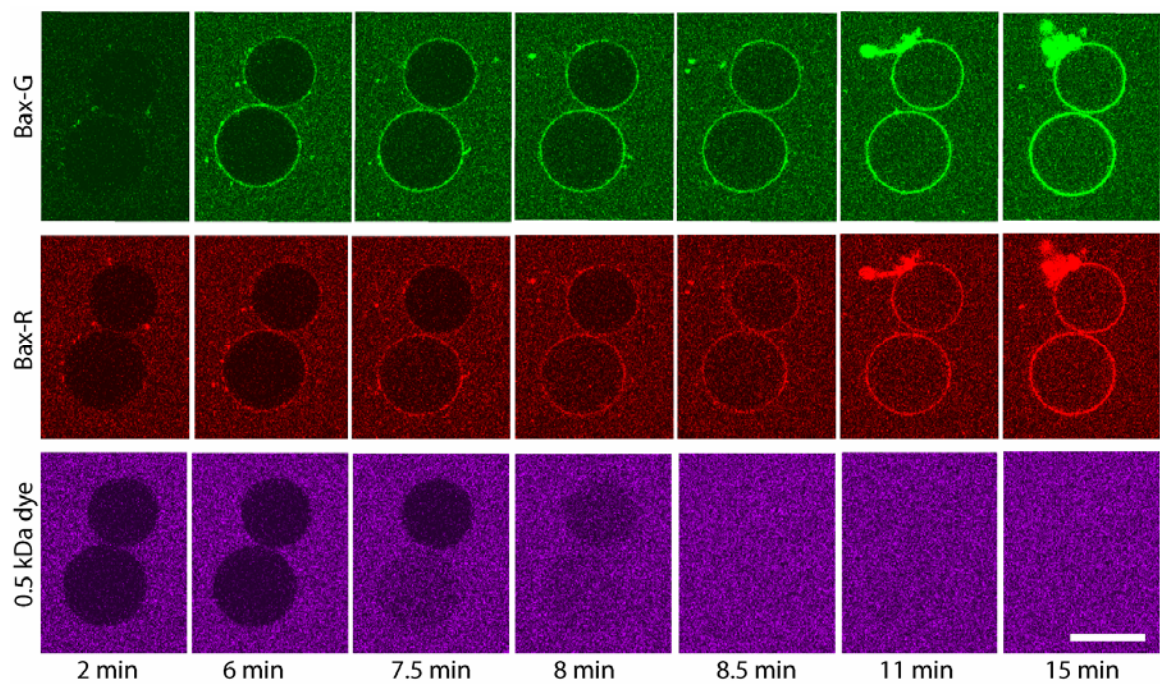
Figure 5-2. GUV permeabilization by Bax-R and Bax-G activated with cBid. Alexa 546 was used as a small soluble 0.5 kDa dye to follow the GUV permeabilization. Time stamps indicate time after protein addition to GUVs. Scale bar is 20 µm.
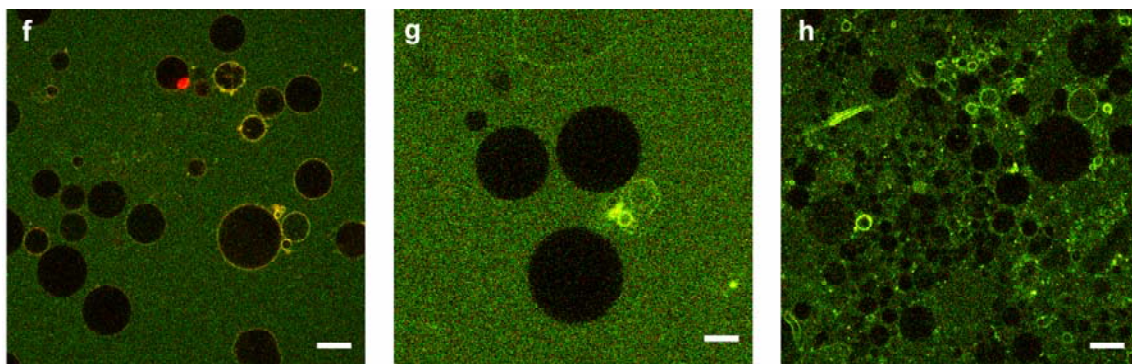
Figure 5-3. f. Bax binding to GUVs in the presence of Bcl-xL (50 nM) and cBid (4 nM). Bax-R and Bax-G total concentration is 50 nM. **g.** Bax does not bind GUVs preincubated for 60 minutes with 50 nM Bcl-xL and 4 nM cBid. **h.** Bax-R and Bax-G binding to GUVs in the absence of the activator cBid protein. In all images scale bar is 20 µm.

Bax changes morphology of GUVs

The ability of Bax to from pores in GUVs has been reported previously but not with the fluorescent protein or with the intent to characterize the evolution of membrane morphology upon prolonged interaction with Bax protein[9, 10]. Here, we used confocal microscopy to establish the effect of the fluorescently labeled Bax on GUVs and to establish the time window for the FCCS measurements. We determined that incubation with 50 nM Bax and 4 nM cBid allowed us to simultaneously observe the accumulation of fluorescent Bax in the GUV membrane and permeabilization of this membrane (Fig. 5-2) and that the GUVs were stable for 7 to 8 hours allowing FCCS measurements. However, after 24 hours this preparation became a mass of collapsed GUV remnants reflecting the multiple effects of Bax on membrane structure. After one hour of incubation with this Bax concentration, 100 % of GUVs were permeabilized and had homogeneous distribution of labelled Bax on the bilayer membrane. At the same time, in these experiments, Bax did not bind to all GUVs equally producing variation in the

fluorescence of Bax in GUV membranes representing a variation of Bax concentration in these membranes (Fig. 5-5). We hypothesize that this heterogeneity of Bax binding to GUVs results from the variation in cardiolipin content of the GUVs which is known to affect the Bax and cBid binding[11, 12] (See next section for discussion). After 3-4 hours of incubation with Bax and cBid the heterogeneity of Bax binding to GUVs was no longer visible suggesting Bax saturation in the lipid membrane of GUVs (Fig. 5-5a). Prolonged incubation of GUVs with these concentrations of Bax and cBid leads to major morphology changes in the GUVs (Fig. 5-3a-d). GUVs change their shape from spherical to potato-like and tubule-like shape reflecting the Bax induced changes in the elastic coupling to lipid bilayer forces in membranes. Additionally, we observed formation of gigantic Bax mega-pores (See Chapter 6) and other large visible Bax aggregates in GUV membranes (Fig. 5-4b). During incubation with Bax occasional GUVs rupture onto smaller liposomes (Fig. 5-4e) and by the 24 hours of incubation with Bax almost no GUVs are left in the observation chamber. This clearly defined the time period when these GUVs could be studied by FCCS. The Bax binding to GUVs and consequent deformation and rupture of GUVs is dependent upon the Bax concentrations demonstrating that mass action and thermodynamics governs this process. Although all of the GUVs were permeabilized by one hour, the membrane density of Bax particles was not sufficient for the FCCS measurements until 30 to 40 minutes, and, therefore, the early pore formation was not accessible to these studies.
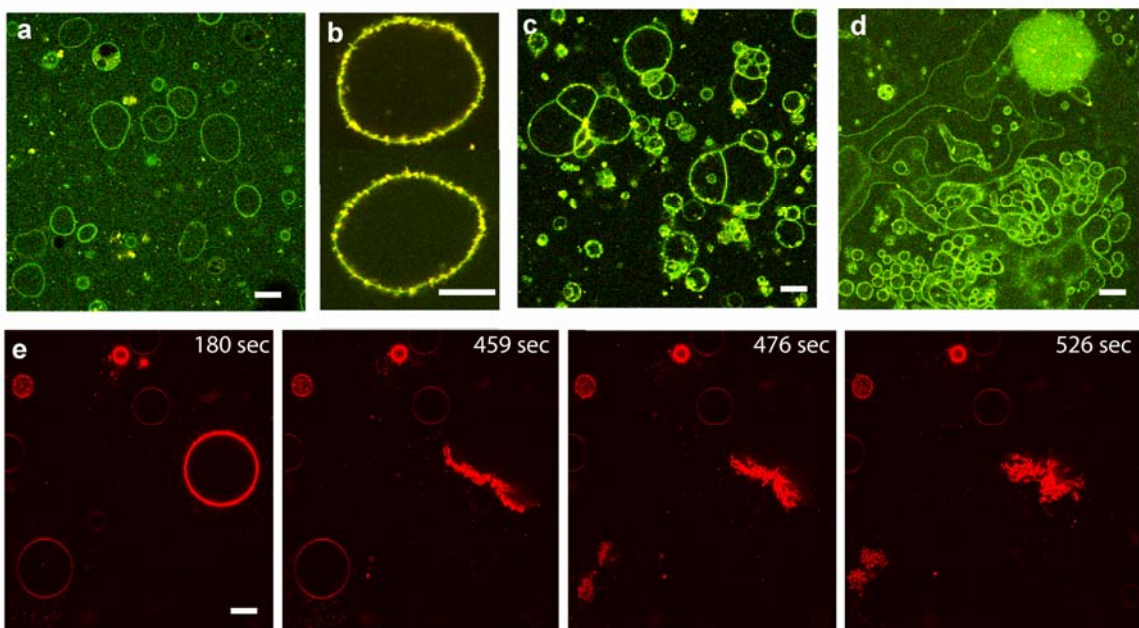
Figure 5-4. Bax binding to GUVs: confocal microscopy images. a. ….**b.** Aggregates of Bax in GUV membranes. **c.** Agglomeration of GUVs after four hours of incubation with Bax. **d.** Formation of tubule-like lipid membrane structures after 7-8 hours of incubation with Bax. **e.** Rupture and collapse of GUVs upon Bax addition. Time steps represent the time after Bax addition. In all images scale bar is 20 µm.

Heterogeneity of Bax binding to GUVs

For all the experiments presented in Chapters 5, 6 and 7 of this dissertation, the lipid composition of GUV was DOPC:bovine heart cardiolipin (80:20 mol%). Assuming homogeneous distribution of lipids among GUVs during electroformation we expected homogeneous Bax binding to GUVs. However, we observed wide variation in the amount of Bax binding to GUVs electroformed from the same lipid mixture (Fig. 5-5a). We hypothesize that the heterogeneity of Bax binding to GUVs is based on the heterogeneity of lipid distribution among GUVs during the electroformation (See Appendix IV for the detailed description of the method). In particular, we hypothesize that the heterogeneity comes from un-equal distribution of cardiolipin among the GUVs. Cardiolipin is known

for its ability to promote non-lamellar lipid bilayer formation (i.e. lipid bilayers with high curvature) and in our GUV preparations with 80:20 mol% of DOPC:cardiolipin we observe formation of both unilamellar and multilamellar vesicles (Fig. 5-5b), with the multilamellar vesicles showing high curvature regions. We hypothesize that these multi-lamellar vesicles contain higher concentration of cardiolipin than the rest of the vesicles from the same GUV preparation. However, we do not have a direct way to measure the cardiolipin concentration in these vesicles.
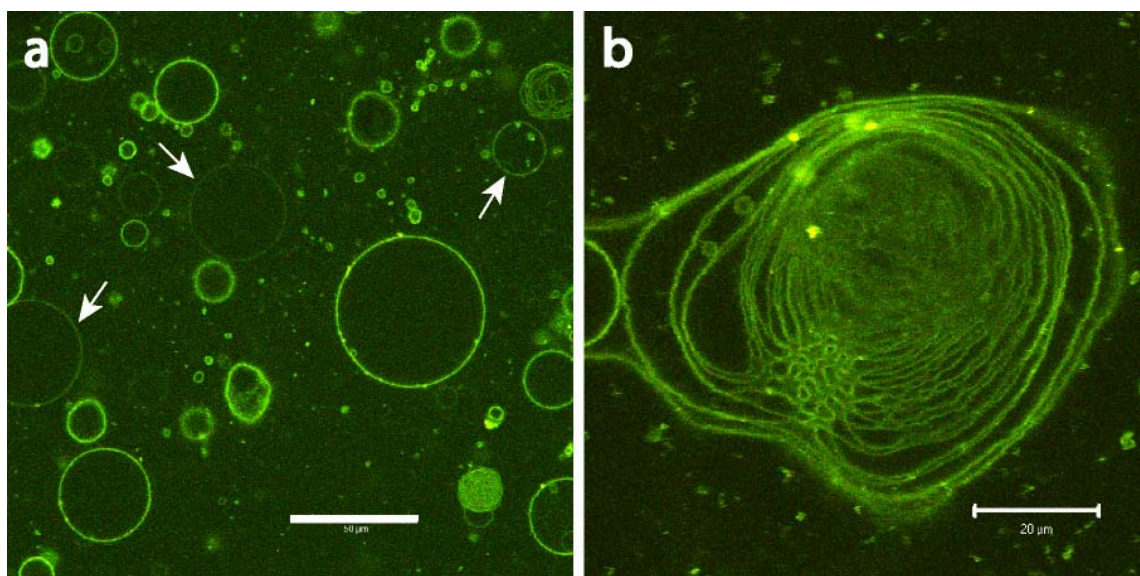
Figure 5-5. Heterogeneity of Bax binding to GUVs. GUVs were prepared by electroformation from DOPC:CL (80:20 mol%) and added to the solution containing Bax-R (50 nM), Bax-G (50 nM) and cBID (10 nM). The confocal image was taken approximately 30 minutes after mixing. The confocal image is an overlay of red and green channels corresponding respectively to Bax-R and Bax-G. **a.** Confocal image of the field view of multiple GUVs with the fluorescently labeled Bax bound. Scale bar is 50 µm. **b.** Confocal image of a giant multilamellar vesicle containing high concentration of the bovine heart cardiolipin which resulted in the production of high curvature in the portions of this vesicle. Scale bar is 20 µm. Images a and b were taken in the same chamber, indicating that these vesicles were from the same preparation and were exposed to the same concentration of the fluorescent Bax and cBid.

Bax and detergents produce similar morphological changes in GUVs.

In addition to permanent transformations of GUV morphology shown in Figure 5-4, we have observed transient changes in GUV morphology upon Bax binding (Fig. 5-6). These transient morphological changes included endocytosis like events, where thransforamtion of the GUV membrane resulted in the formation of smaller daughter vesicles inside the original vesicle (Fig. 5-6a), and fission like events, where GUV disintegrated into a number of smaller vesicles (Fig. 5-6b). Similar morphological transformations have been observed when sub-CMC concentration of n-octylglucoside detergent was added to GUVs (Fig. 5-7). This apparent similarity in the shape transformation of GUVs in the presence of detergents and in the presence of Bax, which have never been exposed to detergents, suggests that Bax acts as a detergent during binding to lipid membranes. When detergents bind lipid membranes changes in the mechano-elastic properties of membranes have been observed, thus we can stipulate that Bax can change mechano-elastic properties of lipid membranes similar to detergents.
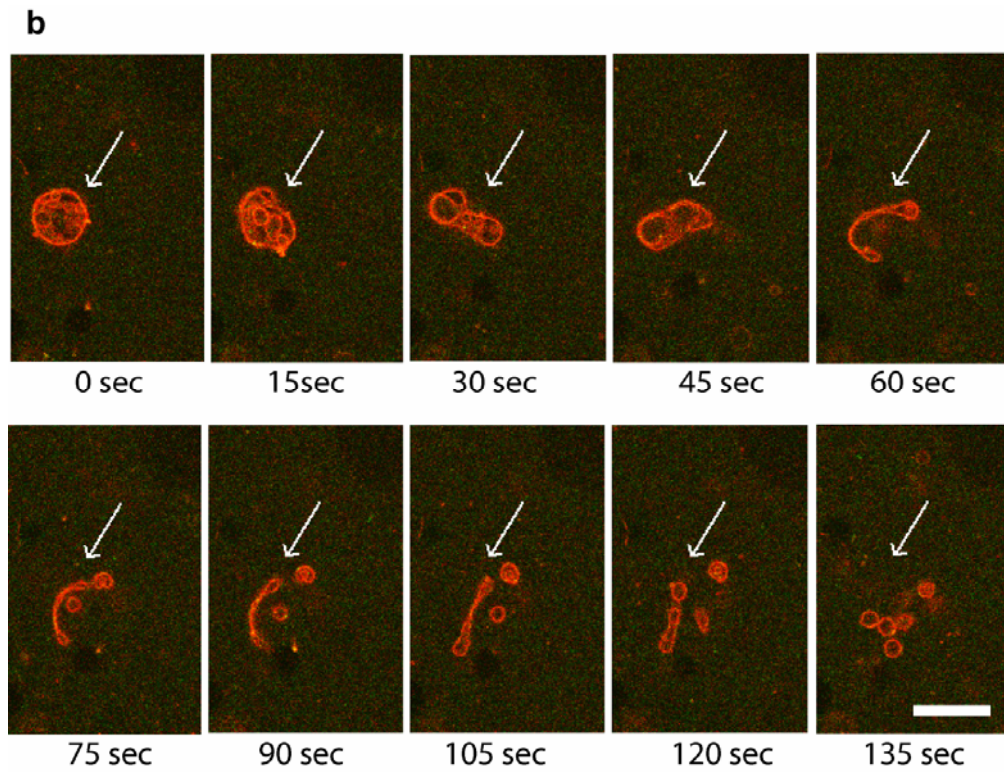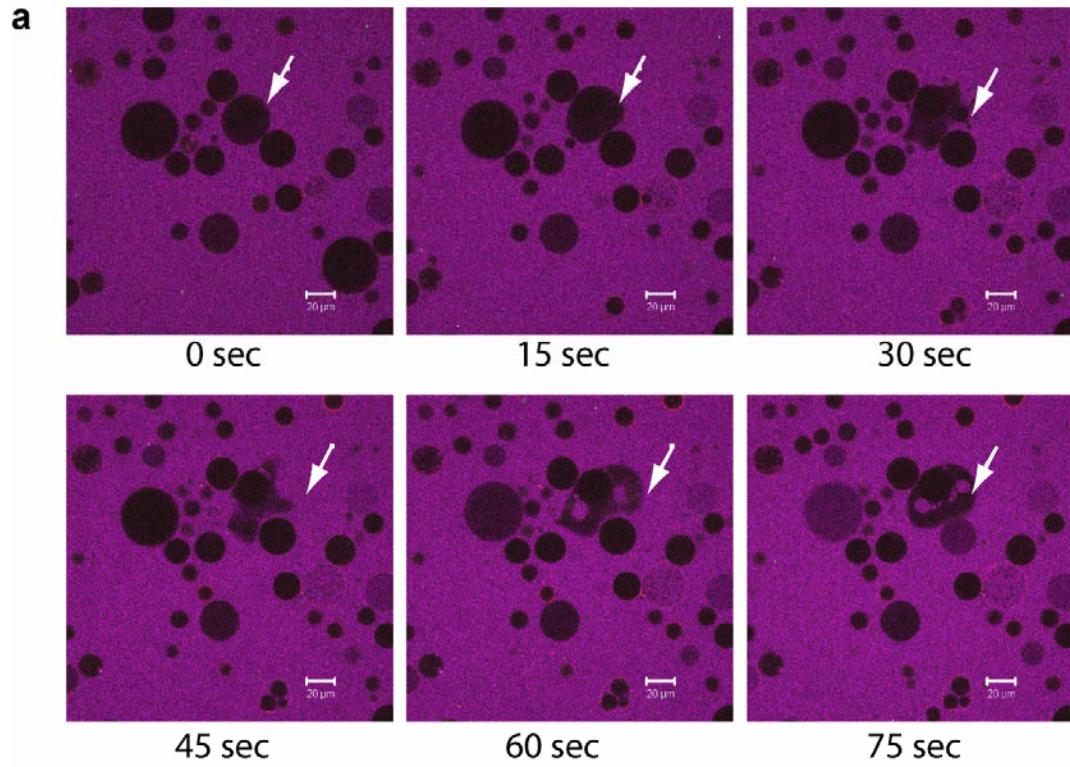
Figure 5-6. Transformation of GUV shapes upon Bax binding.
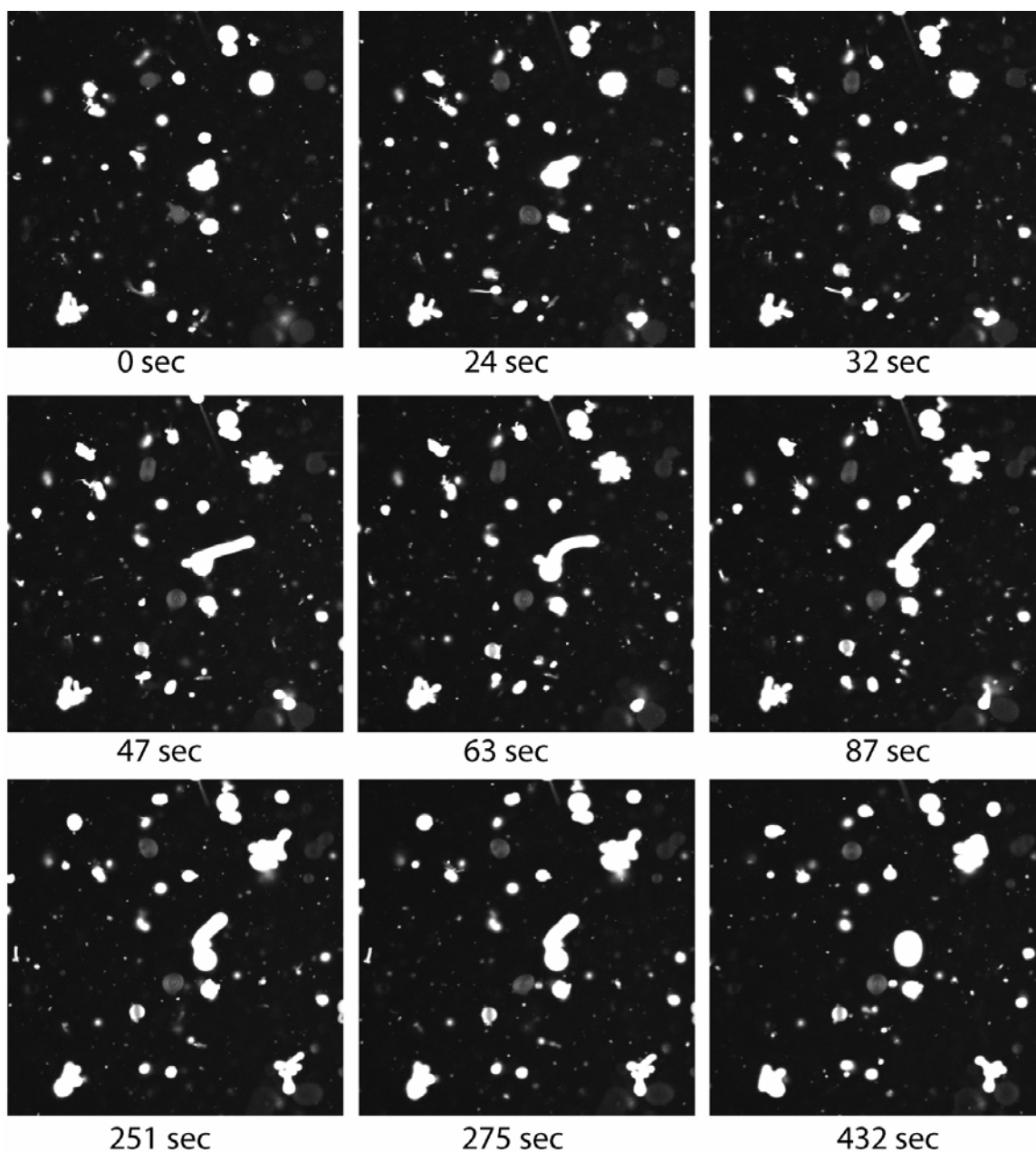
Figure 5-7. Transformation of GUV shapes upon the addition of n-octylglucoside detergent. Time stamps indicate time since the beginning of the observation, which occurred 10-15 sec upon the detergent addition.

Conclusion

Described above confocal microscopy studies of the effects of Bax onto the morphology of GUVs were undertaken with the goal of determining the feasibility and the experimental conditions for the FCCS measurements of Bax diffusion and self-assembly in GUV membranes. As a result of these studies we determined that GUVs can be used as a source of free-standing lipid membranes in the FCCS experiments and that addition of 50 nM Bax and 4 nM cBid result in sufficient for the FCCS measurement amount of Bax accumulated in GUV membranes. In addition, for these Bax and cBid concentrations it was determined that GUVs maintain spherical shape and do not collapse for a period of 4-7 hours which is suitable for FCCS measurements. In addition, the functionality of the two forms of the fluorescently labelled Bax, Bax-R and Bax-G, have been tested for their ability to form pores in LUVs and GUVs indicating that Bax-R and Bax-G can form pores in liposomes similar to the wild-type Bax.

Experimentals

Protein preparation, labeling and functionality check. Human cDNA for Bax, Bid and Bcl-x$_L$ were subcloned into pTYB1 vector (New England Biolabs). For production of the fluorescently labeled Bax two endogenous cysteines of Bax were substituted (C62S, C126A) and additional cysteine was engineered, S4C. All proteins were expressed in BL21(DE3) *E. coli*, and purified as an intein/chitin-binding domain fusion protein without use of detergents (See Appendix V for details). Purified proteins were estimated to be > 95% pure by Coomassie staining SDS-PAGE gels and stored at 4 °C. Bid was cut with recombinant caspase 8 to produce cBid. Mutant Bax with single cysteine was

labeled according to the manufacturer's protocol with Alexa Fluor 488 maleimide (Invitrogen) and Atto 655 maleimide (AttoTech). Functional comparison of the fluorescently labeled Bax to the wild-type Bax was done using carboxyfluorescein assay from liposomes (See Chapter 3 for the method description).

Preparation of giant unilamellar vesicles. GUVs were prepared by the electroformation method[13] from a lipid mixture containing 80 mol% of 1,2-dioleoyl-sn-glycero-3-phosphocholine (DOPC from Avanti Polar Lipids) and 20 mol% of bovine heart cardiolipin (Avanti Polar Lipids). For the detailed protocol of GUV preparation see Appendix IV. For the confocal microscopy observation 50 µl of solution containing GUVs was transferred into a Lab-Tek observation chamber (Fisher Scientific) containing 450 µl of 10 mM HEPES, pH 7.2, 100 mM KCl and a mixture of Bax, cBid and Bcl-x$_L$.

Confocal Microscopy was performed at 22 °C on a laser-scanning confocal microscope Meta 510 system (Carl Zeiss) using 40× NA 1.2 UV-Vis-IR C Apochromat water-immersion objective. For excitation the 488 nm line of an Argon-ion laser (25 µW) and the 633 nm line of the HeNe laser (15 µW) were used. Collection and processing of images was done using Zeiss software provided with the microscope (AIM, version 4.2).

References

1.   Basanez, G. et al. Bax, but not Bcl-xL, decreases the lifetime of planar phospholipid bilayer membranes at subnanomolar concentrations. Proc Natl Acad Sci U S A 96, 5492-7 (1999).

2.   Garcia-Saez, A. J., Chiantia, S. & Schwille, P. Effect of line tension on the lateral organization of lipid membranes. J Biol Chem 282, 33537-44 (2007).

3.   Van Mau, N., Kajava, A. V., Bonfils, C., Martinou, J. C. & Harricane, M. C. Interactions of Bax and tBid with lipid monolayers. J Membr Biol 207, 1-9 (2005).

4.   Schwille, P., Meyer-Almes, F. J. & Rigler, R. Dual-color fluorescence cross-correlation spectroscopy for multicomponent diffusional analysis in solution. Biophys J 72, 1878-86 (1997).

5.   Ivashyna, O. et al. Detergent activated BAX protein is a monomer. J Biol Chem 284, 23935-46 (2009).

6.   Saito, M., Korsmeyer, S. J. & Schlesinger, P. H. BAX-dependent transport of cytochrome c reconstituted in pure liposomes. Nat Cell Biol 2, 553-5 (2000).

7.   Tan, C. et al. Auto-activation of the apoptosis protein Bax increases mitochondrial membrane permeability and is inhibited by Bcl-2. J Biol Chem 281, 14764-75 (2006).

8.   Billen, L. P., Kokoski, C. L., Lovell, J. F., Leber, B. & Andrews, D. W. Bcl-XL inhibits membrane permeabilization by competing with Bax. PLoS Biol 6, e147 (2008).

9.   Schlesinger, P. H. & Saito, M. The Bax pore in liposomes, Biophysics. Cell Death Differ 13, 1403-8 (2006).

10.   Dejean, L. M., Martinez-Caballero, S., Manon, S. & Kinnally, K. W. Regulation of the mitochondrial apoptosis-induced channel, MAC, by BCL-2 family proteins. Biochim Biophys Acta 1762, 191-201 (2006).

11.   Kuwana, T. et al. Bid, Bax, and lipids cooperate to form supramolecular openings in the outer mitochondrial membrane. Cell 111, 331-42 (2002).

12.   Schafer, B. et al. Mitochondrial outer membrane proteins assist Bid in Bax-mediated lipidic pore formation. Mol Biol Cell 20, 2276-85 (2009).

13.   Angelova, M. I. & Dimitrov, S. D. Liposome electroformation. Faraday Discuss. Chem. Soc. 81, 303-311 (1986).

CHAPTER 6

"Bax Mega-Pore: Line Tension Measurement"

Introduction

The size of the Bax pore has become a controversy in the field of apoptosis. In fact, the Bax pore has not been observed *in vivo* by electron microscopy in mitochondria of cells undergoing apoptosis, where Bax appears to aggregate at the fission sites on the surface of the OMM[1]. Nonetheless, *in vitro* studies using electrophysiology and pore-sizing techniques have shown that Bax forms pores of 2-5 nm in diameter[2-6], while electron microscopy and AFM revealed the formation of 100-200 nm disruptions in liposomes and supported lipid bilayers incubated with Bax[7, 8]. In light of this controversy about the size of a Bax pore, the finding of the formation of 5-20 μm in diameter Bax mega-pores support the hypothesis that Bax is able to form pores of various sizes[9].

In addition to extremely large diameters, Bax mega-pores also exhibited uncommonly long life times ranging from 10 min to hours. Based on the life time and size, these Bax mega-pores are very similar to the giant pores formed in GUVs by detergents or by the physical disruption of GUVs[10-15]. The latter two types of giant pores can be differentiated on the basis of the magnitude of the force responsible for closing a pore – the line tension[10, 16]. The line tension is the energy per unit length of the membrane contour at the pore edge, and it arises due to the exposure to water of the hydrophobic lipid tails in the rim of the pore. The line tension is the highest in the giant pores opened by physical disruption (10-20 pN)[10, 15], and it is two orders of magnitude lower in the giant pores stabilized by detergents (0.2 pN)[10]. Therefore, in order to characterize the Bax mega-pores with respect to the other two known types of giant pores, we used an established microscopy technique to measure the line tension in the rim of the Bax mega-pore, which turned out to be two orders of magnitude lower than the line tension in the

rim of a detergent stabilized giant pore. Furthermore, using this line tension measurement together with other knowledge about the Bax interaction with lipid membranes, we propose a model of the formation, existence and closure of the Bax mega-pores.

Results and Discussion

Bax forms longed lived mega-pores in GUVs

While using confocal microscopy to study Bax-R and Bax-G binding to GUVs in the presence of cBid, we were intrigued by the formation of giant Bax pores which we named Bax mega-pores (Fig. 6-1, 6-2). These pores ranged from 5-20 μm in diameter, appeared within 10 minutes of Bax addition to GUVs, and were extremely stable, with life times of 8 minutes up to many hours. Interestingly, all observed Bax mega-pores had increased Bax concentration in the rim of the pore, which did not expand or led to GUV collapse[17]. Although the mega-pores usually closed over the observation period of 1-2 hours, the presence of a simple obstacle in the pore closure path, *e.g.* another liposome, was observed to arrest the closure process (Fig. 6-1c). For comparison, an impedimentary lipid vesicle present in the closure path of a giant pore opened by the stimulation with visible light was cut into two vesicles when the pore closed[10]. This observation shows that Bax reduces the line tension in the pore rim, thus resulting in the arrest of the pore closure by an impedimentary vesicle. Nonetheless, in GUVs where Bax mega-pore did close, the fluorescent Bax concentrated at the rim of the pore dispersed over the GUV surface producing a homogeneous Bax fluorescence signal. Additionally, GUVs which have gone through the process of the mega-pore formation and closure did not have another mega-pore open and appeared to be stable for hours afterwards.
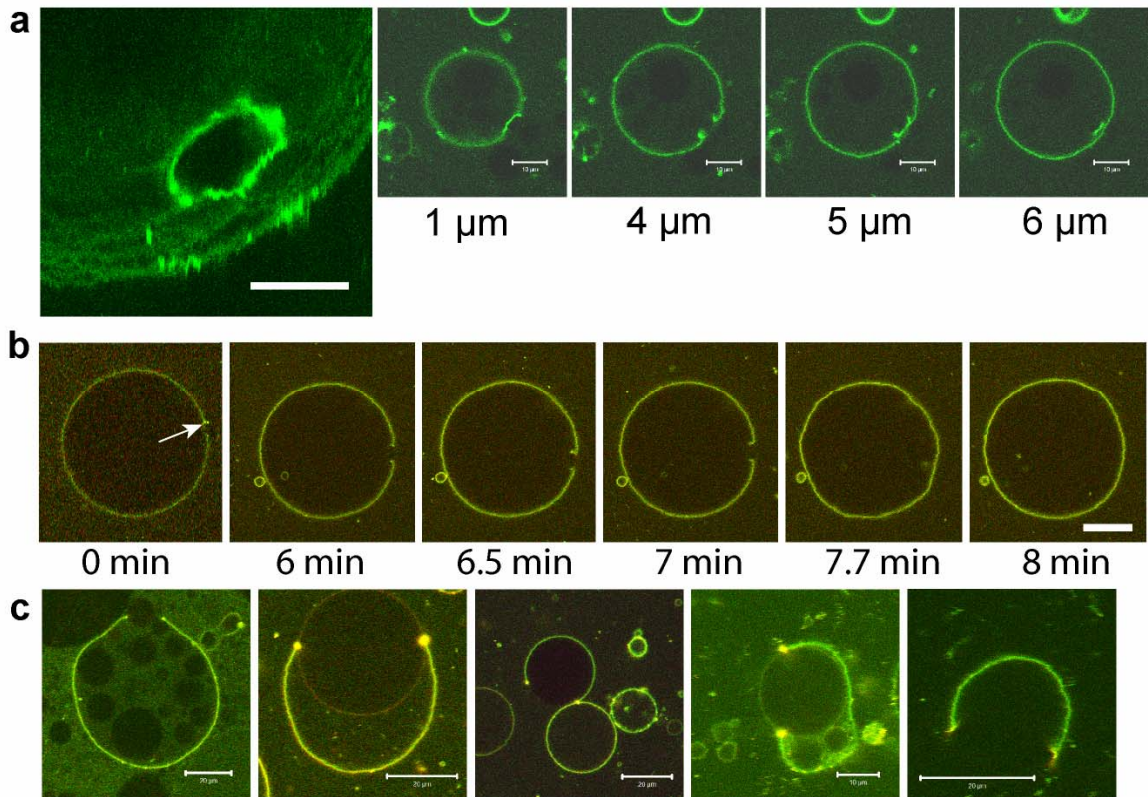
Figure 6-1. Bax mega-pore. a 3D reconstruction of the Bax mega-pore shown together with the confocal images used to produce this reconstruction. Values in μm indicate distance from the coverslip surface. **b.** Time series of opening, existence and closure of the Bax mega-pore. Arrow in the first image indicates the position at which mega-pore will open. Time stamps represent time since the opening of the pore. **c.** Other examples of giant Bax mega-pores.
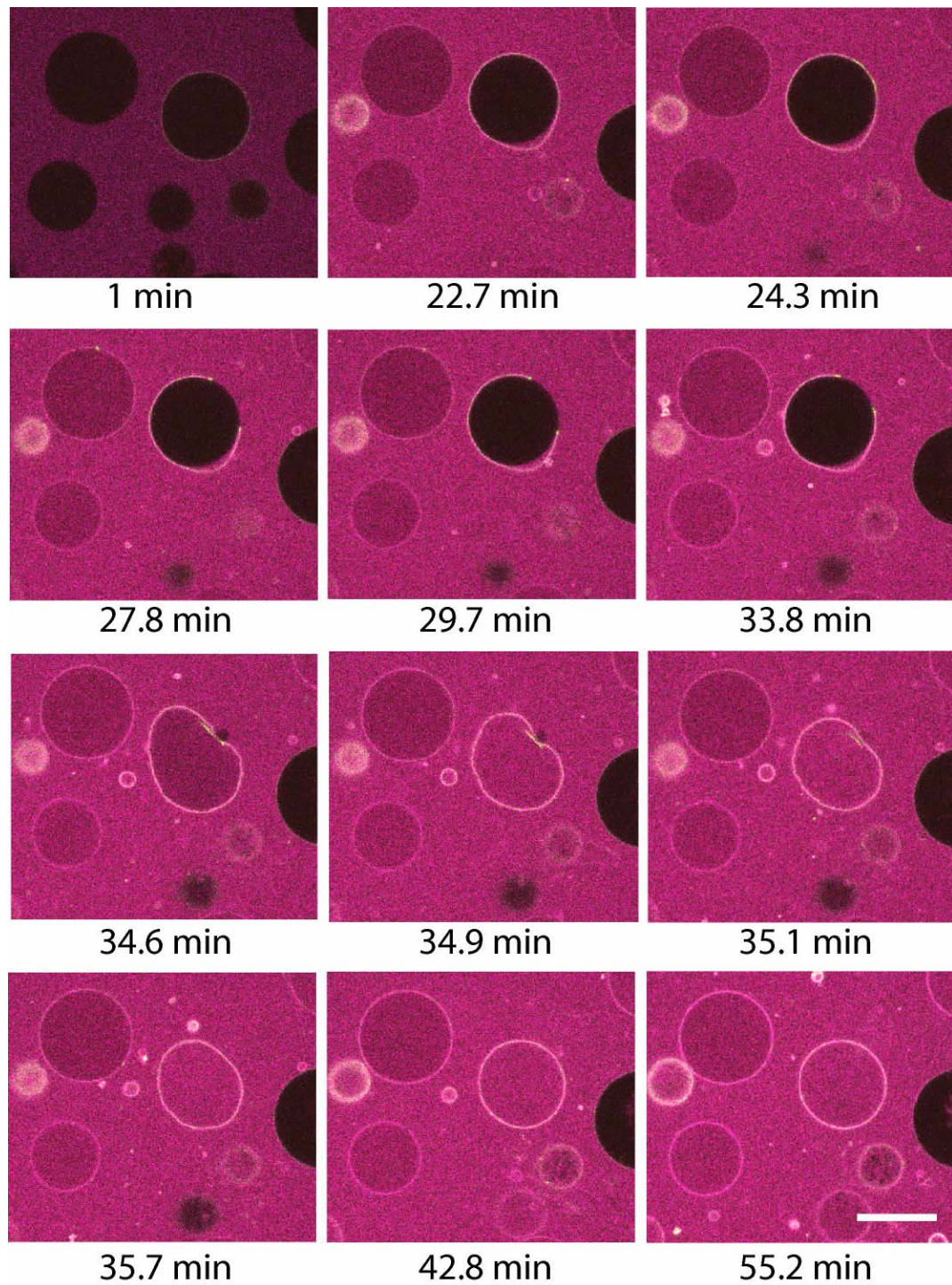
Figure 6-2. Time series of the opening and closure of a Bax mega-pore. These confocal images represent an overlay of three channels: red (Bax-R), green (Bax-G) and pink (Alexa 546). Time stamps indicate time after protein addition to GUVs. Scale bar is 40μm**.**

Size distribution of Bax mega-pores.

To determine whether there exists correlation between the size of a Bax mega-pore and the size of a GUV, we performed the Pearson's correlation test. In this test we compared the distribution of the diameters of the Bax mega-pores with the diameter of corresponding GUVs (Fig. 6-3). As a result only weak correlation was found between these two sets of values (with the Pearson correlation coefficient of 0.25). The maximum value for the Pearson correlation coefficient is 1, and it corresponds to the direct positive correlation between the two sets of values, i.e. increase in the value of one data set will lead to linear increase in the values of the other data set.

a   **b**
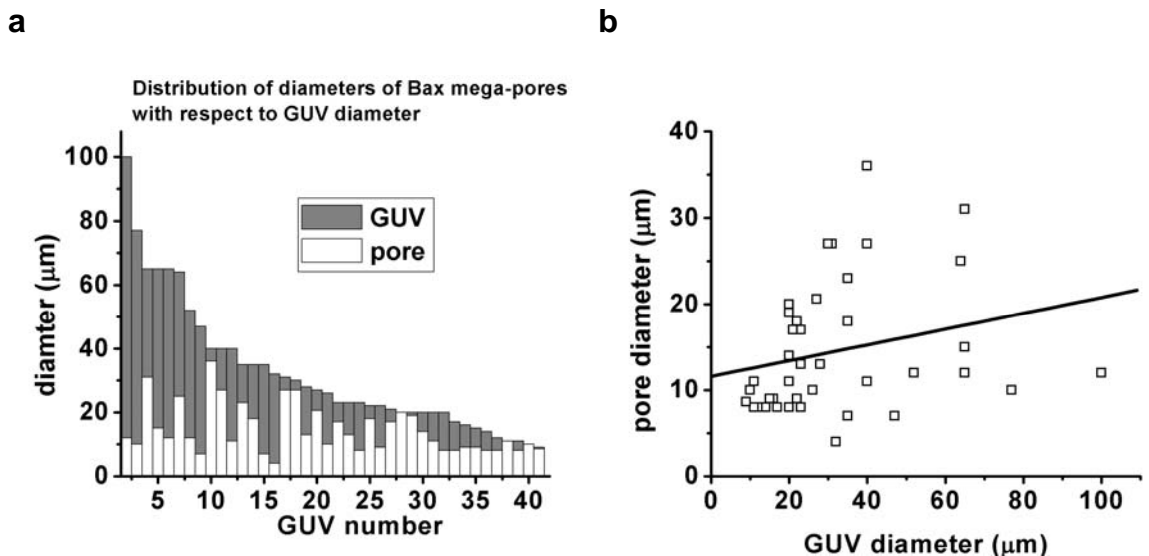
Figure 6-3. Size distribution of Bax mega-pores. a. Bar plot of GUV diameter (gray) and corresponding diameter of a Bax-mega pore (white). Data from 44 GUVs is presented. **b.** Same data as in **a** but plotted as a distribution on Bax mega-pore diameter versus the GUV diameter. As an additional evidence of weak correlation between the two data sets the linear fit of this data shown as a line (R=0.25).

Weak correlation between the diameter of a GUV and the diameter of a Bax mega-pore present in this GUV suggest that the Bax mega-pore formation is a stochastic process which most likely depends on the physical properties of the GUV membrane (i.e. elasticity and bending rigidity etc.). These physical properties of GUV membranes depend directly on the lipid composition of membranes. In Chapter 5 the heterogeneity of cardiolipin distribution among GUVs during the electroformation was discussed, and correlated with the heterogeneous binding of Bax to GUVs. Based on this, it can be concluded, that one of the reasons for the weak correlation between the diameters of Bax mega-pores and GUVs in which they occur is due to heterogeneous lipid distribution among GUVs. We can also speculate, that the other reason for the weak correlation can be the fact that Bax mega-pores formed in GUVs larger than 50μm in diameter destabilize the GUV leading to its collapse (data not shown) which results in a skewed distribution of the Bax mega-pore diameters with GUV diameter. Finally, we should mention that the diameter values for this analysis were collected from a number of confocal images corresponding to the various experiments where concentration of the fluorescently labeled BAX was varied.

Analysis of the line tension in the rim of Bax mega-pore

Kinetics and thermodynamics of giant pores in GUVs can be explained by theoretical models [10, 13] where the energy E_r of a pore of radius r can be described as

$$E_r = 2\pi r \Gamma - \pi r^2 \sigma \qquad \text{(Eqn. 1)}$$

where, Γ is the line tension while σ is the surface tension. Interplay between line and surface tension allows opening, existence and closure of giant pores in GUVs. Following

146

model of Borchard-Wyart *et al.*[14] the life of a pore in a GUV can be described in four steps: (i) pore opens due to the increase of the membrane surface tension (σ) which can be induced by application of an electrical field[11, 18], or by insertion of molecules with non-zero spontaneous curvature such as detergents[10], or by the insertion of the Bax-derived α5 peptide [19]; (ii) while surface tension term in Equation 1 is larger than the line tension term the pore expands to some critical radius (r_c); (iii) while the surface tension and line tension terms in the equation 1 are equal (i.e. pore energy $E_r = 0$) the pore exists in unstable equilibrium state; (iv) when the line tension begins to increase the pore begins to close. Using this theoretical framework the line tension in the rim of the pore during the pore closing stage can be calculated using

$$k = -\frac{2\Gamma}{3\pi\eta} \qquad \text{(Eqn. 2)}$$

where, k is the slope of the $R^2 \ln(r)$ versus time plot and η is the solution viscosity (1.035×10^{-3} Pa·s for 30 mM sucrose solution), R is the radius of a GUV containing a pore of radius r. Examples of the evolution of the radius (r) of Bax mega-pore for three GUVs are shown in Figure 6-4. From these three plots we estimate the line tension in the rim of the Bax mega-pore to be 3.7±1.7 fN which is four orders of magnitude lower than the line tension of a pore opened by the intense illumination in a DOPC vesicle ($\Gamma = 20.7 \pm 3.5$ pN)[10] and two orders of magnitude lower than the line tension of a detergent stabilized giant pore (0.2 pN).

The ability of the Bax to reduce the line tension of artificial lipid membranes have been reported previously but without a direct measurement of the line tension[20]. Here, we measured the line tension in the rim of the Bax mega-pore to be 3.7±1.7 fN which is two

to four orders of magnitude lower than the line tension in the rim of detergent stabilized or mechanically opened pores respectively. It is hypothesized, that the reason for the ability of the cone-shaped detergents to reduce the line tension in giant lipid pores is based on their propensity to partition to the high curvature regions in the edge a pore[10, 16] (Karatekin, May 2000 others). Therefore, the ability of Bax to reduce the line tension lower than that of detergents indicates that Bax is a remarkable protein designed by evolution to stabilize edges of lipid membranes.

Interestingly, the line tension generated by the full length Bax proteins is three orders of magnitude lower than the line tension generated by the pore-forming α5 peptide of Bax in a supported lipid bilayer ($\Gamma = 3.8\pm0.4$ pN)[19]. The lower line tension value measured in the presence of the full length Bax protein indicates that the full length protein is able to stabilize the pore edge more efficiently than a single alpha helix of Bax indicating an additional role for the non-pore forming alpha helices of Bax. Previously the non-pore forming helices of Bax were given two major roles in the function of Bax: first, to prevent the pore-forming helices of Bax (α5 and α 6) from harming the cell by forming pores in various membranes; and second, to facilitate the communication between Bax and other proteins involved in the apoptosis decision such as BH3 domain interactions etc.

The life time of Bax mega-pore

The life time of a lipid pore in DOPC vesicle immersed in water solution is estimated to be 10-200 msec, and it can be extended by increasing the viscosity of solution[13]. Therefore, 66 % glycerol solution which has 30 times higher solution viscosity
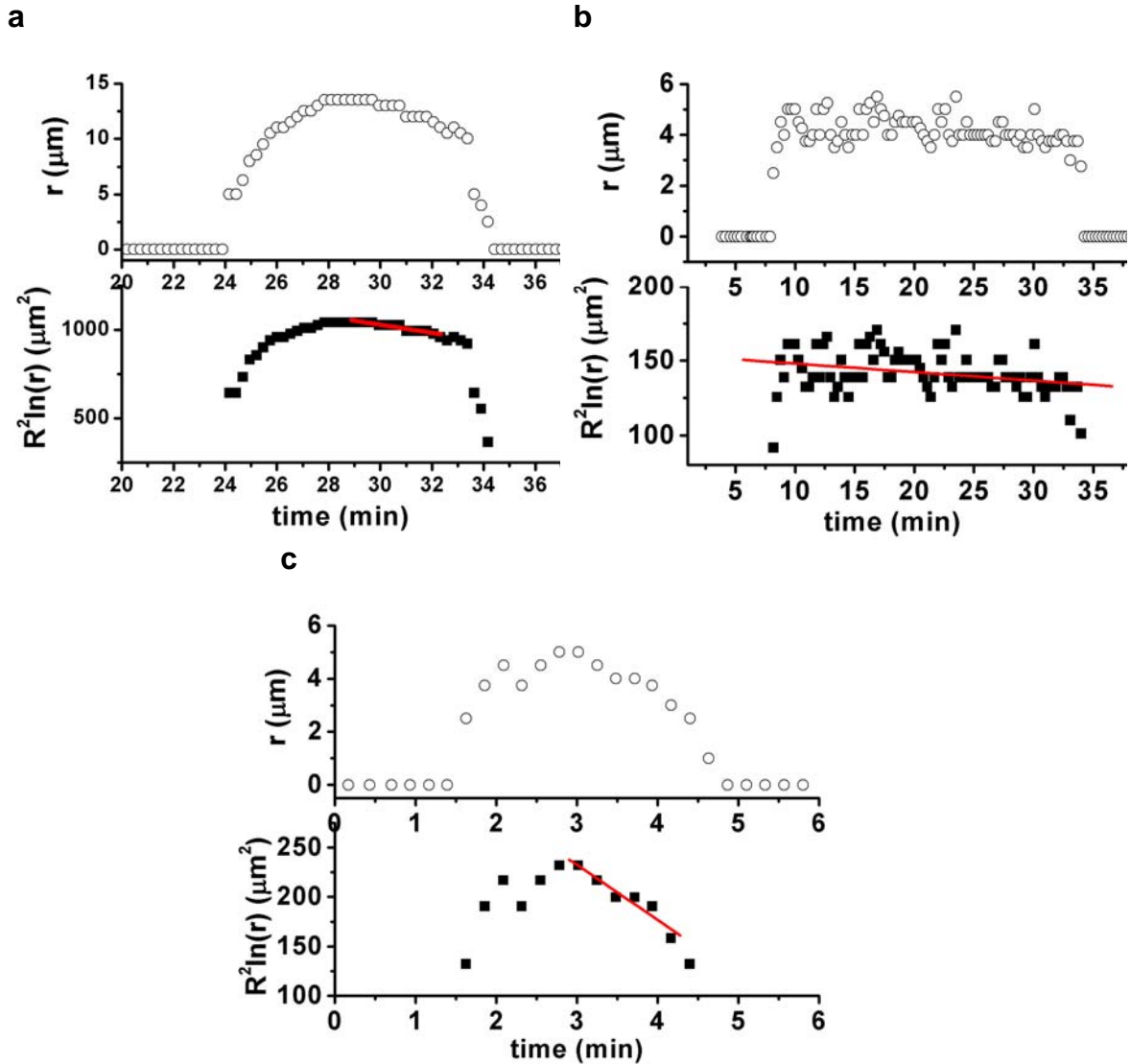
Figure 6-4. Plots of the evolution of the radius of Bax mega-pore with time. GUVs were mixed with 30 nM Bax-G, 25 nM Bax-R and 4 nM cBid. Movies of the Bax-R and Bax-G binding to GUVs as well as transformation of GUVs were taken immediately upon mixing. **a.** GUV initial radius was 40 μm while the slope of the $R^2 \ln(r)$ during the pore closing is $k = -22.8 \pm 2.5$ μm^2/sec. The opening and closing of a pore for this particular GUV is shown in Supp. Movie 1. **b.** GUV initial radius was 20 μm while the slope of the $R^2 \ln(r)$ during the pore closing is $k = -0.57 \pm 0.19$ μm^2/sec. **c.** GUV initial radius was 20 μm, while the slope of the $R^2 \ln(r)$ during the pore closing is $k = -0.93 \pm 0.14$ μm^2/sec.

than water is commonly used to measure the life time of giant lipid pores[10, 12, 14]. The reported life time of giant pores in glycerol ranges from seconds for the lipid pores opened by a physical method to minutes for lipid pores stabilized with detergent[10] while the life time of Bax mega-pores is measured in water solution and ranges from 8 min to many hours. Hence, if the life time of all tree types of giant pores is compared in the same solution, the Bax mega-pore will have the longest life time, which is explained by the extremely low line tension measured in the rim of this pore.

Proposed model of the Bax mega-pore formation, existence and closure

We propose the following mechanism for Bax mega-pore opening, existence, and closure based on a GUV shown in Figures 6-1b and 6-2. In this mechanism Bax inserts into a lipid membrane from the outside of a GUV and transforms from a globular soluble protein[21] to a membrane integrated protein with proposed extended structure shallowly inserted into the membrane[22] (Fig. 6-5a). This produces a dramatic area increase in the outer membrane leaflet while the area of the inner leaflet remains unchanged (Fig. 6-5b). The localized area difference of the two membrane leaflets induces curvature frustration and increase in the surface tension of the membrane[23, 24] ($\Delta\sigma > 0$). When surface tension increases to a critical value the membrane structure ruptures and the mega-pore is formed. Once the pore is formed its line tension provides a force for reclosure of the mega-pore which counteracts the surface energy such that GUV continues to exist and does not collapse (See also Eqn. 1). However, now through the open mega-pore soluble Bax is able to accumulate in the lumen of the GUV and insert into the inner leaflet of the GUV membrane. This results in the area increase of the inner leaflet leading to the

150

increase in surface tension in this leaflet. Meanwhile, membrane Bax has accumulated in the rim of the pore, reducing line tension and decreasing the rate of pore closure as surface energy of the inner and outer leaflets equilibrate (Fig. 6-2b). As a result the Bax
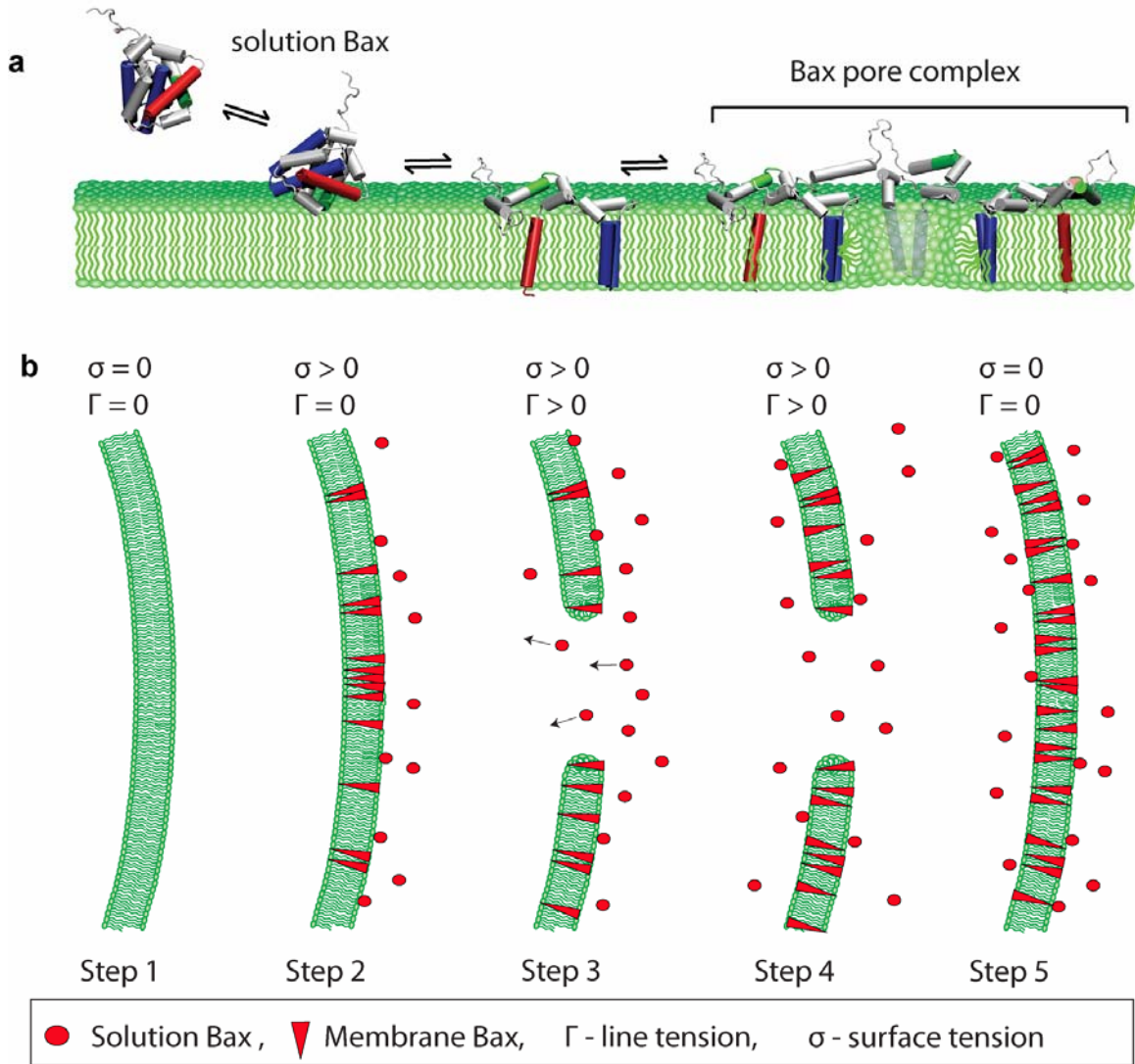
Figure 6-5. Model of Bax interaction with lipid membranes. a. Schematic of Bax binding, integration and oligomerization in a lipid membrane. **b.** Proposed mechanism of the Bax mega-pore opening and closure.

mega-pore closes very slowly over tens of minutes even though the surface energy of the two leaflets is the same. After the pore closure Bax in the form of monomers or small oligomers diffuses away from the position where the membrane resealed such that within seconds after pore closure no heterogeneities are observed on the GUV surface.

Bax mega-pore: connection to physiology

It is clear that the Bax mega-pore structures we observed in GUVs can not occur *in vivo* simply due to their size (5-20 μm) versus the size of mitochondria (0.2-1 μm). Furthermore Bax mega-pores scaled for the smaller size of mitochondria would also need to be scaled for the reported localization of Bax to the fission sites[1]. Finally, the simple lipid composition of GUVs (DOPC:cardiolipin, 80:20 mol %) compared to the complexity of mitochondrial outer membrane and the heterogeneous distribution of lipids and proteins on the mitochondrial surface all limit the space available for Bax pore formation to a submicroscopic size. Therefore, on the mitochondrial surface Bax has a limited membrane area to form a protein-membrane complex, while on the surface of GUV membrane the area available to Bax is many times greater and can generate the mega-pores that we observed.

Conclusion

The existence of microscopic Bax mega-pores further supports the hypothesis that Bax can form a variety of pore sizes in artificial lipid membranes and that the Bax pore is a lipidic pore stabilized by the presence of the Bax protein in the pore rim[5, 20]. The

accumulation of Bax in the pore rim not only reduces the line tension to extremely low values but it also leads to the increase of the pore life time.

Bax is not the first protein which is reported to form giant pores in GUVs. For example, protein talin and other FERM domain containing proteins have been shown to stabilize the edges of giant pores in GUVs but only in conditions of zero salt[25, 26]. At physiological salt concentrations these proteins do not promote the formation of giant pores. Furthermore, the physiological relevance of this pore stabilization ability of talin and other FERM domain containing proteins is not clear. *In vivo* the function of these proteins is to connect actin filaments to the cell membrane. In contrary to these proteins, Bax forms giant pores in physiologic salt conditions and is a bona fide pore-forming protein, whose pore forming activity is directly linked to its function *in vivo*, thus making the discovery of the ability of Bax to form mega-pores more significant.

Experimentals

Protein purification and labeling was done as described in Chapter 5 and Appendix V.

Line tension analysis. Analysis of the line tension in the rim of a Bax mega-pore was done according to Karatekin *et al.*[10] using time-lapse movies of the pore opening and closure collected using laser-scanning microscope Meta 510 system (Carl Zeiss). Diameter of an open Bax mega-pore together with the diameter of a GUV was measured using Zeiss LSM image browser software. Time dependent evolution plots of the pore diameter were fitted using linear square fit analysis in Origin 6.0 software (OriginLab Corp.). The value for the slope of this linear fit was used to calculate the line tension as described in Supplementary Information.

References

1. Karbowski, M. et al. Spatial and temporal association of Bax with mitochondrial fission sites, Drp1, and Mfn2 during apoptosis. J Cell Biol 159, 931-8 (2002).

2. Saito, M., Korsmeyer, S. J. & Schlesinger, P. H. BAX-dependent transport of cytochrome c reconstituted in pure liposomes. Nat Cell Biol 2, 553-5 (2000).

3. Schlesinger, P. H. & Saito, M. The Bax pore in liposomes, Biophysics. Cell Death Differ 13, 1403-8 (2006).

4. Schlesinger, P. H. et al. Comparison of the ion channel characteristics of proapoptotic BAX and antiapoptotic BCL-2. Proc Natl Acad Sci U S A 94, 11357-62 (1997).

5. Qian, S., Wang, W., Yang, L. & Huang, H. W. Structure of transmembrane pore induced by Bax-derived peptide: evidence for lipidic pores. PNAS 105, 17379-83 (2008).

6. Dejean, L. M., Martinez-Caballero, S., Manon, S. & Kinnally, K. W. Regulation of the mitochondrial apoptosis-induced channel, MAC, by BCL-2 family proteins. Biochim Biophys Acta 1762, 191-201 (2006).

7. Schafer, B. et al. Mitochondrial outer membrane proteins assist Bid in Bax-mediated lipidic pore formation. Mol Biol Cell 20, 2276-85 (2009).

8. Epand, R. F., Martinou, J. C., Montessuit, S., Epand, R. M. & Yip, C. M. Direct evidence for membrane pore formation by the apoptotic protein Bax. Biochem Biophys Res Commun 298, 744-9 (2002).

9. Martinez-Caballero, S. et al. Assembly of the mitochondrial apoptosis-induced channel, MAC. J Biol Chem 284, 12235-45 (2009).

10. Karatekin, E. et al. Cascades of transient pores in giant vesicles: line tension and transport. Biophys J 84, 1734-49 (2003).

11. Riske, K. A. & Dimova, R. Electro-deformation and poration of giant vesicles viewed with high temporal resolution. Biophys J 88, 1143-55 (2005).

12. Rodriguez, N., Cribier, S. & Pincet, F. Transition from long- to short-lived transient pores in giant vesicles in an aqueous medium. Phys Rev E Stat Nonlin Soft Matter Phys 74, 061902 (2006).

13. Sandre, O., Moreaux, L. & Brochard-Wyart, F. Dynamics of transient pores in stretched vesicles. Proc Natl Acad Sci U S A 96, 10591-6 (1999).

14. Brochard-Wyart, F., de Gennes, P. & Sandre, O. Transient pores in stretched vesicles: role of leak out. Physica A 278, 32-51 (2000).

15. Zhelev, D. V. & Needham, D. Tension-stabilized pores in giant vesicles: determination of pore size and pore line tension. Biochim Biophys Acta 1147, 89-104 (1993).

16. May, S. A molecular model for the line tension of lipid membranes. European Physical Journal E 3, 37-44 (2000).

17. Bar-Ziv, R., Moses, E. & Nelson, P. Dynamic excitations in membranes induced by optical tweezers. Biophys J 75, 294-320 (1998).

18. Needham, D. & Hochmuth, R. M. Electro-mechanical permeabilization of lipid vesicles. Role of membrane tension and compressibility. Biophys J 55, 1001-9 (1989).

19. Garcia-Saez, A. J., Chiantia, S., Salgado, J. & Schwille, P. Pore formation by a Bax-derived peptide: effect on the line tension of the membrane probed by AFM. Biophys J 93, 103-12 (2007).

20. Basanez, G. et al. Bax, but not Bcl-xL, decreases the lifetime of planar phospholipid bilayer membranes at subnanomolar concentrations. Proc Natl Acad Sci U S A 96, 5492-7 (1999).

21. Suzuki, M., Youle, R. J. & Tjandra, N. Structure of Bax: coregulation of dimer formation and intracellular localization. Cell 103, 645-54 (2000).

22. Annis, M. G. et al. Bax forms multispanning monomers that oligomerize to permeabilize membranes during apoptosis. EMBO J 24, 2096-103 (2005).

23. Zemel, A., Ben-Shaul, A. & May, S. Modulation of the spontaneous curvature and bending rigidity of lipid membranes by interfacially adsorbed amphipathic peptides. J Phys Chem B 112, 6988-96 (2008).

24. Lee, A. G. Lipid-protein interactions in biological membranes: a structural perspective. Biochim Biophys Acta 1612, 1-40 (2003).

25. Saitoh, A., Takiguchi, K., Tanaka, Y. & Hotani, H. Opening-up of liposomal membranes by talin. Proc Natl Acad Sci U S A 95, 1026-31 (1998).

26. Takeda, S. et al. Opening of holes in liposomal membranes is induced by proteins possessing the FERM domain. J Mol Biol 362, 403-13 (2006).

CHAPTER 7

"FCCS Study of Bax Self-Assembly in Lipid Membranes"

Abstract

It is widely accepted that during apoptosis, permeabilization of the outer mitochondrial membrane by the pore-forming members of the Bcl-2 protein family is a critical point after which the cell cannot be resuscitated. However, without direct evidence of how they interact in bilayers the molecular mechanism of the mitochondrial permeabilization remains controversial. Here we have reconstituted the pore formation by protein Bax in giant vesicles and show that in this environment Bax can form a heterogeneous distribution of coexisting pore sizes ranging from 1 nm to 20 μm in diameter. Evidence is provided by directly examining oligomerization and mobility change of Bax molecules in GUVs by fluorescence cross-correlation spectroscopy and by studying the large complexes by confocal microscopy. We show that in the presence of Bcl-x_L, an inhibitor of Bax pore formation, membrane bound Bax was primarily monomeric. We also show that, in the large length scale format of a GUV, Bax form structures that reveal its affinity for highly curved membranes, and that it dramatically reduces line tension while stabilizing its lipidic pores. Finally, our results demonstrate that Bax forms pores by increasing membrane surface energy and changing curvature of lipid membranes, thus manifesting an ability to sculpt lipid bilayers.

Introduction

Bax is a pro-apoptotic member of the BCL-2 protein family and its paramount function is to permeabilize the OMM during apoptosis[1, 2]. Upon apoptotic stimulation Bax translocates to the OMM where it changes conformation, inserts as a monomer, and then undergoes in-membrane homo-oligomerization to form a pore. Once the Bax pore is formed, cytochrome c and other mitochondria-resident proteins escape into the cytoplasm where they activate the cascade of caspases that dismantle the cell. To date the structure of the inactive, cytoplasm-resident, form of Bax is known[3]; however, the structure of the active, membrane-integrated, form of Bax remains unsolved. The absence of a membrane structure for this protein has lead to a vigorous debate about: the nature of the Bax pore (lipidic versus barrel-stave)[4-6], the number of Bax monomers participating in the pore formation[7-10], the possible molecular interactions formed among them in a pore[11, 12], and the progression and variety of pores formed by Bax (i.e. dimer, tetramer and higher order polymers)[5, 6, 13, 14]. To address these questions we used two-focus two-color scanning FCCS[15-17] to non-intrusively measure the mobility and self-association of the fluorescently-labeled Bax in a hydrated lipid membrane of GUVs for 5-7 hours after Bax insertion into the lipid membrane (See Chapter 5 for the confocal microscopy analysis of the fluorescent Bax binding to GUV). In these FCCS experiments the microscope output was multiplexed for simultaneous determination of the membrane diffusion coefficients and concentrations of Bax-R, Bax-G and Bax-RG complexes, and the analysis of the Bax pore activation. Using the membrane diffusion coefficients for the monomeric Bax-R and Bax-G proteins and for the Bax-RG complexes we estimated the hydrodynamic radius of these complexes in lipid membranes which is comparable to values reported in literature.

Furthermore, using the values for the membrane diffusion coefficient of Bax we were able to clearly differentiate between two monomeric species of Bax in lipid membranes – membrane associated and membrane integrated Bax. In support of this analysis we used cBid to activate Bax and Bcl-x_L to inhibit the membrane integration and self-association of Bax.

Results and Discussion

Bax is monomeric in solution and oligomerizes only in lipid membranes

It has been shown by a FRET study that Bax does not oligomerize prior to membrane binding[14]. Using FCCS we observe similar result that Bax-R and Bax-G in the presence of cBid are monomeric and do not oligomerize in solution (Fig. 7-1b). In solution, diffusion coefficient for Bax-G is 114±6 μm^2/sec (mean±s.e., n=3) and for Bax-R it is 134±12 μm^2/sec (mean±s.e., n=3) which is similar to that of monomeric tBid and Bcl-x_L[17]. We observe oligomerization of Bax-R and Bax-G only in the environment of a lipid membrane as shown by the increased cross correlation in Fig. 7-1c (blue line).

In a lipid membrane Bax forms a population of varying in size oligomers

Two-color two-focus scanning FCCS allows simultaneous measurement of the fluorescent protein concentration, diffusion coefficient and self-association in a lipid membrane[15-18]. To study Bax self-association in a lipid membrane we used Bax-R and Bax-G proteins (50 nM total concentration) activated with 4 nM cBid (as was determined by the confocal microscopy experiments described in Chapter 5).
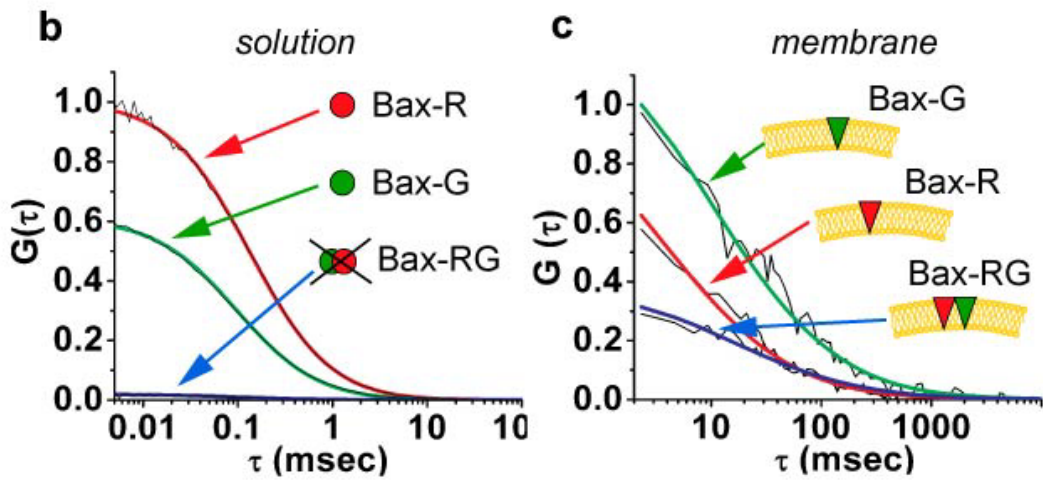
Figure 7-1. FCCS on Bax in solution and in a lipid membrane. b. Normalized auto-correlation curves and cross-correlation curve (blue) for Bax-R and Bax-G in solution in the presence of cBid. **c.** Normalized auto-correlation curves and cross-correlation curve (blue) for Bax-R and Bax-G in a lipid membrane in the presence of cBid.
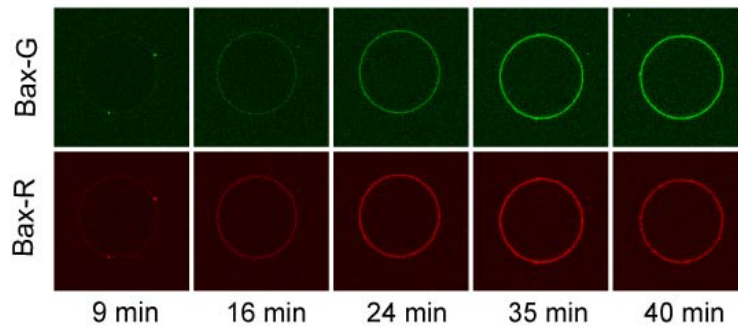
Figure 7-2. Confocal microscopy images of Bax binding to a GUV. Bax-R (25 nM), Bax-G (25 nM) and cBid (4 nM) were added to GUVs upon which collection of the time-series of images was initiated. Time stamps represent the time after protein addition to GUVs.

After the establishment of sufficient fluorescent signal of Bax in GUV membranes (as shown in Fig. 7-2), the FCCS measurements were done on a population of GUVs (10 min measurement time per GUV) (Fig. 7-3 d, e). The FCCS analysis of membrane Bax produced a clear result that Bax protein complexes increased in size with time, as can be seen from the decrease in the average mobility of these Bax-RG containing complexes (Fig. 7-3 e, blue squares). At the same time, the number of membrane Bax particles (which include monomers and oligomers) was increasing, so it was clear that for the >6 hours of these experiments Bax was continuing to accumulate in the membrane. Each time point on the Figure 7-3 d and 7-3 e represents an independent GUV measurement such that amount of Bax in the membrane and the average diffusion coefficient of the Bax particles is not uniform and reflects the variation in the vesicle lipid composition (See Chapters 2 and 5 for discussion).

The average diffusion coefficient of Bax-RG complexes in GUV membranes incubated for five hours with 50 nM of the fluorescent Bax and 4 nM cBid is 2.0±0.4 μm^2/sec (mean±s.d., n=21). This diffusion coefficient is slower than the membrane diffusion coefficient of monomeric tBid and Bcl-$x_L\Delta C$ measured by the same technique (5 μm^2/sec)[17], suggesting formation of a bulky slowly-diffusing Bax-RG complex in a lipid membrane (Table 7-1). Since the diffusion coefficient of a particle in a lipid membrane depends on the in-membrane hydrodynamic diameter of the particle, we can use the value for the diffusion coefficient of Bax-RG complexes to determine their approximate in-membrane hydrodynamic diameter using a modified Saffman-Delbruck formula[19] but for this the membrane diffusion coefficient of a Bax monomer should be
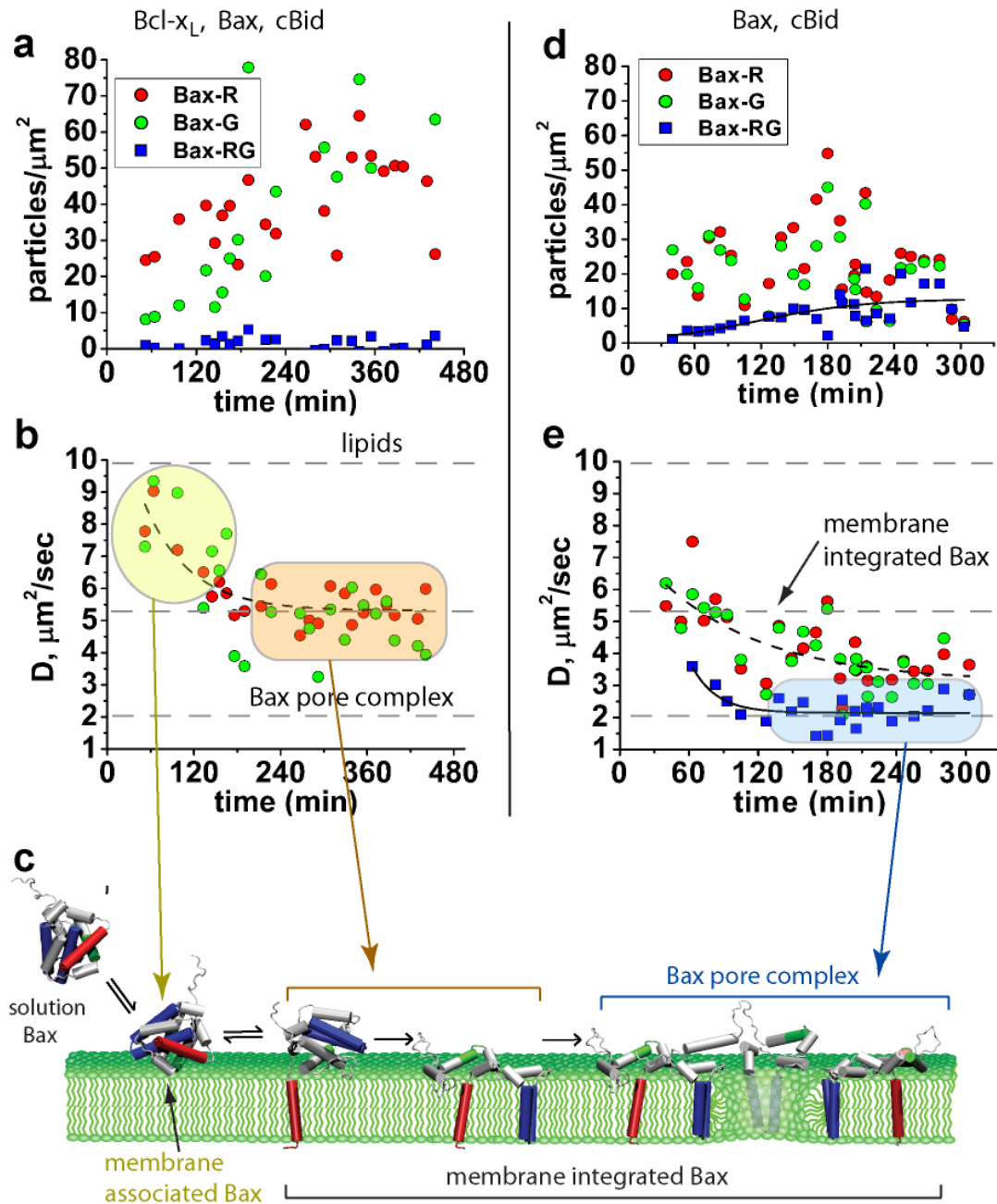
Figure 7-3. Two-color two-focus scanning FCCS experiments on Bax. a and **b** represent FCCS results of Bax-R/Bax-G cross-correlation (50 nM total Bax concentration) in the presence of 50 nM Bcl-x_L and 4 nM cBid, while **d** and **e** represent similar results but in the absence of Bcl-x_L. **c.** Schematic of various diffusion species of Bax in a lipid membrane.

known. The value for the diffusion coefficient of a Bax monomer will be used to ensure the accuracy of calculations.

Bcl-x$_L$ prevents the self-assembly of Bax in lipid membranes.

To determine the membrane diffusion coefficient of a Bax monomer, Bax self-assembly and pore formation in a lipid membrane should be inhibited. This was accomplished by using full length human Bcl-x$_L$ protein, which is an anti-apoptotic member of the Bcl-2 family that inhibits Bax pore formation[20]. When GUVs were preincubated with Bcl-x$_L$ (50 nM) and cBid (4 nM) for one hour and then Bax (50 nM) was added, no binding of Bax to GUV membranes was observed (Fig. 5-3, Chapter 5), which does not allow for the FCCS measurements. However, this observation reflects the ability of Bcl-x$_L$ to sequester cBid in an inactive complex which is unable to activate and promote membrane integration of Bax[14, 17, 20]. Simultaneous addition to GUVs of Bax, cBid and Bcl-x$_L$ at these same concentrations resulted in sufficient membrane binding of Bax for the FCCS measurements but did not result in GUV permeabilization (Fig. 5-3, Chapter 5). Comparison of the fluorescence intensity of Bax-R accumulation in the GUV membranes in the presence and absence of Bcl-x$_L$ shows that in the presence of Bcl-x$_L$ the amount of Bax binding to the GUV membranes is lower than in the absence of Bcl-x$_L$ (Fig. 7-4).

Based on the results of the FCCS experiments shown in Figures 7-3 a-c, in the presence of Bcl-x$_L$ the membrane concentration of Bax increased over 7 hours and its diffusion coefficient decreased from 8.3±1.0 μm^2/sec (mean±s.d, n=6) to 5.2±0.7 μm^2/sec (mean±s.d., n=26). The latter diffusion coefficient value is typical of a transmembrane
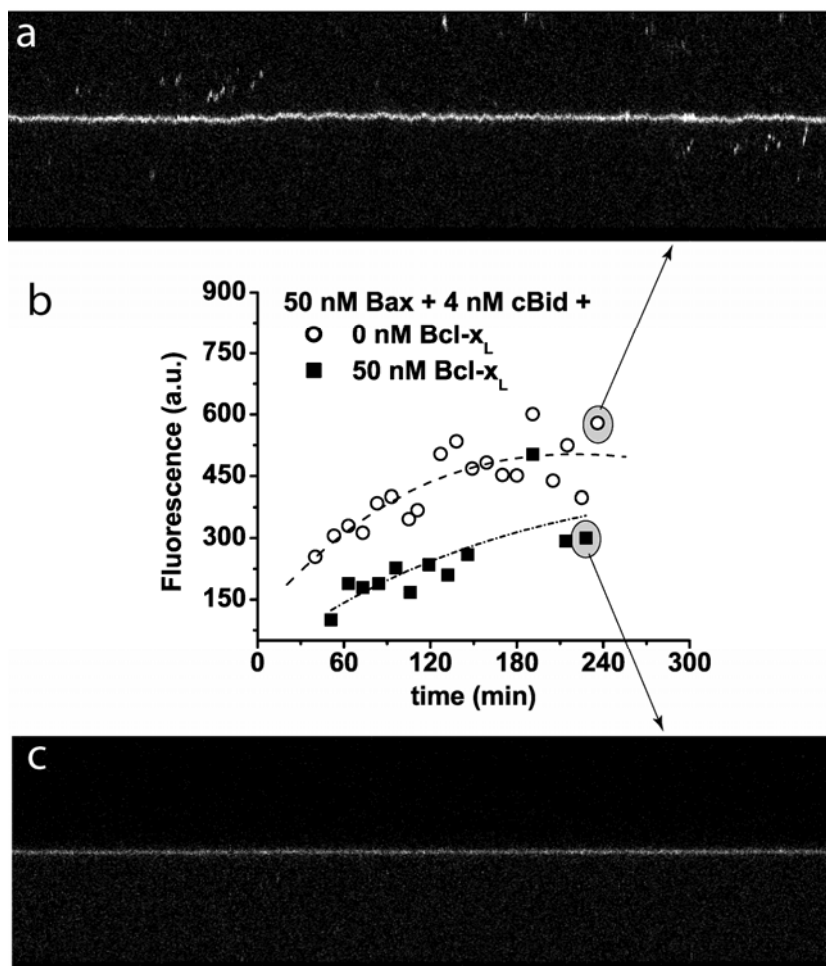
Figure 7-4. Comparison of Bax-R binding to GUV membranes in the presence and absence of Bcl-x_L. **a.** Map of fluorescence intensity changes in a line scan through the GUV membrane (vertical direction) with time (horizontal direction). This membrane trace comes from a GUV exposed only to Bax-R protein and cBid. **b.** Change in cumulative fluorescence intensity in membranes of GUVs exposed to Bax-R and cBid in the absence and presence of Bcl-x_L. The trace for the last point in each measurement is shown in a and c. **c.** Map of fluorescence intensity changes in a GUV exposed to Bax-R, cBid and Bcl-x_L. In these experiments following protein and lipid concentrations were used: 25 nM Bax-R, 25 nM Bax-G, 50 nM Bcl-x_L, 4 nM cBid, and 5 μM total lipid.

alpha-helical peptide[21] and it is also similar to the in-membrane diffusion coefficient of monomeric membrane integrated tBid or C-terminal truncated Bcl-x_L described by the Saffman-Delbruck model of membrane protein diffusion (Table 7-1)[17, 22]. In addition, we observed no cross-correlation between Bax-R and Bax-G at this concentration of Bcl-x_L (Fig. 7-3b). Based on these results we conclude that the diffusion coefficient of a membrane integrated Bax monomers is 5.2±0.7 μm^2/sec.

Furthermore, we propose that the gradual decrease in the membrane diffusion coefficient of Bax in the presence of inhibiting concentrations of Bcl-x_L represents the transition of Bax from being a monomeric membrane-associated protein sliding on the membrane surface with fast diffusion to becoming a monomeric membrane-integrated protein with appropriately slower diffusion (Fig. 7-3c). However, we do not discount the

Table 7-1. Comparison of the various diffusion coefficients of Bax with the diffusion coefficient of lipids.

Type of molecule	Diffusion coefficient, μm^2/sec	in-membrane diameter, nm
in solution:		-
monomeric inactive Bax	114±5	
monomeric tBid[17]	143±9	
monomeric Bcl-xLΔC[17]	78±10	
in a lipid membrane:		
lipids	10.0±0.5	1
monomeric membrane associated Bax	8.3±1.0	-
monomeric membrane integrated Bax	5.2±0.7	~ 1
monomeric tBid[17]	5.0±0.3	-
monomeric Bcl-x_LΔC[17]	4.8±0.7	-
Bax pore complex (at 50 nM total Bax concentration)	2.0±0.4	53±12

possibility that the monomeric integrated Bax forms hetero-dimers with Bcl-x$_L$ in lipid membranes[20]. In the Saffman-Delbruck theory scaling of the diffusion coefficient with the in-membrane diameter of the protein is logarithmic implying that integrated monomeric Bax would have membrane diffusion coefficient similar to that of a Bax/Bcl-x$_L$ hetero-dimer.

Calculation of the Bax pore complex diameter

Traditionally the Saffman-Delbruck equation is used to calculate the hydrodynamic radius of a membrane inclusion from its diffusion coefficient[21-25] (See Eqn. 1 in the Experimentals section). It has been shown, that Saffman-Delbruck equation faithfully describes diffusion of membrane inclusions traversing both leaflets of a lipid membrane in the case of small proteins, however, in the case of larger membrane inclusions (for example, such as lipid rafts) this theory underestimates the diameter of membrane inclusions. As a consequence of this, a modified version of a Saffman-Delbruck equation has been developed by Petrov and Schwille for the description of the diffusion of large membrane inclusions[19] (See Eqn. 2 in the Experimentals section).

In the case of Bax diffusion in lipid membranes, the diffusion coefficient of a Bax monomer (5.2±0.7 μm^2/sec) is consistent with the Saffman-Delbruck theory, however, the diffusion coefficient of Bax-RG protein complex is two times slower than the diffusion of a Bax monomer, and thus according Petrov and Schwille the in-membrane hydrodynamic diameter of this complex should be calculated according to the modified Saffman-Delbruck formula. As a result the diameter of the Bax-RG protein complex

diffusing with diffusion coefficient of 2.0 ± 0.4 μm^2/sec is 53 ± 12 nm. This value is one order of magnitude larger than the size of a Bax pore measured by the dextran blocking of a pore and by the electrophysiology methods[13, 26]. However, this value is consistent with the electron microscopy imaging of a Bax pore in liposomes and the AFM measurement of the Bax pores in supported lipid bilayers[5, 27], where it has been shown that the diameter of a Bax pore can be 100-200 nm.

It is worth noting here that the calculated hydrodynamic radius of a Bax-RG complex does not necessarily represent the size of a pore formed by this complex. In spite of the obvious connection between the calculated diameter of a Bax-RG complex and the electron microscopy and AFM experiments, it is still possible that the size of the pore is smaller than 53 nm and the rest of the size of the pore is occupied by the lipids trapped in the concerted motion of a lipidic pore.

Titration of Bax in lipid membranes: mass action law

We next asked a question, whether by increasing the amount of Bax in a lipid membrane we can control for the size and the concentration of Bax-RG complexes. For this purpose various amounts of total soluble Bax-R and Bax-G proteins were added to the constant concentration of GUVs, and the FCCS measurements were done on these GUV populations. In each case, Bax binding to GUVs was activated by the addition of 4 nM cBid. As a result of these experiments we find that with the increasing concentration of total Bax added to the system the higher concentration of Bax particles is found in a lipid membrane (Fig 7-4, grey bars). It is important to note that these Bax particles include monomers and oligomers of Bax. Additionally, with increasing concentration of
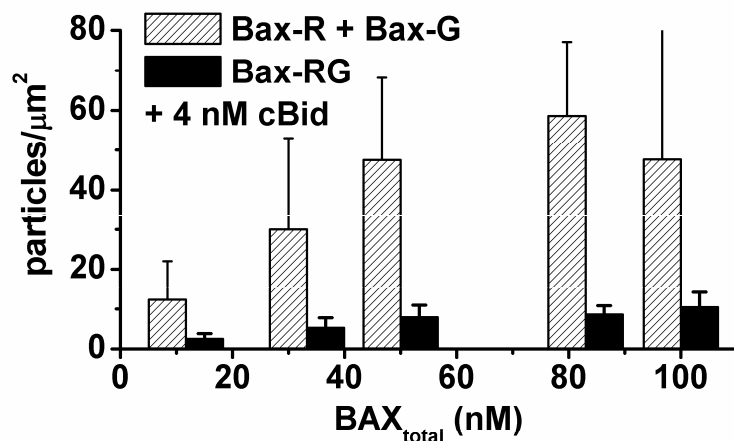
Figure 7-5. Titration of Bax. Bax-R and Bax-G were added to GUVs (5µM total lipid concentration) in the presence of cBid. FCCS measurements were done on a population of no less than 10 GUVs upon 1-2 hours after protein addition to GUVs.

Table 7-2. FCCS results of the titration of Bax. Experimental conditions were the same as described in the legend to Figure 7-5. The hydrodynamic diameter was calculated using modified Saffman-Delbruck formula[19].

Total Bax concentration, nM	Bax-RG complexes, particles/μm^2	measured diffusion coefficient, μm^2/sec	calculated in-membrane hydrodynamic diameter, nm
50	7.9	2.0±0.4	53.2
83	8.8	1.5±0.4	102.2
100	9.6	1.4±0.3	120

Bax particles in a lipid membrane, the greater number of the Bax-RG complexes was observed (Fig. 7-5, black bars). Analysis of the diffusion coefficients for the Bax-RG complexes formed at different total concentrations of Bax also showed an increase in the average size of these complexes (Table 7-2). Such correlation between the size and concentration of Bax-RG complexes with the total concentration of Bax in a system shows that Bax pore formation follows the mass action law.

Moderating the activity of Bax with cBid

To study the effects of increasing concentrations of cBid onto the distribution of Bax particles in a lipid membrane, we varied cBid concentrations in our FCCS experiments while keeping Bax and total lipid concentration constant. As a result, we observed correlation between the increase of cBid concentration and the resulting concentration of Bax particles in the lipid membrane (Fig. 7-6). However, the concentration of Bax-RG complexes did not follow this correlation pattern.
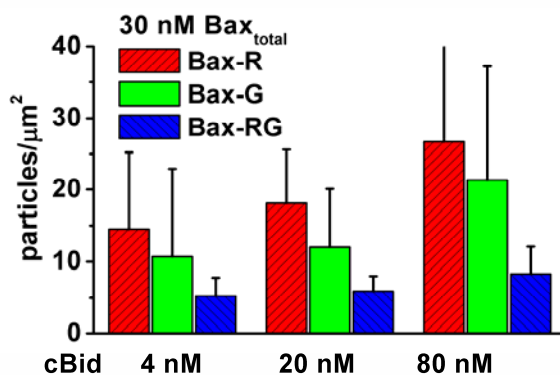
Figure 7-6. Effects of cBid titration on the distribution of the membrane forms of Bax. Results were obtained using two-color two-focus scanning FCCS analysis.

The concentration of Bax-RG complexes in a lipid membrane remained constant (within the margin of error) for all cBid concentrations (Fig. 7-6, blue bars). This observation indicates that cBid must be affecting only the kinetics of Bax integration into the lipid membranes without a significant effect on the resulting concentration of the Bax oligomers.

Interactions among Bax, cBid, and Bcl-x$_L$: rheostat model

In Figure 7-3 we have shown that Bcl-x$_L$ inhibits oligomerization of Bax in a lipid membrane. However, we were intrigues to know whether the inhibitory effect of Bcl-x$_L$ on Bax can be rescued by the addition of excess cBid. According to the rheostat model proposed by Korsmeyer *et al.* the apoptosis decision in cells depends on the relative concentrations of pro- and anti-apoptotic proteins[28]. Therefore, in our minimal *in vitro* system we expect to observe an increase in the oligomerization of Bax in a lipid membrane containing Bcl-x$_L$ when cBid concentration is increased, due to the competition for cBid between Bax and Bcl-x$_L$[29].

Simultaneous addition to GUVs of 50 nM Bax and Bcl-x$_L$ at 1:1 protein to protein ratio with 4 nM cBid resulted in complete inhibition of Bax oligomerization as can be seen from the absence of Bax-RG complex formation, while in the absence of Bcl-x$_L$ the same concentrations of Bax and cBid resulted in the formation of 16% of Bax-RG complexes (normalized to the total concentration of Bax particles in the membrane) (Fig. 7-7). However, when excess of cBid is added, with 1:1:1 stoichiometry of Bax, Bcl-x$_L$ and cBid in the system, there is sufficient cBid for the interaction with both Bax and Bcl-x$_L$, and as a result we observe rescue of the Bax-RG complex formation (Fig. 7-7). These

observations are consistent with the rheostat model where cBid can interact with both Bax and Bcl-x_L while having higher affinity for the interaction with Bcl-x_L[14, 17, 29] and thus when Bcl-x_L is present majority of the cBid molecules is sequestered in the interaction with Bcl-x_L (assuming 1:1 stoichiometry of protein binding) leaving few cBid molecules for the interaction with Bax. Therefore, using minimal *in vitro* system we were able to show that the outcome of the interaction among Bax, cBid and Bcl-x_L can be described by the rationale of the rheostat model.
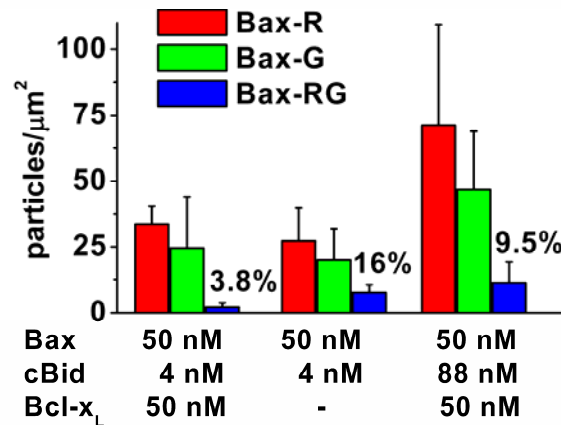
Figure 7-7. Bax, cBid and Bcl-x_L: rheostat model. Results were obtained using two-color two-focus scanning FCCS analysis.

Discussion

For use with two-color two-focus FCCS we produced two forms of the fluorescently labeled full length Bax protein, Bax-R and Bax-G. These fluorescently labeled Bax proteins have been shown to have the pore formation activity similar to that of the recombinant wild type Bax (See Chapter 5 for details). Furthermore, we show that

these two fluorescent forms of Bax are monomeric in solution and oligomerize only in lipid membranes (Fig. 7-1).

Bax binding to lipid membranes: associated versus integrated Bax

Using two-color two-focus scanning FCCS we show that prior to oligomerization in a lipid membrane monomeric Bax associates with the lipid membrane, and then becomes membrane integrated. The transition between the membrane associated and integrated forms of Bax most likely occurs via a conformational change, which is aided by cBid protein already present in the membrane. We differentiate between these two monomeric forms of Bax based on their diffusion coefficient: membrane associate monomeric Bax, due to incomplete insertion into a lipid bilayer, has faster diffusion coefficient (8 μm^2/sec) than the monomeric membrane integrated Bax (5 μm^2/sec). It is important to note, that this transition from associated to integrated Bax could only be observed by scanning FCCS in the presence of Bcl-x_L protein in GUV membranes. Bcl-x_L slows down membrane binding of Bax, and thus allowed us to observe this transition process. Bcl-x_L have been proposed to inhibit the pore formation by Bax in three ways: by directly binding monomeric integrated Bax, by binding cBid protein and thus eliminating it as an activator of Bax, and by preventing Bax binding to a lipid membrane[20, 30]. However, the mechanism of a letter inhibition pathway is not clear. Therefore, Bcl-xL inhibition of Bax binding, oligomerization and pore formation in lipid membranes, which were observed in our experiments, agree with literature.

In the absence of Bcl-x_L in the membrane, the association and integration of Bax is rapid, and can not be resolved by the scanning FCCS. In this case we observe the

decrease in the average diffusion coefficient of Bax from 5 μm^2/sec to 2 μm^2/sec, which is likely represents the transition form monomeric integrated Bax to a proteo-lipidic complex containing multiple Bax monomers. Furthermore, the time frame of the Bax transition from the associated to integrated protein in the presence of Bcl-x_L is longer than the time frame of the transition from the monomeric membrane integrated protein to the proteo-lipid complex in the absence of Bcl-x_L (Fig. 7-3 b and e), thus supporting our proposal that Bcl-x_L slows down the process of Bax integration in a lipid membrane. Our observation of the transition from membrane integrated to membrane associated forms of Bax can be further supported by the SPR studies[31] and by the studies of the conformation of Bax loosely associated with the lipid membrane of LUVs[32].

Self-assembly of Bax in lipid membranes

It has been shown that in order to form a pore in artificial lipid membranes, Bax need to undergo self-assembly in the lipid membrane environment[5, 10, 13, 14, 33], while *in vivo,* during apoptosis, Bax has also been shown to form large aggregates[10, 34, 35]. Therefore, our observation of the Bax-RG complex formation was expected. However, what was unexpected, is the progressive decrease in the diffusion coefficient of Bax upon membrane integration. According to the Saffman-Delbruck formula, diffusion of a membrane protein is primarily affected by the in-membrane hydrodynamic diameter of the protein. Therefore, dimerization and even tetramerization of a protein in a lipid bilayer would not result in a significant change in the diffusion coefficient of the resulting complex, compared to that of a monomer[36, 37]. Therefore, our observation of the significant decrease in the diffusion coefficient of Bax-RG complex compared to that of a

Bax monomer, indicates that Bax is not simply oligomerizing, but most likely is forming lipidic pores[4, 5, 38]. These lipidic pores involve lipids which contribute to the size of the in-membrane hydrodynamic diameter of a complex (See Fig. 7-3 c for a proposed model of a Bax lipidic pore). Therefore, our estimation of the diameter of these slowly diffusing Bax-RG proteo-lipidic complexes most likely over-estimates the size of pores formed by these complexes in a lipid bilayer. However, we do not have direct experimental evidence for the presence of pores in these complexes. The reason for our assumption, that these Bax-RG proteo-lipidic complexes contain a pore, is based on the transmission electron microsocopy and AFM measurement of the Bax pore diameters, which show that Bax is capable of forming pores with the diameter of 100-200 nm. Calculated in-membrane diameter of a Bax-RG complex falls into this range.

Rheostat model: connection to physiology

The finding that pro- and anti-apoptotic proteins of the Bcl-2 family can heterodimerize, and that their relative concentrations to each other affects the decision whether a cell should undergo apoptosis, have lead to the proposal of the rheostat model by Korshmeyer *et al*[28]. The results obtained using our model system of Bax pore formation in GUVs support this hypothesis (Fig. 7-7). These results show that, when equimollar concentrations of Bax and Bcl-x_L are present in a lipid membrane together with low concentration of cBid, there is no oligomerization and pore formation by Bax. However, when cBid is added, such that there is approximately one cBid molecule for each Bax and Bcl-x_L molecule, then oligomerization and pore formation by Bax is

rescued. Similarly, in the presence of low cBid concentration and the complete absence of Bcl-x_L, Bax is able to oligomerize and form pores.

The results of scanning FCCS shown that Bax, cBid and Bcl-x_L obey the law of mass action (Fig. 7-5, 7-6, 7-7). These results show that increase in the concentration of soluble protein leads to the concentration increase of the membrane bound protein, with a certain saturation limit. Results of the titration experiments with Bax-R and Bax-G show that not only the total concentration of membrane bound Bax monomers increases, but also that the distribution of Bax-RG proteo-lipidic complexes changes, resulting in the larger mean diameter of complexes (Table 7-2).

Conclusions

The work presented in this chapter represents the first example of the application of two-color two-focus scanning FCCS to study oligomerization and pore formation by Bax in lipid membranes of GUVs. The results of this study provide an insight into the mechanism of Bax pore formation in lipid membranes and the regulation of this mechanism by the pro-apoptotic BH3-only protein cBid and anti-apoptotic protein Bcl-x_L. These results show that Bax binds lipid membranes containing cBid as a monomer, by first associating with the lipid membrane, likely via electrostatic interaction, and then undergoing conformational transition to become a membrane integrated protein, likely due to the interaction with cBid. Once in lipid membrane, integrated Bax monomers initiate self-association which leads to the formation of pores. Formation of pores reduces the concentration of monomeric Bax monomers in the lipid membrane, thus allowing for the integration of additional Bax proteins. This continual insertion of Bax monomers into

the lipid membrane leads to increase in the average Bax pore size resulting in the heterogeneous distribution of Bax pores. Increase in the number of Bax pores in the lipid membrane leads to the disruption of elastic forces of the lipid membrane, thus leading to the deformation and destruction of GUVs.

Experimentals

Protein purification and labeling was done as described in Chapter 5 and Appendix V.

Sample preparation for the FCCS experiments.

For the FCCS experiments GUVs were prepared from a lipid mixture of DOPC:bovine heart cardiolipin (80:20 mol%) using the electroformation method described in Appendix IV. After the preparation 50 µl of GUVs were transferred to an observation well containing 450 µl of 1xEB buffer (10 mM Hepes, pH 7.2, 100 mM KCl) and a mixture of proteins (Bax, cBid, Bcl-x_L) depending on the experiment. For all experiments observation chambers (8 well LabTak, Nunc) were treated for at least one hour with a solution containing 4 mg/ml BSA. BSA treatment was done with the purpose to prevent protein adsorption to the plastic walls of the observations chamber. All FCCS measurements were performed at room temperature (22 °C) in a dark room.

Fluorescence cross-correlation spectroscopy.

FCCS measurements were performed on a laser-scanning microscope Meta 510 system (Carl Zeiss) using 40× NA 1.2 UV-Vis-IR C Apochromat water-immersion objective. For excitation the 488 nm line of an Argon-ion laser (25 µW) and the 633 nm line of the HeNe laser (15 µW) were used, while detection was done using a home-built

detection unit at the fiber output channel. A dichroic mirror and band-pass filters (D555, HQ520/40 and HQ700/75; AHF Analyze Technik) were used behind a collimating achromat to split the emission for the dual-color detection and to reject residual laser and background light. We then used achromats (LINOS Photonics) to image the internal pinhole onto the apertures of the fibers connected to the avalanche photodiodes (APD, PerkinElmer). The photon arrival times were recorded in the photon mode of the hardware correlator Flex 02-01D (http://correlator.com).

For scanning FCCS, the detection volume was repeatedly scanned perpendicularly through the equator of a GUV. We controlled its movement directly with the Zeiss LSM operation software. We used the frame mode with *Nx2* pixels to scan the two parallel lines. We measured their distance *d* by repeatedly scanning over a film of dried fluorophores and measuring the distance between the bleached traces in a high-resolution LSM image.

Data analysis was performed with software written in MATLAB (MathWorks). For scanning FCCS, we binned the photon stream in bins of 2 μs and arranged it as a matrix such that every row corresponded to one line scan. Corrected for movements of the membrane was done by calculating the position of the maximum of a running average over several hundred line scans and shifting it to the same column. We fitted an average over all rows with a Gaussian and we added only the elements of each row between -2.5σ and 2.5σ to construct the intensity trace. We computed the auto- and cross-correlation curves of the resulting intensity traces with a multiple tau correlation algorithm and fitted them with a nonlinear least-squares fitting algorithm. In all FCCS data processing, we excluded from further analysis irregular curves resulting from major instabilities

identified by distortions of the curves and a systematic change in the intensity trace. For details of data fitting see Supplementary information.

Calculation of the diameter for the Bax pore complex.

According to the Saffman-Delbruck theory of the diffusion of particles in lipid membranes translational diffusion coefficient (D) of the particle depends on the radius (R) of the particle in the following way

$$D = \frac{k_B T}{4\pi\mu_{mem}h}\left(\ln\frac{\mu_{mem}h}{\mu_{sol}R} - \gamma\right) \qquad (\text{Eqn.1})$$

where μ_{mem} is membrane viscosity, μ_{sol} is solution viscosity, h is membrane thickness, T temperature, k_B is Boltzmann constant, and γ is Euler's constant (0.5772)[22].

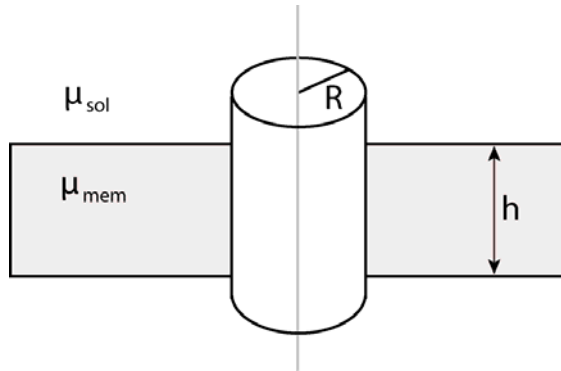Schematic representation of a diffusing particle in a lipid membrane is shown in Figure 7-8.

Figure 7-8. Schematic representation of the hydrodynamic model of a particle diffusing in a lipid membrane described by the Saffman-Delbruck equation (Eqn. 1).

As was mentioned previously that Saffman-Delbruck formula describes well diffusion of small proteins is a lipid membrane, but it fails to describe the membrane diffusion of larger complexes such as lipid rafts[19]. Since Bax-RG proteo-lipidic complexes have diffusion coefficient two times smaller that the diffusion coefficient of a Bax monomer we used modified Saffman-Delbruck formula[19] to determine the in-membrane hydrodynamic radius of these complexes. In our analysis we made assumptions that membrane viscosity is 0.7 cP[15], membrane thickness is 5 nm. The expression for the modified Saffman-Delbruck formula is following

$$D(\varepsilon) = \frac{k_B T}{4\pi \mu_{mem} h} \frac{\left(\ln\left(\frac{2}{\varepsilon}\right) - \gamma + \frac{4\varepsilon}{\pi} - \left(\frac{\varepsilon^2}{2}\right) \ln\left(\frac{2}{\varepsilon}\right) \right)}{\left(1 - \left(\frac{\varepsilon^3}{\pi}\right) \ln\left(\frac{2}{\varepsilon}\right) + c_1 \varepsilon^{b_1} \Big/ \left(1 + c_2 \varepsilon^{b_2}\right) \right)} \qquad \text{(Eqn. 2)}$$

where, ε is the reduced radius, $\varepsilon = 2R\mu_{sol}/\mu_{mem}$, while c_1, c_2, b_1, and b_2 are constant ($c_1 = 0.73761$, $c_2 = 0.52119$, $b_1 = 2.74819$, $b_2 = 0.61465$).

To calculate the error for this value we used the fact that membrane viscosity is not very well defined and according to Ramadurai et al.[15] it varies for a lipid membrane composed of DOPC/DOPG mixture from 0.6 cP to 0.8 cP. Using this uncertainty in the actual value for the membrane viscosity together with the fact that lipid composition used in our work has similar viscosity as the one used in Ramadurai et al. based on the measurements of translational lipid diffusion (see Appendix VI) we estimated that standard error for the diameter of the Bax pore complex is 12 nm. Therefore, we estimate that the diameter of the Bax pore complex in a lipid membrane is 53±12 nm.

References

1.   Chipuk, J. E., Moldoveanu, T., Llambi, F., Parsons, M. J. & Green, D. R. The BCL-2 Family Reunion. Mol Cell 37, 299-310 (2008).

2.   Youle, R. J. & Strasser, A. The BCL-2 protein family: opposing activities that mediate cell death. Nat Rev Mol Cell Biol 9, 47-59 (2008).

3.   Suzuki, M., Youle, R. J. & Tjandra, N. Structure of Bax: coregulation of dimer formation and intracellular localization. Cell 103, 645-54 (2000).

4.   Qian, S., Wang, W., Yang, L. & Huang, H. W. Structure of transmembrane pore induced by Bax-derived peptide: evidence for lipidic pores. PNAS 105, 17379-83 (2008).

5.   Schafer, B. et al. Mitochondrial outer membrane proteins assist Bid in Bax-mediated lipidic pore formation. Mol Biol Cell 20, 2276-85 (2009).

6.   Martinez-Caballero, S. et al. Assembly of the mitochondrial apoptosis-induced channel, MAC. J Biol Chem 284, 12235-45 (2009).

7.   Hsu, Y. T. & Youle, R. J. Bax in murine thymus is a soluble monomeric protein that displays differential detergent-induced conformations. J Biol Chem 273, 10777-83 (1998).

8.   Ivashyna, O. et al. Detergent activated BAX protein is a monomer. J Biol Chem 284, 23935-46 (2009).

9.   Antonsson, B., Montessuit, S., Lauper, S., Eskes, R. & Martinou, J. C. Bax oligomerization is required for channel-forming activity in liposomes and to trigger cytochrome c release from mitochondria. Biochem J 345 Pt 2, 271-8 (2000).

10.   Antonsson, B., Montessuit, S., Sanchez, B. & Martinou, J. C. Bax is present as a high molecular weight oligomer/complex in the mitochondrial membrane of apoptotic cells. J Biol Chem 276, 11615-23 (2001).

11.   Bleicken, S. et al. Molecular details of Bax activation, oligomerization and membrane insertion. J Biol Chem (2009).

12.   Dewson, G. & Kluck, R. M. Mechanisms by which Bak and Bax permeabilise mitochondria during apoptosis. J Cell Sci 122, 2801-8 (2009).

13.   Saito, M., Korsmeyer, S. J. & Schlesinger, P. H. BAX-dependent transport of cytochrome c reconstituted in pure liposomes. Nat Cell Biol 2, 553-5 (2000).

14. Lovell, J. F. et al. Membrane binding by tBid initiates an ordered series of events culminating in membrane permeabilization by Bax. Cell 135, 1074-84 (2008).

15. Ries, J., Chiantia, S. & Schwille, P. Accurate determination of membrane dynamics with line-scan FCS. Biophys J 96, 1999-2008 (2009).

16. Ries, J. & Schwille, P. Studying slow membrane dynamics with continuous wave scanning fluorescence correlation spectroscopy. Biophys J 91, 1915-24 (2006).

17. Garcia-Saez, A. J., Ries, J., Orzaez, M., Perez-Paya, E. & Schwille, P. Membrane promotes tBID interaction with BCL(XL). Nat Struct Mol Biol 16, 1178-85 (2009).

18. Yu, S. R. et al. Fgf8 morphogen gradient forms by a source-sink mechanism with freely diffusing molecules. Nature 461, 533-6 (2009).

19. Petrov, E. P. & Schwille, P. Translational diffusion in lipid membranes beyond the Saffman-Delbruck approximation. Biophys J 94, L41-3 (2008).

20. Billen, L. P., Kokoski, C. L., Lovell, J. F., Leber, B. & Andrews, D. W. Bcl-XL inhibits membrane permeabilization by competing with Bax. PLoS Biol 6, e147 (2008).

21. Ramadurai, S. et al. Lateral diffusion of membrane proteins. J Am Chem Soc 131, 12650-6 (2009).

22. Saffman, P. G. & Delbruck, M. Brownian motion in biological membranes. Proc Natl Acad Sci U S A 72, 3111-3 (1975).

23. Peters, R. & Cherry, R. J. Lateral and rotational diffusion of bacteriorhodopsin in lipid bilayers: experimental test of the Saffman-Delbruck equations. Proc Natl Acad Sci U S A 79, 4317-21 (1982).

24. Guigas, G. & Weiss, M. Size-dependent diffusion of membrane inclusions. Biophys J 91, 2393-8 (2006).

25. Gambin, Y. et al. Lateral mobility of proteins in liquid membranes revisited. Proc Natl Acad Sci U S A 103, 2098-102 (2006).

26. Schlesinger, P. H. et al. Comparison of the ion channel characteristics of proapoptotic BAX and antiapoptotic BCL-2. Proc Natl Acad Sci U S A 94, 11357-62 (1997).

27. Epand, R. F., Martinou, J. C., Montessuit, S., Epand, R. M. & Yip, C. M. Direct evidence for membrane pore formation by the apoptotic protein Bax. Biochem Biophys Res Commun 298, 744-9 (2002).

28. Korsmeyer, S. J., Shutter, J. R., Veis, D. J., Merry, D. E. & Oltvai, Z. N. Bcl-2/Bax: a rheostat that regulates an anti-oxidant pathway and cell death. Semin Cancer Biol 4, 327-32 (1993).

29. Nickells, R. W. Variations in the rheostat model of apoptosis: What studies of retinal ganglion cell death tell us about the functions of the Bcl2 family proteins. Experimental Eye Research, 1-7 (2010).

30. Cheng, E. H., Levine, B., Boise, L. H., Thompson, C. B. & Hardwick, J. M. Bax-independent inhibition of apoptosis by Bcl-XL. Nature 379, 554-6 (1996).

31. Christenson, E., Merlin, S., Saito, M. & Schlesinger, P. Cholesterol effects on BAX pore activation. J Mol Biol 381, 1168-83 (2008).

32. Yethon, J. A., Epand, R. F., Leber, B., Epand, R. M. & Andrews, D. W. Interaction with a membrane surface triggers a reversible conformational change in Bax normally associated with induction of apoptosis. J Biol Chem 278, 48935-41 (2003).

33. Kuwana, T. et al. Bid, Bax, and lipids cooperate to form supramolecular openings in the outer mitochondrial membrane. Cell 111, 331-42 (2002).

34. Karbowski, M. et al. Spatial and temporal association of Bax with mitochondrial fission sites, Drp1, and Mfn2 during apoptosis. J Cell Biol 159, 931-8 (2002).

35. Kim, H. et al. Hierarchical regulation of mitochondrion-dependent apoptosis by BCL-2 subfamilies. Nat Cell Biol 8, 1348-58 (2006).

36. Garcia-Saez, A. J. & Schwille, P. Fluorescence correlation spectroscopy for the study of membrane dynamics and protein/lipid interactions. Methods 46, 116-22 (2008).

37. Haustein, E. & Schwille, P. Fluorescence correlation spectroscopy: novel variations of an established technique. Annu Rev Biophys Biomol Struct 36, 151-69 (2007).

38. Terrones, O. et al. Lipidic pore formation by the concerted action of proapoptotic BAX and tBID. J Biol Chem 279, 30081-91 (2004).

CHAPTER 8

"Conclusions and Future Directions"

Conclusions

Protein Bax, a member of the Bcl-2 family, participates in the apoptosis decision by forming pores in the mitochondrial outer membrane. In non dying cells, Bax is found in the cytoplasm, therefore, in order to form pores in the mitochondrial outer membrane it needs to undergo a conformational change, which is associated with the activation of Bax. The molecular mechanism of Bax activation is one of the major unanswered questions in the field of apoptosis. In addition to this question, there are other questions about the pore formation mechanism of Bax, which remain unanswered due to the absence of the structure for membrane integrated active Bax, the form of Bax involved in the formation of pores. These questions include (i) the molecular mechanism of Bax integration into a lipid membrane; (ii) the details of molecular interactions between Bax monomers, leading to the formation of a pore; (iii) the progression, oligomeric state and the size of pores formed Bax; (iv) the nature of a Bax pore – lipidic versus barrel-stave; (v) the molecular interactions among monomers in a pore. To answer some of these questions we developed and used approaches to study fluorescently labeled Bax in three model *in vitro* systems –detergent micelles, LUVs and GUVs – using single-molecule sensitivity fluorescence techniques based on FCS. These single-molecule sensitivity techniques provide us with a non-invasive method to study the mechanism of Bax pore formation in lipid membranes.

Determination of the oligomeric state of Bax in micelles of activating detergents

It has been observed that Bax can be activated via interaction with detergent micelles. Additional biochemical analysis of the complexes formed by Bax and detergent

micelles revealed that these proteo-micellar complexes have a hydrodynamic volume larger than the combined volumes of a Bax monomer and a single detergent micelle. Due to the propensity of Bax to oligomerize in the hydrophobic environment of a lipid membrane during pore formation, it was hypothesized that Bax oligomerizes in detergent micelles, and that this oligomerization leads to the activation of Bax. Additionally, it was proposed that the oligomer of detergent activated Bax (consisting of up to 8 monomers) binds lipid membranes and then leads to the formation of a pore. This is in contrast to the *in vitro* studies where it was shown that Bax binds the mitochondrial outer membrane as a monomer, and then undergoes oligomerization culminating in the formation of a pore.

Using a truncated version of Bax, BaxΔC, labeled with a single fluorophore per protein monomer, we determined the oligomeric state of Bax in the micelles of several activating detergents using the fluorescence intensity distribution analysis (FIDA). To show that the fluorescently labeled BaxΔC used in our study has similar pore forming ability to that of BaxΔC used in the preceding studies where it was shown to enlarge the size of detergent micelles, we compared the pore forming ability of the two proteins using the assay of dye release from liposomes. The results of this assay showed that the fluorescently labeled BaxΔC has similar but slightly reduced pore forming ability compared to unlabeled BaxΔC. We attribute this slight reduction in the pore forming activity of fluorescently labeled BaxΔC to the presence of the fluorescent label on this protein.

The detergents used in this study were n-octylglucoside, dodecylmaltocide, Triton X-100, Tween 20, and cholic acid, and the results of FIDA for all of these detergents showed that BaxΔC does enlarge the hydrodynamic volume of detergent micelles, but

there is only one protein monomer per detergent micelle. Cholic acid was an exception to the first part of this statement, since Bax did not enlarge the size of micelles of cholic acid. We ascribe the absence of enlargement of the micelles of cholic acid upon interaction with Bax to the fact that cholic acid is an ionic detergent, and it naturally forms extremely small micelles of 4 kDa (in comparison the size of Bax is 21 kDa while the size of Triton X-100 detergent micelles is 70-100 kDa).

The result, showing that BaxΔC is present as a monomer in the proteo-micellar complexes, provides a connection between the detergent activation of Bax *in vitro* and the physiologic pattern of Bax activation observed *in vivo,* showing that active Bax is a monomer prior to membrane binding, and oligomerizes only in the environment of a lipid membrane to form a pore. However, independent reviewers of our study pointed out that the use of the truncated version of Bax, BaxΔC, might be a problem. Furthermore, two recently published studies used micelles of Triton X-100 to study the homo-oligomerization of full length Bax using cross-linking. The comment of the authors of these studies on our study was that the reason for difference in the observed results is the use of BaxΔC, which might have different oligomerization propensity than full length Bax.

BaxΔC has 19 amino acids truncated at the C-terminus, and thus lacks helix 9 which is implicated in binding lipid membranes. When expressed *in vivo,* BaxΔC can release cytochrome c from mitochondria, thus showing that it has pore forming activity comparable to that of full length Bax. The reason why we chose to use BaxΔC in our studies is because the full length Bax in our hands forms visible by eye precipitates upon incubation with activating detergents, thus rendering it unusable in FIDA analysis.

However, we do agree that repeating FIDA with the full length fluorescently labeled Bax is one of the future experiments which need to be done.

Imaging studies with fluorescently labeled Bax

Before continuing to the two-color two-focus scanning FCCS experiments on the fluorescently labeled full length Bax in lipid membranes, we performed confocal microscopy characterization of the interaction of fluorescent Bax with GUVs. In these confocal microscopy experiments we used cBid to promote Bax binding to GUVs, and we have made a number of informative observations: (i) permeabilization of GUVs by Bax is a stochastic process, i.e. GUVs exposed to the same concentration of solution Bax are not permeabilized simultaneously; (ii) after the initial permeabilization of a GUV, Bax continues to bind the GUV membrane until it saturates; (iii) shortly after the addition of Bax to GUVs, Bax is able to open stable giant pores in GUVs, which we named Bax mega-pores; (iv) Bax binding was not homogenous among the GUVs, i.e. some GUVs accumulated high membrane Bax concentrations than others, suggesting heterogeneity in the lipid composition of GUVs; (v) after prolonged incubation with GUVs Bax causes morphological changes in GUV structure, GUVs may form tubule-like structures, or have a potato-like shape, GUVs can form agglomerates or disintegrate; (vi) large, visible by confocal microscopy aggregates of Bax were observed in GUV membranes after prolonged incubation with Bax; (vii) the inhibitor of Bax pore formation, protein Bcl-x_L, does not completely inhibit Bax binding to GUV membranes but it does inhibit permeabilization of GUVs by Bax; (viii) within 24 hours of Bax addition, the majority of GUVs are disintegrated and are unfit for FCCS measurements, while GUVs which were

187

not treated with Bax maintain their spherical shape and remained present in the observation chamber after 24 hours. The results of these confocal imaging studies not only allowed us to determine the optimal experimental conditions and the time frame for performing scanning FCCS measurement on Bax in GUV membranes, but also they showed that Bax binding changes the morphology of GUVs.

Bax mega-pore

It has been observed that Bax forms a wide variety of pores in artificial lipid membranes and in isolated mitochondria, with the largest size of a Bax pore ranging between 100-200 nm in diameter. In contrast to these studies, we observed the formation of Bax mega-pores with diameters of 5-20 μm. All of these pores had fluorescent Bax concentrated at the rim of the pore which allowed us to perform 3D reconstructions of these pores.

These Bax mega-pores spent an unusually long time in an open state ranging from 10 minutes to hours. Giant pores of similar diameter can be opened in GUVs by application of detergents or by mechanical disruption, however, these only have a life time on the order of seconds and microseconds respectively. By analyzing the closure kinetics of Bax mega-pores, we have determined that the reason for such long lifetime of these pores compared to the other giant pores is explained by the extremely low line tension in the rim of the pore (3.7±1.7 fN), which is caused by the presence of Bax in the pore rim. Furthermore, the line tension in the rim of a Bax mega-pore formed by full length Bax is three orders of magnitude lower than that formed by the pore forming helix

5 of Bax, thus suggesting that the non-pore forming helices of Bax participate in the stabilization of a pore.

The existence of Bax mega-pores shows that Bax can form pores spanning four orders of magnitude in size. However, it is not clear whether all of these Bax pores have similar molecular interactions among Bax monomers in the pore rim, suggesting for the need to further explore the formation mechanism of various Bax-containing pores.

FCCS studies with Bax

For FCCS studies, we have produced two fluorescently labeled forms of Bax. One is labeled with Alexa Fluor 488 (Bax-G) and the other is labeled with Atto 655 (Bax-R). The pore forming activity of these proteins was identical to that of the wild-type full length Bax. Furthermore, these proteins behaved as monomers in solution and did not associate in solution in the absence of lipid membranes. Association of Bax-R and Bax-G resulted in the formation of a stable Bax-RG complex, and was observed only in GUV membranes using two-color two-focus scanning FCCS. Using this scanning FCCS technique, we have also observed that the diffusion of Bax-RG complexes decreases with time, suggesting a time dependent enlargement in the hydrodynamic in-membrane size of the complexes. The size of these Bax-RG complexes ranged from 50-120 nm in diameter, which is consistent with the size of the Bax pores observed in LUVs by transmission electron microscopy (with maximal size of 10-200 nm in diameter). However, it is important to mention that the in-membrane size of the Bax-RG complexes may not be the same as the size of pores possibly formed inside these complexes, since if the Bax pore is a lipidic pore, then lipids would be participating in the formation of the

pore, and their contribution to the diffusion of the Bax-RG complex would lead to a decrease in the overall diffusion coefficient of the complex, and thus lead to higher values in the estimation of the hydrodynamic diameter of the complex.

In the presence of Bcl-x_L protein the oligomerization of Bax was inhibited and the amount of Bax binding to the lipid membrane was decreased. We have also found that the diffusion coefficient of Bax was changing with time from 8 μm^2/sec to 5 μm^2/sec. This change in the diffusion coefficient of monomeric Bax is consistent with the hypothesis that, during membrane integration, Bax transitions from being a membrane associated protein to being a membrane integrated protein, where the membrane associated Bax monomer would have fast diffusion coefficient, comparable to that of lipids (~10 μm^2/sec), while the membrane integrated Bax monomer would have a slow diffusion coefficient, similar to that of transmembrane monomeric proteins (~5 μm^2/sec). This change in the diffusion coefficient of Bax in the presence of Bcl-x_L occurred over two hours after protein addition to GUVs, while in the absence of Bcl-x_L, Bax became oligomeric and reduced its diffusion coefficient to 3-4 μm^2/sec after 40 min of addition to GUVs, thus indicating that Bcl-x_L prevents pore formation by Bax not only by keeping it monomeric but by also keeping Bax mostly in the membrane associated state preventing the membrane integration of Bax.

Overall the results of scanning FCCS studies on Bax in GUV membranes provide direct observation that Bax binds lipid membranes as a monomer (membrane associated monomeric Bax), undergoes membrane insertion (membrane integrated monomeric Bax) and then undergoes in-membrane oligomerization and self-assembly into large complexes 50-120 nm in diameter which we feel are proteo-lipid pores.

Future Directions

Scanning FCCS can be used to study hetero-oligomerization among proteins of the Bcl-2 family

To the best of our knowledge, the approach, implementation and data analysis presented in this dissertation of using single-molecule sensitivity fluorescence techniques to study the mechanism of pore formation by Bax, and in fact by any other pore forming protein, is the first of its kind. Therefore, we foresee further studies utilizing this approach to study other pore forming proteins and peptides, and in particular, Bax. Our scanning FCCS studies provided an initial characterization of the diffusion coefficients of various Bax species in a lipid membrane. However, since *in vivo* Bax is kept in check by other members of the Bcl-2 protein family, it is important to investigate in future experiments the effect of other Bcl-2 members on Bax. This can be done by studying not the homo-oligomeirzation of Bax, as was done in this dissertation, but the hetero-oligomerization of Bax with other Bcl-2 family members. This type of hetero-oligomerization studies by scanning FCCS in lipid membranes can, for example, provide information about the affinity of the interaction among various Bcl-2 family members, and in particular help to determine whether activator and de-repressor BH3-only proteins interact with Bax in the environment of a lipid membrane. Another set of hetero-oligomerization experiments can address the question whether the major mechanism of inhibition of Bax pore formation by the anti-apoptotic proteins is by directly binding Bax in the lipid membrane or not. Our preliminary evidence suggests that Bax and Bcl-x_L do not form a stable complex in a lipid membrane; however, Bcl-x_L did inhibit the pore formation by Bax in these experiments. Information obtained in the described above

experiments about the mechanisms of interaction among the Bcl-2 family members in lipid membranes can potentially be used to develop small molecules which can help modulate these Bcl-2 family interactions and thus can be used in cancer treatment of prevention of cell death after trauma or cardiac infarction.

Cholic acid can be used to determine the structure of active Bax

Our FCS studies with the micelles of Bax activating detergents have shown that the majority of activating detergents form large proteo-micellar complexes with Bax. The large hydrodynamic size of these complexes prohibits NMR determination of the structure of active Bax contained inside these complexes. However, we have shown that cholic acid activates Bax without the formation of large hydrodynamic volume complexes, in fact, the size of Bax-cholic acid complexes is almost identical to the size of an inactive Bax monomer whose structure have been successfully determined by NMR. Therefore, we predict that cholic acid can be used to determine the structure of active Bax by NMR.

Single-molecule TIRF can be used to study the sequence of interactions among proteins of the Bcl-2 family

Single-molecule TIRF microscopy allow to study interactions among individual molecules near a surface. Supported lipid bilayers can form such a surface, and thus they have been used in single-molecule TIRF experiments. We hypothesize that single-molecule TIRF can be used to study homo- and heterotypic interactions among proteins of the Bcl-2 family, provided that these proteins are fluorescently labeled. These types of

studies would provide information about the sequence of interactions among the proteins of the Bcl-2 family, since such information can not be easily obtained using scanning FCCS technique used in this dissertation.

APPENDIX

Appendix I

Structural information on human α Bax protein

Amino acid sequence:

```
MDGSGEQPRG   GGPTSSEQIM   KTGALLLQGF   IQDRAGRMGG   EAPELALDPV   PQDASTKKLS

        70           80           90          100          110          120
ECLKRIGDEL   DSNMELQRMI   AAVDTDSPRE   VFFRVAADMF   SDGNFNWGRV   VALFYFASKL

       130          140          150          160          170          180
VLKALCTKVP   ELIRTIMGWT   LDFLRERLLG   WIQDQGGWDG   LLSYFGTPTW   QTVTIFVAGV

       190
LTASLTIWKK  MG
```

Number of amino acids: 192

Molecular weight: 21184.4

Theoretical pI: 5.08

Amino Acid composition:
Ala (A) 14   7.3%
Arg (R) 11   5.7%
Asn (N) 3 1.6%
Asp (D) 13   6.8%
Cys (C) 2 1.0%
Gln (Q) 9 4.7%
Glu (E) 10 5.2%
Gly (G) 21   10.9%
His (H) 0 0.0%
Ile (I) 9   4.7%
Leu (L) 22   11.5%
Lys (K) 9 4.7%
Met (M) 8   4.2%
Phe (F) 10 5.2%
Pro (P) 8   4.2%
Ser (S) 11 5.7%
Thr (T) 13   6.8%
Trp (W) 6   3.1%
Tyr (Y) 2   1.0%
Val (V) 11   5.7%

Total number of negatively charged residues (Asp + Glu): 23
Total number of positively charged residues (Arg + Lys): 20
Extinction coefficients:

Ext. coefficient   35980 M^{-1} cm^{-1}, at 280 nm measured in water.

Abs 0.1% (=1 g/l)   1.698, assuming all Cys residues are reduced

Appendix II

Protocol for the preparation of large unilamellar vesicles

For my thesis I have used the reverse phase method of LUV preparation (ref). The other existing method for the LUV preparation is the freeze-thaw method (ref). Using either of these methods it is possible to prepare LUVs in various aqueous buffer solutions. In my thesis research I mainly prepared two types of LUV: filled with quenched concentration of carboxyfluorescein or filled with buffer solution. In order to prepare LUVs by either method lipids have to be dried in a glass vial/tube.

Drying lipids:

1. Deposit lipids dissolved in chloroform into a glass tube (1x10 cm, diameter x height). The total amount of lipids per tube can be from 0.5 – 10 mg.

2. Dry lipids using a stream of nitrogen gas. Dried lipids are extremely vulnerable to oxidation by the oxygen in the atmosphere, therefore, care must be taken to keep the dry lipids either under 100% nitrogen or 100% argon atmosphere.

3. To remove the chloroform from lipids completely the liophilization vacuum system is used for 2 hours.

4. At this points glass tubes with dried lipids can be stored at -20 °C under 100% nitrogen or 100% argon atmosphere. For convenience 50 ml disposable plastic conical tubes can be used. In this form lipids can be stored for 1-2 months.

LUV preparation by reverse phase method:

1. Defrost a container containing the glass tube/tubes with dried lipids by leaving it on a bench at room temperature for 5-10 minutes.

2. Return the rest of the glass tubes to -20 °C.

3. To the glass tube with dried lipids add 1 ml of diethyl ether to dissolve the lipids. Make sure that all lipids are dissolved by checking for the white residue of dry lipids on the sides of a glass tube. (Note, a bottle of diethyl ether which is over 1 year old is dangerous since it can be explosive due to the formation of diethyl ether hydroperoxide).

4. Next, add 0.5 ml of buffer which will be incorporated into the interior of the liposomes (for example, 1x EB* or 50 mM rarboxyfluorescein in 1x EB). At this point the ether and water phases will be separated with ether phase being on top of the water phase.

5. Sonicate the water-ether solution using a table top, water bath sonicator for 10-30 seconds. At this point the solution in the glass tube should become homogeneous and milky. If the solution is not homogeneous repeat the sonication cycle.

6. The milky solution in a tube is an emulsion of aqueous buffer in ether.

7. Transfer the emulsion to a bulb-like vial and connect it to a rotary evaporator to evaporate the ether from the emulsion. Slow evaporation of ether forces lipids in solution to organize into lipid bilayers of liposomes. At this point liposomes would be non-unilamellar (i.e. there would be daughter liposomes inside of a larger mother liposome) and would have diameters anywhere between 600 nm and 50-30 nm.

8. To form unilamellar liposomes of a 200 nm to 100 nm in diameter the liposomes from the Step 7 should be extruded 7-21 times through a membrane with pore of a specified diameter.

9. At this point dynamic light scattering can be used to asses the quality of the extrusion process.

10. Depending on the lipid composition resulting extruded LUVs can be stored for 1 month. For example, extruded LUVs made with lipids containing tow oleoyl carbon tails can be store at room temperature for 1 month.

Preparation of LUVs filled with quenched carboxyfluorescein:

1. Prepare a 50 mM carboxyfluorescein solution in a buffer of choice. Keep 7.0 pH.

2. Follow steps 1-3 of the above LUV preparation protocol.

3. Add 0.5 ml of 50 mM carboxyfluoresceine in 1x EB to the glass tube containing lipids dissolved in ether. Separation of the aqueous and ether pahses would be clearly visible.

4. Sonicate the buffer-ether solution using a table top, water bath sonicator for 10-30 seconds. At this point the solution in the glass tube should become homogeneous and milky. If the solution is not homogeneous repeat the sonication cycle.

5. The milky solution in a tube is an emulsion of aqueous buffer in ether.

6. Transfer the emulsion to a bulb-like vial and connect it to a rotary evaporator to evaporate the ether from the emulsion. Slow evaporation of ether forces lipids in solution to organize into lipid bilayers of liposomes. At this point liposomes would be non-unilamellar (i.e. there would be daughter liposomes inside of a larger mother liposome) and would have diameters anywhere between 600 nm and 50-30 nm.

7. To form unilamellar liposomes of a 200 nm to 100 nm in diameter the liposomes from the Step 7 should be extruded 7-21 times through a membrane with pore of a specified diameter.

8. To separate the extruded LUVs filled with the carboxyfluoresceien from the carboxyfluoresceine present outside the LUVs use a Sephadex G-25 column. The appropriate dimentions of such Sephadex G-25 column should be 1 cm x 30 cm (diameter versus length) to enshure clear separation of the liposomes filled with the carboxyfluorescein from free carboxyfluoresceine in solution.

9. After the gel filtration thotuhg the Spehadex G-25 column perform dynamic light scattering on the sample of LUVs to ensure the correct size.

10. To ensure that the liposomes are filled with quenched carboxyfluorescein use a small sample of liposomes (5-10 µl) in a clear ependorf tube (note the brightness of the sample) then add 5 µl of 20% Triton X-100 to the sample. Triton X-100 is a detergent which when added to the liposomes would solubilize the liposomes releasing their content into solution. If the sample changes brightness this would mean that the liposomes are filled with qunenched carboxyfluoresceien and are ready for use. The same type of control can be sone using a plate reader or a conventional fluorimeter.

11. Liposomes filled with quenched carboxyfluoresceine and filtered throught he Sphadex G-25 column can be used only over a 5 day period due to the gradual leakage of carboxyfluoresceine from liposomes.

* 1x EB – equilibration buffer containing 10 mM HEPES pH 7.2, 100 mM KCl

Appendix III

Protocol for preparation of giant unilamellar vesicles

Giant unilamellar vesicles (GUVs) used in all experiments described in this dissertation were prepared by the electroformation method[2, 3]. In this method chloroform mixture of lipids (1-2 mg/ml of total lipid) is deposited onto the surface of two parallel platimun wires (5 µl of mixture per wire). Deposition of lipid mixture onto the platinum wires is done using a plastic gel-loading pipette tip. Lipids are allowed to dry on the surface of the wires after which the wires are immersed into the di-ionized water solution of 300 mM sucrose. The platinum wires and the sucrose solution are contained in a Teflon chamber (Fig. A1a). Next, wires are connected to an AC function generator set to sine wave-shaped output of AC current with 10 Hz, 2V for 1-2 hours (Fig. A1b, A1c). During this 1-2 hour time period GUVs are formed on the surface of the platinum wires (like grapes on a wine). After that the frequency of the AC current is changed to 2 Hz for another 30 min to 1 hour. This leads to detachment of GUVs from the platinum wires into the sucrose solution resulting in GUVs ready for use in an experiment. While pipetting the GUVs care must be taken not to rupture them by cutting the tip of 200 µl pipette tip (this increases the diameter of the pipette opening and results in a smaller shear forces experienced by GUVs while passing through the opening during pipetting).
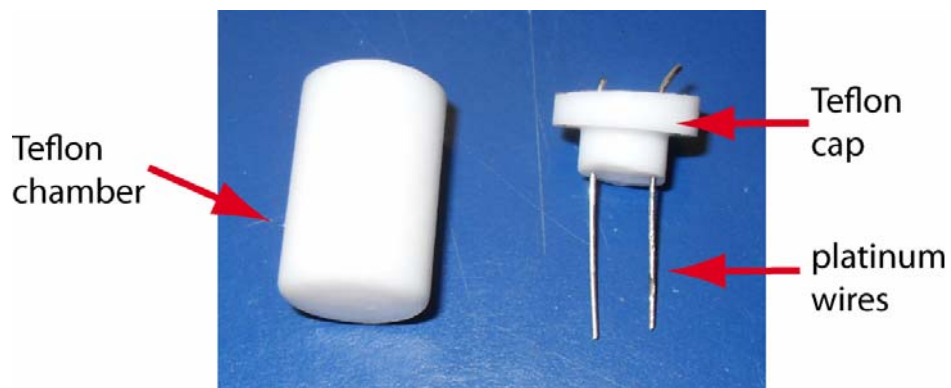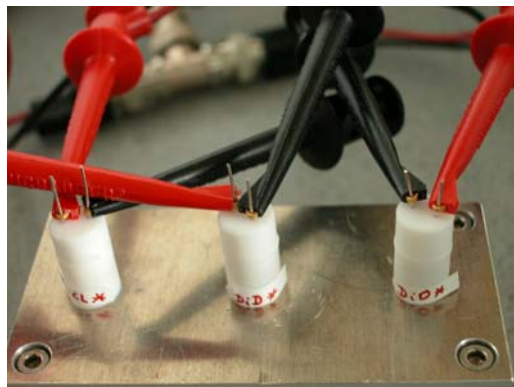
Figure A1. Illustrations to the method of GUV electroformation. **a.** Electroformation chamber made of Teflon with two platinum wires. **b.** Function generator; this figure shows for function generators. **c.** Assembled electroformation chambers connected to the function generator.

Appendix IV

Protocol of protein purification and labeling.

Human full length Bax, BaxΔC, BaxΔC(G40C), Bid, Bcl-x$_L$, and mutant Bax_S4C were expressed in BL21(DE3) *E. coli,* and purified as an intein/chitin-binding domain fusion protein without use of detergents. Briefly, bacterial cultures were grown at 37 °C in Terrific Broth[4] to an *A*600 of 1.5–2.0, and then the cultures were induced with 0.1 mM isopropyl 1-thio-D-galactopyranoside (Research Products International. Corp.), and the temperature was changed to 25 °C. After 12–15 h, bacteria were collected via centrifugation; the resulting pellet was resuspended in lysis buffer (phosphate-buffered saline, pH 7.2, 1mM EDTA, 0.25 mM phenylmethylsulfonyl fluoride), and cells were broken by four passages through a microfluidizer (Microfluidics) at the pressure of 1000 bar. Lysate was clarified by centrifugation, and the supernatant containing protein of interest was incubated with chitin affinity resin (New England Biolabs) overnight at 4 °C on a rocker. Resin was subjected to a high salt wash and then equilibrated in cleavage buffer (10 mM HEPES/NaOH, pH 8.0, 100 mM NaCl, 50mM dithiothreitol) and incubated for 48 h at 4 °C. The purity of the proteins was assessed by SDS-PAGE. Bax_S4C was labeled with either Alexa Flupr 488 maleimide (Invitrogen) or Atto 655 maleimide (AttoTech) according to the manufacturer's protocol. Labeled protein was separated from the free dye using a Sephadex G-25 column. The degree of protein labeling was determined using a Nano-Drop spectrophotometer (Thermo Scientific) by measuring absorbance at 280 nm (for protein concentration) and 488 nm (for Alexa Fluor 488 concentration) and 655 nm (for Atto 655 concentration). Resulting proteins Bax-R and Bax-G were 80% and 100% labeled respectively and were stored in EB buffer (10

mM HEPES/KOH, pH 7.2, 100 mM KCl) at 4 °C. Proteins were used within one month of purification and labeling.

Bid was cut with recombinant caspase 8 to produce cBid.

Protein functionality check: fluorescently labeled Bax is functional. To determine whether fluorescent labeling and mutagenesis of the human full length Bax protein (Figure 1B) interferes with the capacity of Bax to form pores the experiments of carboxyfluorescein release from liposomes [5, 6] were performed. In these experiments the ability to form pores in liposomes of the wild-type Bax and the two forms of the fluorescently labeled Bax (Bax-G labeled with Alexa 488 and Bax-R labeled with Atto 655) were compared. As a result, identical kinetics of carboxyfluorescein release was observed for the wild-type Bax and for Bax-R and Bax-G which implies that fluorescent labeling and mutagenesis of Bax did not interfere with its pore forming ability. In these experiments 100 nM Bax was activated by the activator protein cBid (20 nM). To show that the wild-type Bax as well as Bax-R and Bax-G can be inhibited by the full-length Bcl-x_L we also performed carboxyfluorescein releases in the presence of 100 nM Bcl-x_L (Supplementary Fig. 2b-d). For these experiments liposomes were prepared from the lipid mixture of DOPC and bovine heart cardiolipin (80:20 mol%). Lipids were purchased from Avanti Polar Lipids.

Appendix V

Lipid diffusion in DOPC versus DOPC:CL (80:20 mol%) lipid bilayer.

To determine whether lipid diffusion and viscosity of a lipid membrane is affected by the presence of cardiolipin in a lipid bilayer we have measured the lipid diffusion in GUVs formed from DOPC or DOPC:CL (80:20 mol%) lipid mixtures. We have also compared the results using dual-focus scanning FCS versus static volume FCS which is normally done in a fixed position at the top a GUV (See Chapter 3 for the description of FCS in lipid membranes). The results of our analysis show no difference in diffusion of classic lipidic probes (DiO and DiD) in DOPC versus DOPC:CL lipid membranes (Table A1) indicating the presence of cardiolipin does not affect lipid diffusion and the viscosity of a lipid membrane.

Table A1. Comparison of lipid diffusion in GUVs prepared from lipid mixture of DOPC and DOPC:CL (80:20 mol%). The lipid probe used was DiO or DiD (Invitrogen, Molecular Probes). Comparison was also done with regard to the dual focus scanning FCS versus static volume FCS[7] which was done using Zeiss Confocor 2 instrument.

Membrane composition	Probe	D, μm^2/sec	Number of GUVs measured	Method
DOPC:CL (80:20 mol%)	DiO, DiD	10.0±0.5	9	dual focus scanning FCS
DOPC	DiD	10.9±1.9	12	static volume FCS (single point measurement at the top of a GUV)
DOPC:CL (80:20 mol%)	DiO	10.6±2.9	10	static volume FCS (single point measurement at the top of a GUV)

References

1.   Korsmeyer, S. J., Shutter, J. R., Veis, D. J., Merry, D. E. & Oltvai, Z. N. Bcl-2/Bax: a rheostat that regulates an anti-oxidant pathway and cell death. Semin Cancer Biol 4, 327-32 (1993).
2.   Angelova, M. I. & Dimitrov, S. D. Liposome electroformation. Faraday Discuss. Chem. Soc. 81, 303-311 (1986).
3.   Garcia-Saez, A. J., Ries, J., Orzaez, M., Perez-Paya, E. & Schwille, P. Membrane promotes tBID interaction with BCL(XL). Nat Struct Mol Biol 16, 1178-85 (2009).
4.   Tartof & Hobbs. Improved media for growing plasmid and cosmid clones. Focus 9, 12 (1987).
5.   Saito, M., Korsmeyer, S. J. & Schlesinger, P. H. BAX-dependent transport of cytochrome c reconstituted in pure liposomes. Nat Cell Biol 2, 553-5 (2000).
6.   Ivashyna, O. et al. Detergent activated BAX protein is a monomer. J Biol Chem 284, 23935-46 (2009).
7.   Kahya, N., Scherfeld, D., Bacia, K., Poolman, B. & Schwille, P. Probing lipid mobility of raft-exhibiting model membranes by fluorescence correlation spectroscopy. J Biol Chem 278, 28109-15 (2003).